SANDIA REPORT

SAND2011-3342
Unlimited Release
Printed December 2011

LNG Cascading Damage Study Volume I: Fracture Testing Report

Robert J. Kalan, Jason P. Petti

Prepared by
Sandia National Laboratories
Albuquerque, New Mexico 87185 and Livermore, California 94550

Sandia National Laboratories is a multi-program laboratory managed and operated by Sandia Corporation, a wholly owned subsidiary of Lockheed Martin Corporation, for the U.S. Department of Energy's National Nuclear Security Administration under contract DE-AC04-94AL85000.

Issued by Sandia National Laboratories, operated for the United States Department of Energy by Sandia Corporation.

Available to DOE and DOE contractors from
U.S. Department of Energy
Office of Scientific and Technical Information
P.O. Box 62
Oak Ridge, TN 37831

Telephone: (865)576-8401
Facsimile: (865)576-5728
E-Mail: reports@adonis.osti.gov
Online ordering: http://www.osti.gov/bridge

Available to the public from
U.S. Department of Commerce
National Technical Information Service
5285 Port Royal Rd
Springfield, VA 22161

Telephone: (800)553-6847
Facsimile: (703)605-6900
E-Mail: orders@ntis.fedworld.gov
Online order: http://www.ntis.gov/help/ordermethods.asp?loc=7-4-0#online

SAND2011-3342

Unlimited Release

Printed December 2011

LNG Cascading Damage Fracture Testing Report

Robert J. Kalan
Mechanical Environments, Org. 01534
Sandia National Laboratories
P.O. Box 5800
Albuquerque, NM 87185

Jason P. Petti
Structural & Thermal Analysis, Org. 06233
Sandia National Laboratories
P.O. Box 5800
Albuquerque, NM 87185

Abstract

As part of the LNG Cascading Damage Study, a series of structural tests were conducted to investigate the thermal induced fracture of steel plate structures. The thermal stresses were achieved by applying liquid nitrogen (LN_2) onto sections of each steel plate. In addition to inducing large thermal stresses, the lowering of the steel temperature simultaneously reduced the fracture toughness. Liquid nitrogen was used as a surrogate for LNG due to safety concerns and since the temperature of LN_2 is similar (-190^{o}C) to LNG (-161^{o}C). The use of LN_2 ensured that the tests could achieve cryogenic temperatures in the range an actual vessel would encounter during a LNG spill. There were four phases to this test series. Phase I was the initial exploratory stage, which was used to develop the testing process. In the Phase II series of tests, larger plates were used and tested until fracture. The plate sizes ranged from 4 ft square pieces to 6 ft square sections with thicknesses from ¼ inches to ¾ inches. This phase investigated the cooling rates on larger plates and the effect of different notch geometries (stress concentrations used to initiate brittle fracture). Phase II was divided into two sections, Phase II-A and Phase II-B. Phase II-A used standard A36 steel, while Phase II-B used marine grade steels. In Phase III, the test structures were significantly larger, in the range of 12 ft by 12 ft by 3 ft high. These structures were designed with more complex geometries to include features similar to those on LNG vessels. The final test phase, Phase IV, investigated differences in the heat transfer (cooling rates) between LNG and LN_2. All of the tests conducted in this study are used in subsequent parts of the LNG Cascading Damage Study, specifically the computational analyses.

CONTENTS

FIGURES

TABLES

ACKNOWLEDGMENTS

The authors would like to acknowledge the following Sandia, DOE, and expert panel members.

- Mike Hightower, Sandia National Laboratories, Overall LNG Project Manager
- Luis Abeyta, Sandia National Laboratories, Testing Support and Data Acquisition
- Amarante Martinez, Sandia National Laboratories, Testing Support and Photometrics
- Carlos Lopez, Sandia National Laboratories, LNG Cascading Damage Thermal Lead
- Gerald Wellman, Sandia National Laboratories, Test Planning and Design
- Frank Dempsey, Sandia National Laboratories, Test Planning and Design
- Doug Ammerman, Sandia National Laboratories, Internal Sandia Review
- Robert Corbin, DOE Project Manager
- Christopher Freitas, DOE
- Commander Nick Caron, U.S. Coast Guard, Expert Review Panel
- Charles Rawson, U.S. Coast Guard, Expert Review Panel
- Professor Stan Rolfe, Kansas University, Expert Review Panel
- Dr. James Rawers, DOE, Expert Review Panel
- Dr. John Moorhouse, British Gas (*formerly of*), Expert Review Panel
- John Dasch, DNV, Expert Review Panel
- Chris Zerby, FERC, Expert Review Panel
- Tony Galt, Freeport LNG, Expert Review Panel

EXECUTIVE SUMMARY

The combination of recent and expected future growth of imports of liquefied natural gas (LNG) with the increased safety and security concerns resulting from the incidents of September 11, 2001, have led to an exploration of possible impacts that an attack on potentially hazardous cargos would have on the public and other assets. A number of studies (Hightower, et al., 2004, Hightower et al., 2006) have been performed at Sandia National Laboratories in the aftermath of September 11, 2001, in order to examine the potential hazards from LNG vessels experiencing an unintended release of LNG cargo. An unintended release of LNG has two significant components: 1) the effects of the cryogenic LNG contacting the steel structure of the tanker vessel, and 2) the flammable nature of LNG and the potential fire hazards to the tanker and to the public if in a harbor location. Stored LNG has a temperature of approximately -161^{o}C which is well below the brittle transition for the marine steels that comprise LNG tankers. Rupture of the LNG containment vessel will results in the LNG flowing out and coming into contact with the tankers steel structures. Due to the complex nature of this type of event, the US Government Accountability Office (GAO) has studied the current state of knowledge of the relevant issues/phenomenon (GAO, 2007). This report was compiled in order to identify the areas of additional research required in order to gain an improved understanding of these events. The top two areas recommended for further study were related to improving the understanding of large LNG fire physics and to improving the state of knowledge surrounding the potential for cascading damage to LNG vessels. Under two separate projects, Sandia National Laboratories is examining both areas of concern. This report summarizes one component, the large-scale fracture testing, performed under LNG Cascading Damage Study. An understanding of the potential for fracture of the steel that comprises the LNG vessels is potentially critical in assessing the likelihood of cascading failure of the vessel. Here, cascading failure is defined as damage that causes the spread of sufficient LNG cargo and/or LNG fires that then lead to additional damage or breaches to the vessel beyond the damage that produced the initial spill. This report summarizes the testing performed to better understand the brittle fracture of steel structures subjected to cryogenic liquids.

The types and method of testing performed here for the LNG Cascading Damage Study are directly related to how the testing information will be used in the computational analysis component of the project. The goal of the project is to provide an assessment of LNG vessels subjected to unintended LNG spills. This will be accomplished through a series of computational finite element analysis of the vessels. The models created for these analyses are relatively large, but even so, the smallest elements are approximately 4 inches by 4 inches. While this resolution provides sufficient stress/strain resolution to capture the global behavior of the vessel, this resolution is several orders of magnitude too large to capture the stress/strain fields that are generated at the tip of a crack in the steel that comprises the hulls of LNG tankers. The progression of brittle cracks in steel plates depends on a number of factors including the specific geometry, the material properties, the temperature state caused by contact with cryogenic liquids, and the microstructure of the material. Specifically, the dependence on the microstructure of the steel plating from point to point makes the tracking of individual brittle cracks using continuum mechanics in finite element models impossible. However, this level of detail is not necessary to assess the global behavior of the vessel. What is necessary is an estimate of the general crack path and directionality. The “damage” caused by crack initiation and crack propagation will be represented in the finite element models by the removal or “death”

of 4 inch by 4 inch elements along the crack propagation path. The "death" of a finite element is achieved by removing that element from the analysis after a defined criteria has been reached in that element causing material separation. For these analyses, a strain/temperature locus is employed. Due to the transition from ductile to brittle behavior as the temperature drops, the strain required to "kill" a finite element drops drastically as the temperature falls. The temperature at which the strain drops most dramatically varies from steel to steel; however, all of the marine steels used in LNG tanker construction enter the brittle regime at temperature well above LNG temperatures. The initial strain/temperature locus was developed using basic material tests (stress-strain tests at multiple temperatures). These test results are not presented in this report, but are described in the analysis report when discussing the strain/temperature locus calibration. The fracture tests presented here were used in the secondary calibration and validation of the strain/temperature locus. The goal of the large-scale fracture tests was therefore to provide examples of fractured steel plates and structures. Finite element models were created for the relevant fracture structures to test the ability of the finite element code, element death modeling, and the strain/temperature locus to reproduce the general crack path and directionality. These finite element analyses also used 4 inch by 4 inch elements in order to have the same stress/strain resolution as the models of the full vessel. The analyses of the test structures and the full vessel have the temperatures of the finite elements reduced at an appropriate rate to induce thermal strains. The temperature fields were generated with either a heat transfer analysis or by ramping the temperatures down manually. Since the stresses and strains generated in the 4 inch element in the analysis would not match the resolution of the strain obtained with strain gauges, only temperature data was taken for each test. The temperature data was then used to link the tests with the finite element analyses. The details of the test analyses and the locus calibration are provided in a separate report on the computational analyses (Volume III, Petti, et al., 2011). This report focuses on the fracture testing structures, procedures, and results.

As part of the LNG Cascading Damage Study, the series of structural tests conducted here were used to investigate thermally induced fracture of steel plate structures. The thermal stresses were achieved by applying liquid nitrogen (LN_2) onto sections of each steel plate causing differential thermal contraction. In addition to inducing large thermal stresses, the lowering of the steel temperature simultaneously reduced the fracture toughness. Liquid nitrogen was used as a surrogate for LNG due to safety concerns and since the temperature of LN_2 is slightly colder (-190^{o}C) than LNG (-161^{o}C). This ensured that the tests could achieve temperatures in the range an actual vessel would see during a spill.

There were four phases to this test series. Phase I was the initial exploratory stage, which was used to develop the testing process. The first several tests studied the cooling of steel plates subjected to LN_2. In addition, tests were conducted on various thermocouple types. Finally, to better represent the typical condition of steel, the plates were coated with paints typically used in commercial vessels, painting of the steel surface in contact with the LN2 was shown to significantly increase the cooling rate. Since both the interior and exterior surfaces of LNG vessel hulls have surface coatings, all subsequent test phases used surface coatings.

In the Phase II series of tests, larger plates were used and tested until fracture. Phase II was divided into two sections, Phase II-A and Phase II-B. Phase II-A used standard A36 steel, while Phase II-B used marine grade steels. The three test structure in Phase II-A included plate sizes ranging from 4 ft square pieces to 6 ft square sections with thicknesses from ¼ inches to ¾

inches. This phase investigated the cooling rates on larger plates and the effect of different notch geometries (stress concentrations used to initiate brittle fracture). Each of the three Phase II-A test structures were tested multiple times. For each subsequent test, stress concentrations were introduced and then made more severe until a fracture was initiated in the plate. Phase II-B used similar test structures and techniques but with marine grade steels. Specifically, ABS Grade A and ABS Grade EH were used in construction of the test articles. Two Gr. A plate and two Gr. EH plate structures were tested.

In Phase III, the three test structures were significantly larger than for Phase II. Each of the structures was built with a main plate spanning 12 ft by 12 ft and then a height of 3 ft. These structures were designed with more complex geometries to include features similar to those on LNG vessels. They included multiple material, intersecting plates, and stiffening elements. However, they were not scaled versions of any specific section of an LNG vessel. The Phase III tests showed that stiffening elements and intersecting plates did not arrest brittle cracks. The cracking that occurred in these test followed the extent of the cooled region and propagated, in general, in the direction perpendicular to the maximum stress.

The final test phase, Phase IV, investigated differences in the heat transfer (cooling rates) between LNG and LN_2.

1. Introduction

The combination of the expected future growth of imports of liquefied natural gas (LNG) with the increased safety and security concerns resulting from the incidents of September 11, 2001, have led to an exploration of possible impacts that an attack on potentially hazardous cargos would have on the public and other assets. A number of studies (Hightower, et al., 2004, Hightower et al., 2006) have been performed at Sandia National Laboratories in the aftermath of September 11, 2001, in order to examine the potential hazards from a LNG tanker vessel experiencing an unintended release of LNG cargo. An unintended release of LNG has two significant components: 1) the effects of the cryogenic LNG contacting the steel structure of the tanker vessel, and 2) the flammable nature of LNG and the potential fire hazards to the tanker and to the public if in a harbor location. Stored LNG has a temperature of approximately -161^{o}C which is well below the brittle transition for the marine steels that comprise LNG tankers. Due to the complex nature of this type of event, the US Government Accountability Office (GAO) commissioned a study on the current state of knowledge of the relevant issues/phenomenon (GAO, 2007). This previous report was compiled in order to identify the areas of additional research required in order to gain an improved understanding of these events. The top two areas recommended for further study were related to improving the understanding of large LNG fire physics and to improving the state of knowledge surrounding the potential for cascading damage to LNG vessels. Under two separate projects, Sandia National Laboratories is examining both areas of concern. This report summarizes one component, the large-scale fracture testing, performed under the LNG Cascading Damage Study. An understanding of the potential for the fracture of the steel that comprises the LNG tankers is critical in assessing the likelihood of cascading failure of the vessel. Here, cascading failure is defined as damage that causes the spread of sufficient LNG cargo and/or LNG fires that then lead to additional damage or breaches to the vessel beyond that produced during the initial spill. This report summarizes the testing performed to better understand the brittle fracture of steel structures subjected to cryogenic liquids. An explanation of why these specific tests were performed and how the results of these tests are used in computational analyses is provided in the next section. The computational analysis portions of the LNG Cascading Damage Study are contained within additional reports (Figueroa and Lopez, 2011, Petti et al., 2011).

2. Testing Purpose

The types and methods of testing performed for the LNG Cascading Damage Study are directly related to the information needed and used in the computational analysis component of the project. The goal of the project is to provide an assessment of LNG vessels susceptibility to damage and possibly failure when subjected to unintended LNG spills. This will be accomplished through a series of computational finite element analysis of models of the two most common commercial LNG vessels. The models created for these analyses are relatively large. However, the analysis will be capable of characterizing the materials response on elements, the smallest of which are approximately 4 inches by 4 inches. While this level of resolution provides sufficient stress/strain analysis to capture the global behavior of the vessel, this scale is several orders of magnitude too large to capture the stress/strain fields that may be generated at the tip of a crack in the steel that comprises the hulls of LNG tankers when subjected to thermal stresses resulting from contact with the LNG. In addition,

the progression of brittle cracks in steel plates depends on a number of factors including the specific geometry, the material properties, the temperature state caused by contact with cryogenic liquids, and the microstructure of the material. Specifically, the dependence on the microstructure of the steel plating from point-to-point makes it impossible to predict the individual brittle crack behavior using continuum mechanics in finite element models. However, specific knowledge at the microscopic level of detail is not necessary to assess the global behavior of the vessel. What is necessary is an approximate estimate of the general crack path and directionality. The "damage" caused by cracks will be represented in the finite element models by the failure or "death" of a path of 4 inch by 4 inch elements. The "death" of a finite element is achieved by removing that element from the analysis after a defined criteria has been reached for that element, causing material separation. For these analyses, a strain/temperature locus is employed as the failure criterion. Due to the transition from ductile to brittle behavior as the temperature drops, the strain required to "kill" a finite element drops drastically as the temperature falls. The temperature at which the strain drops most dramatically varies from steel to steel; however, all of the marine steels used in LNG tanker construction enter the brittle regime at temperatures well above LNG temperatures. The initial strain/temperature locus was developed using basic material tests (stress-strain tests at multiple temperatures). These test results are not presented in this report, but are described in the analysis report when discussing the strain/temperature locus calibration. The fracture test results presented here were used in the secondary calibration and validation of the strain/temperature locus. The goal of the large-scale fracture tests was therefore to provide examples of fractured steel plates and structures. Finite element models were created for a selected number of the fractured structures to test the ability of the finite element code, element death modeling, and the strain/temperature locus to reproduce the general crack path and directionality observed experimentally. These finite element analyses also used 4 inch by 4 inch elements in order to reflect the same stress/strain resolution as the models of the full vessels. The analyses of the test structures and the full vessel have the temperatures of the finite elements in the cooled regions reduced at an appropriate rate to induce thermal strains. The temperature fields were generated with either a heat transfer analysis or by ramping element temperatures down manually. Since the stresses and strains generated in the 4 inch element in the analysis would not match the resolution of the strain obtained from experimental strain measurements, the temperature data was then used to link the tests with the finite element analyses. The details of the test analyses and the locus calibration are located in Volume III of this study (Petti et al., 2011). This report focuses on the fracture testing structures, procedures, and results.

3. Testing Overview

As part of the LNG Cascading Damage Study, a series of structural fracture tests were conducted to investigate the effect of liquid natural gas (LNG) flowing on steel structures. These tests were designed to induce large thermal stresses in the test plates due to differential thermal contraction while simultaneously lowering their ductility. Liquid nitrogen (LN_2) was chosen as the cryogenic fluid to use in place of LNG. It is significantly safer to work with and the temperature of LN_2 is slightly colder (-190^oC) than LNG (-161^oC). The use of LN2 ensures that the tests could achieve temperatures in the range an actual vessel would see during a LNG spill. There were four phases in this test series. Phase I was the initial exploratory stage that provided preliminary data to the material's response to LN2 (LNG) and

the insight and direction for the series of larger scale tests. In the Phase II series of tests, larger plates were used than for Phase I. The plate sizes ranged from 4 ft square pieces to 6 ft square sections. This phase investigated the cooling rates on these plates and the effect of different notch geometries (stress concentrations used to initiate brittle fracture) from which the crack would initiate. Phase II was broken in to two sections, Phase II-A and Phase II-B. Phase II-A used standard A36 structural steel, while Phase II-B used marine grade steels. In Phase III, significantly larger 12 ft square structures with more complex geometries were tested. The final test phase, Phase IV, investigated the heat transfer (cooling) rate differences between LNG and LN_2. Not including the initial exploratory tests conducted as part of Phase I, twenty two tests were conducted in Phases II and III. Cracking was only achieved in a fraction of the tests. The same test article could then be retested using a different, more severe test conditions. Two additional series of the tests were performed for Phase IV. Each of those series included 6 individual tests.

This report presents the details of the testing described above. Due to the large number of thermocouples used and the large number of tests conducted, only a small portion of the temperature data is presented within the main report. The complete set of data can be found in the Appendix B.

4. Fracture Testing

4.1 Phase I Exploratory Tests

Initial tests conducted for the LNG study were exploratory in nature. The tests used small plates to develop the basic test methods and procedures using a low pressure dewar to supply the LN_2. These tests explored methods to cool steel plates, flow distribution, surface coatings, and thermocouple types.

The initial test used ¾ inch thick carbon steel plates (standard A36), which was sectioned into a 24 in. x 24 in. square as shown in Figure 1. The trough used to hold the LNG was made from polyurethane foam. It is sealed to the plate with silicone caulk and held in place with 1 inch angles and studs. The inner trough dimensions were 2 in. wide and 5 in. high. The thermocouples were Type T 30 gauge Teflon and were held in place using Kapton tape (Type T thermocouples are copper-Constantan). They have an operating temperature range of -250°C to 350°C. The location of the thermocouples is shown in Figure 2. There were ten thermocouples (1-10) on the top surface and ten thermocouples (11-20) directly below them on the bottom surface.

Figure 1. Phase I test plate and trough

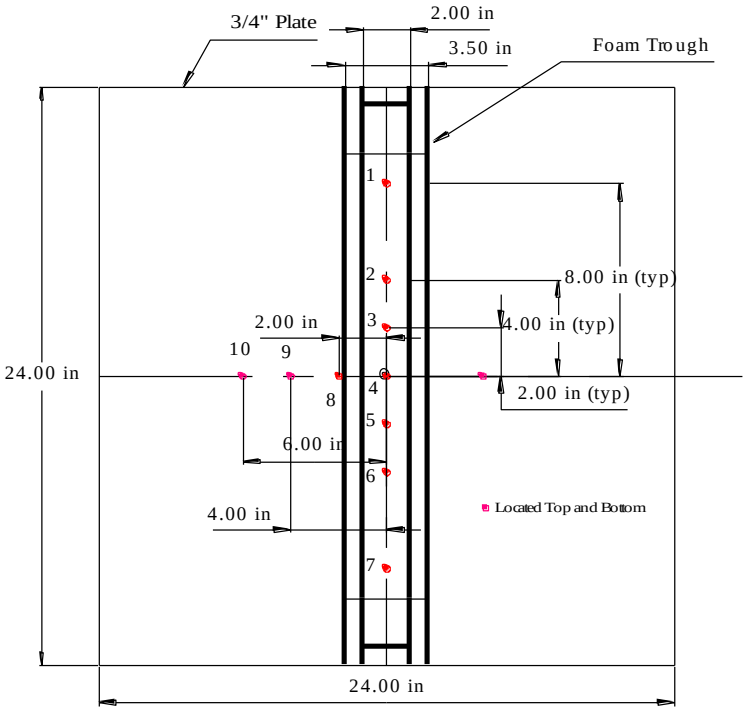

Figure 2. Thermocouple locations for Phase I test plates

The trough was filled with LN_2 using a low-pressure dewar and a ½ in. filler tube which was placed centered on top of the trough (above TC 4). The filler tube is shown in Figure 3. The temperature data was recording using a National Instrument SCXI-1000 Data Acquisition Unit (DAQ) and a TC-2095 Thermocouple Connector Module. Temperature data from the test is shown in Figure 4. The data shows a large spread in the temperature of the top thermocouples and slow cooling of the plate through the thickness.

Figure 3. Filler tube

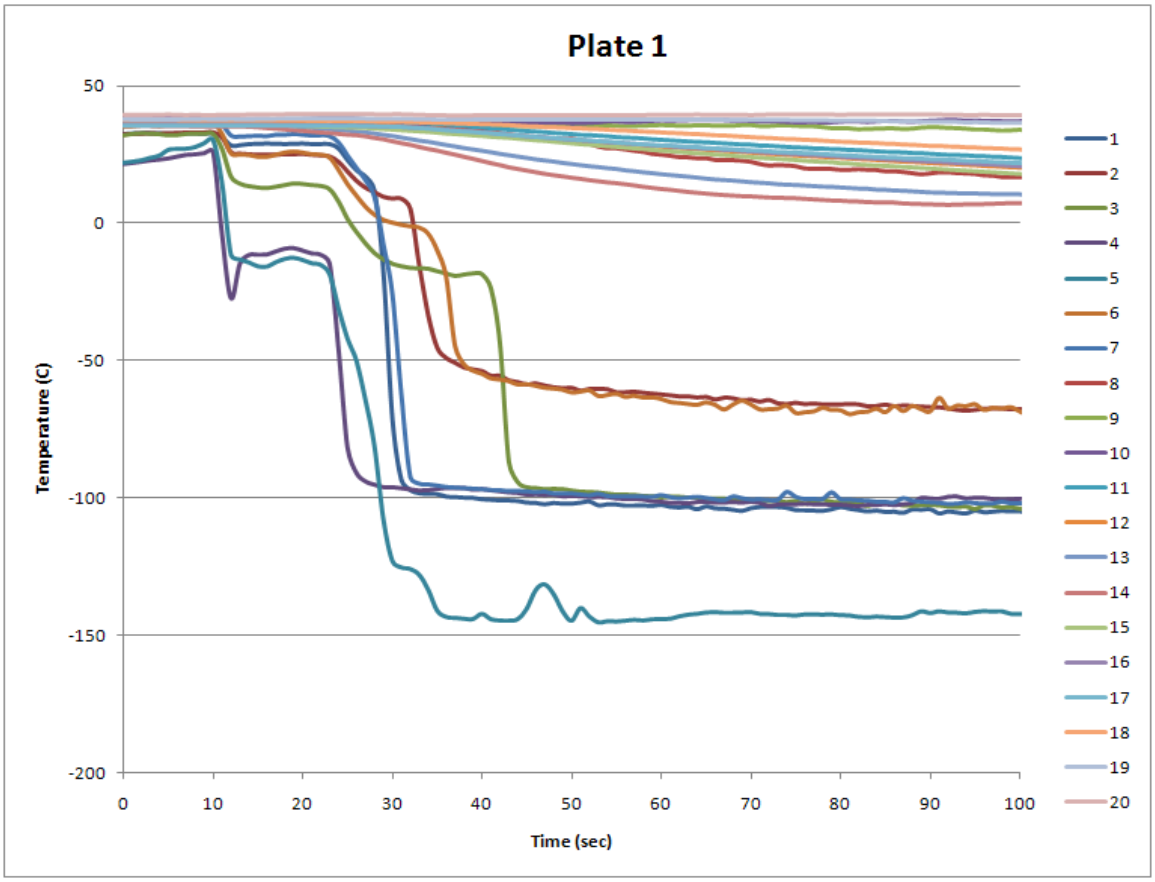

Figure 4. Thermocouple data from initial test

The differences observed in the temperatures along the top thermocouples led to an attempt to distribute the flow of the nitrogen along the length of the trough more evenly. The nozzle was modified as shown in Figure 5 to include a pipe ½ in. diameter pipe with 16 – 7/64 in. diameter holes. The nozzle had a minimal effect in normalizing the temperature distribution along the length of the trough and was not used in future tests.

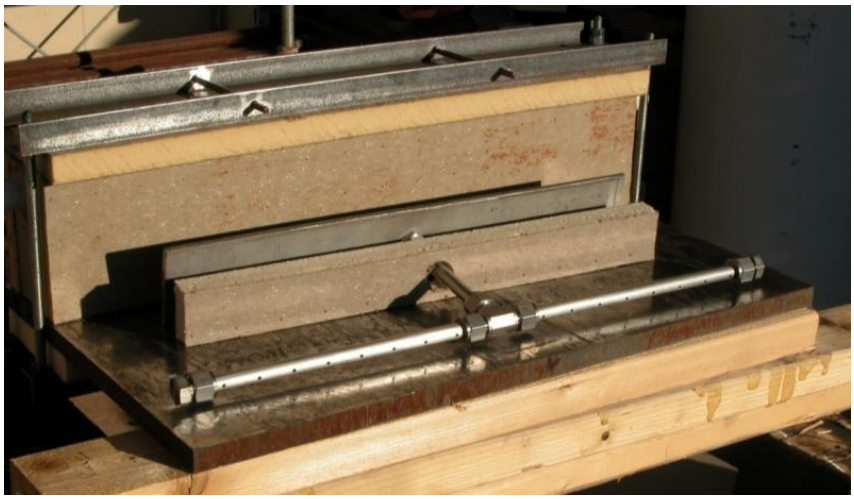

Figure 5. Spray manifold

The next exploratory test was conducted to determine whether the Type T Teflon thermocouples fastened with Kapton tape were the most appropriate thermocouples for determining the plate temperature. A test plate shown in Figure 6 was developed to examine alternate fastening methods along with type E thermocouples. Type E thermocouples leads are made of Nickle-Chromium and Copper-nickel. Type E is recommended for use at temperature above 40K. The Seebeck coefficient for Type E is greater than all other standard thermocouples, which along with its low thermal conductivity make it ideally suited for low temperature applications (ASTM, 1993). A complete list of the thermocouples tested is shown in Table 1. The location of the thermocouples is presented in Figure 7. The thermocouples were mounted 1 in. from the center of the plate in a radial pattern every 45° as shown in Figure 7. The test plate was a 12 in. x 12 in. x ¼ in. thick. A dam was made from a 12 in. x 12 in. x 2 in. thick Styrofoam board with a 4 in. diameter hole in the middle. The Styrofoam was attached to the plate with a bead of room temperature vulcanizing (RTV) sealant around the hole.

Figure 6. Thermocouple test after painting

Table 1. List of thermocouples and mounting methods

Type	Material Type	Mounting Technique
T	30 ga. Teflon Insulated	Kapton Tape
E	30 ga. Teflon Insulated	Kapton Tape
T	30 ga. Teflon Insulated	Epoxy embedded in 0.020 in. deep by .040 in. wide slot
T	0.020 in. Sheathed	Epoxy embedded in 0.020 in. deep by .040 in. wide slot
E	30 ga. Teflon Insulated	Epoxy embedded in 0.020 in. deep by .040 in. wide slot
E	0.020 in. Sheathed	Epoxy embedded in 0.020 in. deep by .040 in. wide slot
T	0.020 in. Sheathed	Capicity Discharge (CD)weld using 0.003 in x 0.250 in. NiCr Strap
E	0.020 in. Sheathed	Capacity Discharge (CD) weld using 0.003 in. x 0.250 in. NiCr Strap
T	30 ga. Teflon Insulated	Epoxy embedded in 0.040 in. hole hole From back side to within 0.020 in. of Surface
E	30 ga. Teflon Insulated	Epoxy embedded in 0.040 in. hole from back side to within 0.020 in. of surface
E	30 ga. Teflon Insulated	Intrinsic (CD welded) Front surface

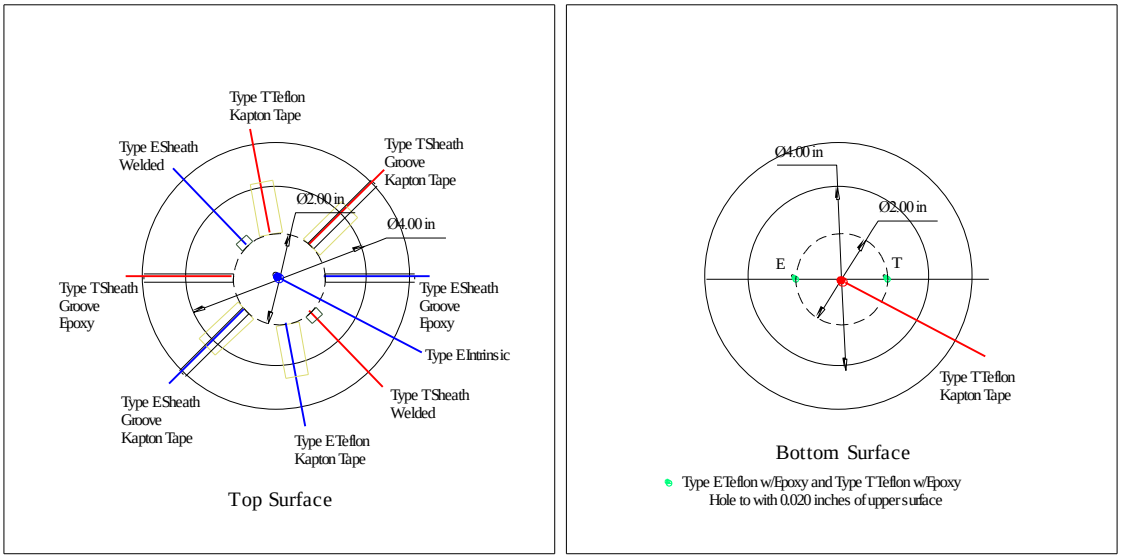

Figure 7. Layout of the thermocouples

Two tests were run, one with the plate as received (bare steel surface), and one with the exposed surface painted with a spray-on enamel paint (painted version shown in Figure 6). The intrinsic CD welded Type E thermocouple provided the best measurement of the plate temperature. A critical, though not unexpected, observation from these tests is apparent in temperature data presented in Figure 8. The graph shows the temperature of the intrinsic thermocouple on the top surface and the Kapton taped thermocouple on the back surface. The graph clearly shows that there is a higher cooling rate for the painted plate than for the bare plate. The paint layer acts as an insulation layer that affects the boiling behavior of the cryogenic liquid when in contact with the paint relative to bare steel. This change in behavior due to the paint enhances the contact between the surface and the liquid which results in an increased cooling of the steel plate. Therefore, all subsequent tests were conducted using a single flow nozzles, intrinsic Type E thermocouples with a National Instrument DAQ, and paint applied to the wetted plate surfaces. Since both the interior and exterior hull surfaces of LNG vessels are all painted with epoxy primer and/or polyurethane, painting the surfaces in this testing program is the most appropriate choice.

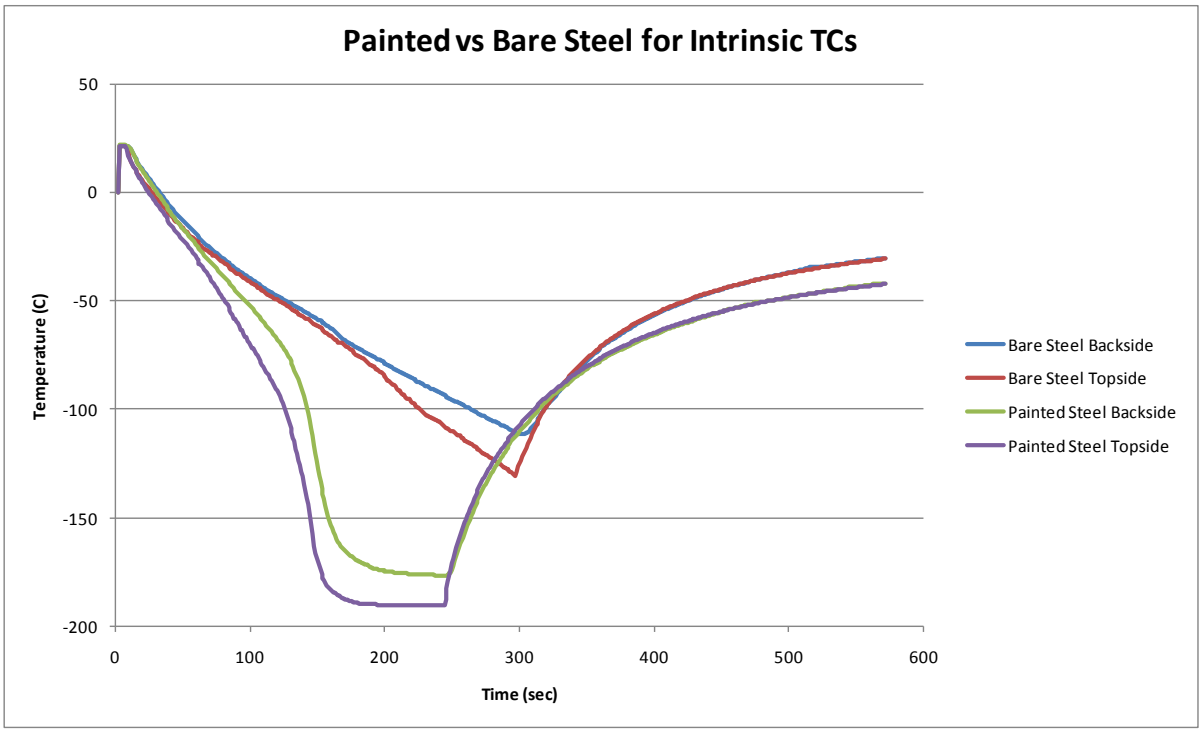

Figure 8. Temperature data from the thermocouple test plate

4.2 Phase II-A Moderate-Scale Fracture Testing – A36 Steel

The initial tests on the exploratory 24 in. x 24 in. x ¾ in. plates showed a very slow cooling rate through the thickness of the plate. In addition to the lack of paint in those tests, the slow cooling was believed to be due to the large mass of the plate and the relatively small size of the cooling trough. In order to more quickly cool the plate and to provide addition constraint to generate thermal stresses, the second phase of testing includes of a series of 48 in. x 48 in. x ¼ in. thick plates. These A36 carbon steel plates also had W8x40 I-beams welded around their circumference. The induction of thermal strain is caused by a region of material becoming cold while the surrounding material remains warm. The cold material tries to contract while the warm surrounding material holds the cold material from contracting freely. This constraint provided by the warm surrounding material causes the generation of a large amount of tension within the cold material. As the temperature drops, the tension increases in addition to the continued decrease in the fracture toughness of the steel. Once the stress increases sufficiently to cause a flaw in the steel microstructure to reach a critical stress level, a brittle crack initiates and propagates outward with a velocity near that of the speed of sound. The propagation is based on the structure geometry, the loading on the structure, the distribution of the cold region, and the material microstructure. Thus, the I-beams welded to the outer edges of the plate provide additional constraint to the structure helping to induce larger stresses in the cool regions.

A diagram of a 48 in. plate with the support welded I-beams and the trough location is show in Figure 9. A foam trough 12 in. wide by 42 in. long and 5 in. deep (inside dimensions) runs along the center of the plate. The trough was filled with LN_2 using a 160 liter low-pressure dewar with a single ½ in. fill pipe locate in the center of the top trough cover. The surface of the plate inside the trough was painted with Krylon spray enamel. As describes earlier, the paint increases the heat transfer between the nitrogen and the plate, resulting in more rapid cooling. The trough was fastened to the plate using silicone caulk and two 1 in. steel angles. The bottom surface of the plate beneath the trough was insulated with Styrofoam (14 in. x 48 in. x 3 in. thick) in order to enhance the heat transfer. The bottom surface foam was also held in place by the steel angles.

Two plate configurations were initially tested with 48 in. size plates. The first is just a plain ¼ in. thick plate welded to I-beams around the perimeter. The second plate consists of two half sections (24 in. x 48 in. x ¼ in.) welded to each other along the center. The weld runs through the centerline of the long trough dimension axis. Welding changes the local microstructure and thus the overall material's response to the stress loadings. The purpose of the weld is to provide a region of increased stress due to the residual stress in the weld and to provide flaws for possible crack ignition sites. The plates are also welded to I-beams around the perimeter. The welded test plate is shown in Figure 10.

In addition to the 48 in. plates with I-beams, one 72 in. x 72 in. plate was also tested as part of Phase II-A tests. The larger plate used the same size trough and therefore employs the extra surrounding warm plate material to provide the constraint in place of the I-beams.

For all tests in Phase II-A, eleven type E intrinsic thermocouples were attached to the top and bottom surface of the plate using a CD welder. The location of the thermocouples is shown in Figure 11. The same test configuration for all of the Phase II-A test is shown in Figure 12.

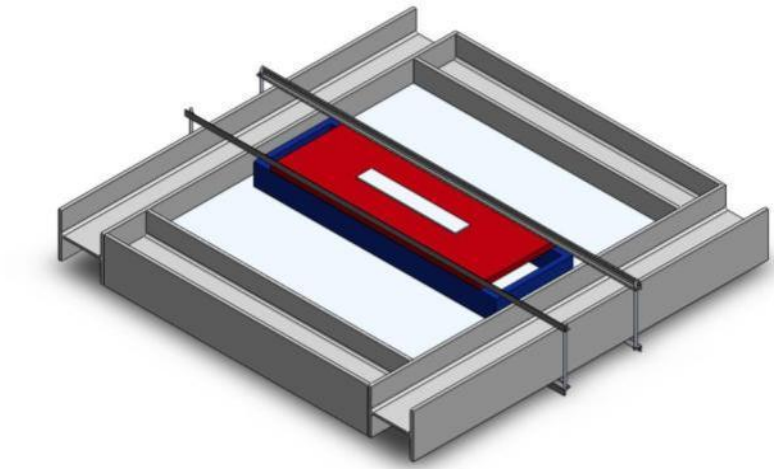

Figure 9. 48 in. x 48 in. x ¼ in. plate and beam test configuration

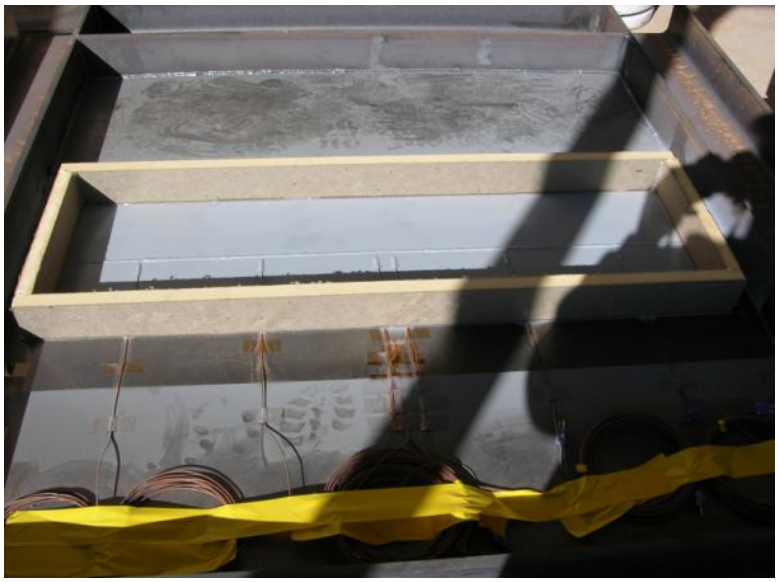

Figure 10. Welded 48 in. x 48 in. x ¼ in. Phase II test plate

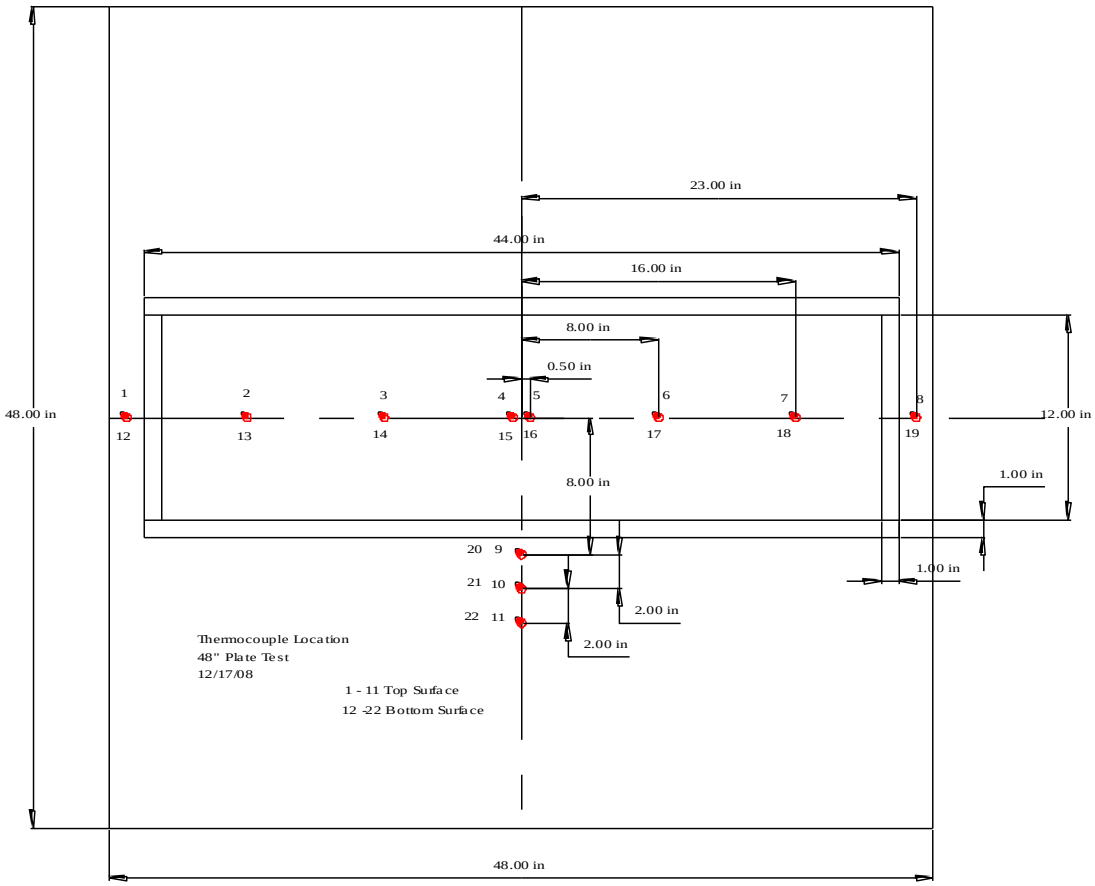

Figure 11. Location of the thermocouples for 48 in plates

Figure 12. Test configuration for the 48 in. x 48 in. Phase II plates

A list of all of the Phase II-A tests using the three test articles described above is summarized in Table 2. As described, each of the three test articles was tested multiple times. Each subsequent test included the addition or slight modification to a stress concentration. These stress concentration include changing the number of holes, the hole geometry, the shape of the holes, and the addition of notches and varying the notch geometry (shape and depth). These holes/notches were increased in severity from test to test until the hole/notch configuration was sufficient to initiate a brittle fracture. The test numbers in Table 2 represent the order in which the test were conducted. Tests 1, 3, and 5 used the 48 in. plain plate. Tests 2, 4, and 6 used the 48 in. welded plate. Finally, Tests 7 through 10 used the 72 in. plate.

Table 2 Phase II-A Testing

Test Number	Note	Material	Plate Size	Notch Type	Test Results
1		A36 Steel	48” x 48” x ¼” thick w/ I-beams	No notch	Did not crack
2		A36 Steel	48” x 48” x ¼” thick w/ I-beams	No notch, weld seam along center of plate	Did not crack
3	Same Plate tested in Test 1	A36 Steel	48” x 48” x ¼” thick w/ I-beams	Three 3/8” holes drilled along centerline	Did not crack
4	Same Plate tested in Test 2	A36 steel	48” x 48” x ¼” thick w/ I-beams	Three 3/8” holes drilled along centerline	Did not crack
5	Same Plate tested in Test 1 & 3	A36 Steel	48” x 48” x ¼” thick w/ I-beams	Three 3/8” holes drilled along centerline with notch	Cracked
6	Same Plate tested in Test 2 & 4	A36 Steel	48” x 48” x ¼” thick w/ I-beams	Three 3/8” holes drilled along centerline with notch	Cracked
7		A36 Steel	72”x 72” x ¾” thick	No notch	Did not crack
8	Same Plate tested in Test 7	A36 Steel	72”x 72” x ¾” thick	Small groove 2 1/8” x ¼” deep cut using circular saw	Did not crack
9	Same Plate tested in Test 7 & 8	A36 Steel	72”x 72” x ¾” thick	Small groove 2 7/8” x 5/8” deep x 5/16” wide cut using die grinder	Did not crack
10	Same Plate tested in Test 7, 8 & 9	A36 Steel	72”x 72” x ¾” thick	4.75” Groove in Test 9 notched with jig saw	Cracked

Each of the Phase II-A tests ran for approximately 10 minutes. The temperature profiles for the Test 1 upper and lower thermocouples are presented in Figure 13 and Figure 14, respectively. With the large trough and a thinner plate, the temperature on the upper and lower surface dropped quickly and in a similar manner. The temperature time histories for Test 2 were similar to Test 1. However, as reported in Table 2, the Test 1 and Test 2 plates did not crack.

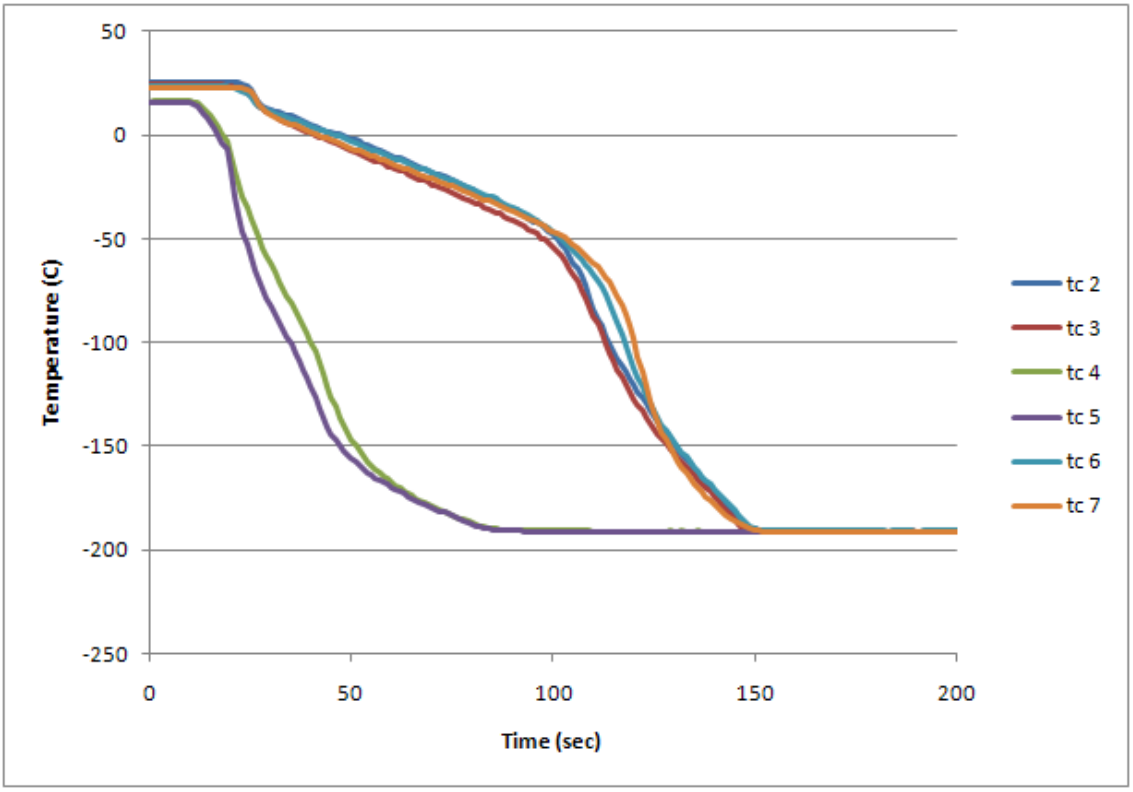

Figure 13. Phase II Test 1 upper surface temperature profile

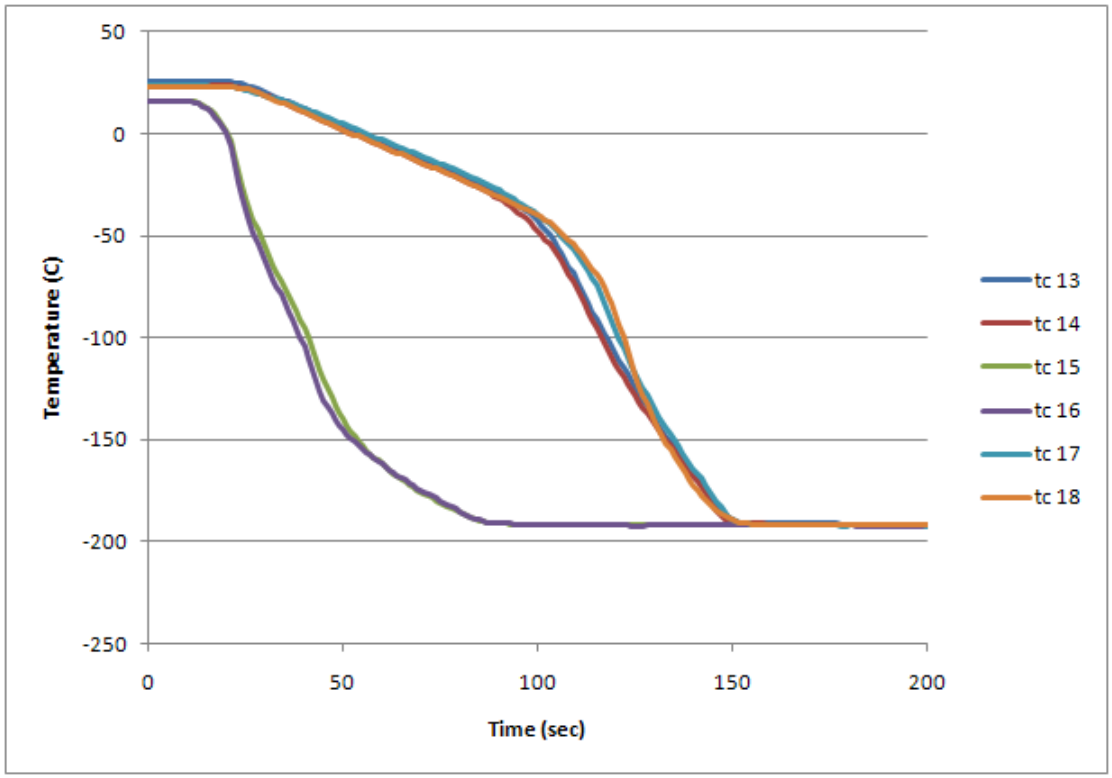

Figure 14. Phase II Test 1 lower surface temperature profile

Since the plane plate and welded plate did not contain a flaw large enough to initiate a brittle fracture given the stress state induced by the cooling applied, stress concentrations were introduced. This was accomplished by drilling three 3/8 in. diameter holes spaced along the long dimension of the trough. The locations of the holes are presented in Figure 15. The holes were sealed with cork material and silicone caulk in order to prevent LN_2 from leaking through the plates. This cork and silicone material adds relatively no strength back to the steel plate. The holes act as a stress concentration since the material directly adjacent to the holes will theoretically experience a stress three times that of the test without holes. If the material in the stress concentrated zone contains a microstructural flaw large enough, and the stress level is sufficiently high, and the material is in the brittle failure regime, brittle fracture will occur. The Appendix at the end of this report provides additional discussion on stress concentrations and fracture mechanics.

These re-tests (Test 3 and 4) were run for approximately 5 minutes, and again, the plates did not crack. The cooling rates for Tests 3 and 4 were similar to Tests 1 and 2. In order to further increase the stress, notches were introduced to the sides of the 3/8 in. holes using a jigsaw. The notches were between 3/4 in. and 7/8 in. long (total length from notch tip to notch tip). Each notch had a width of approximately 1/16 in. The introduction of the notches increased the stress significantly more than the three times achieved by the holes alone. The center holes for Test 5 and Test 6 are shown in Figure 16. These severe notches did lead to fractures initiating approximately 1.5 minutes in to the cooling of each plate. The temperature data from Test 5 is given in Figure 17. The cooling rates for Test 5 were very close to the previous tests (Tests 1 through 4). The cooling rates for Test 6 were also similar to that of Test 5 and the previous tests. The cracks run in Figure 18 and Figure 19 from the edge of the center hole (hole 2 in each plate, and the location of maximum stress) perpendicular to the long dimension of the trough (this happens to also be perpendicular to the direction of maximum stress). The crack was arrested by the material just under the foam trough where the plate temperature increased sharply since it was not cooled directly during the test. As shown in Figure 19, there was a bifurcation of the crack in the plate with the center weld. This type of bifurcation is typical in brittle fracturing of steel plates.

As explained earlier, the goal of this testing program is to explore the propagation of brittle cracks in steel plate structures, and not to determine the exact conditions required for crack initiation. LNG vessels are large complex structures that have sufficient stress concentration to initiate a brittle cracking when subjected to thermal stresses due to contact with LNG. These tests are being used to provide example fractured structures to calibrate/validate a computation failure model as discussed in Section 2.

The tests performed on the two 48 in. plates do not appear to differ significantly. The introduction of the weld does not appear to have affected the test outcome. However, this does not in any way demonstrate that welds on LNG vessels will not contain likely sites for flaws and stress concentrations. The welded plate test was one single test on a simple, non-fatigued, geometry. As later tests in this report will demonstrate, combining welds with more complex geometries increases the likelihood of inherent flaws falling within any spill region.

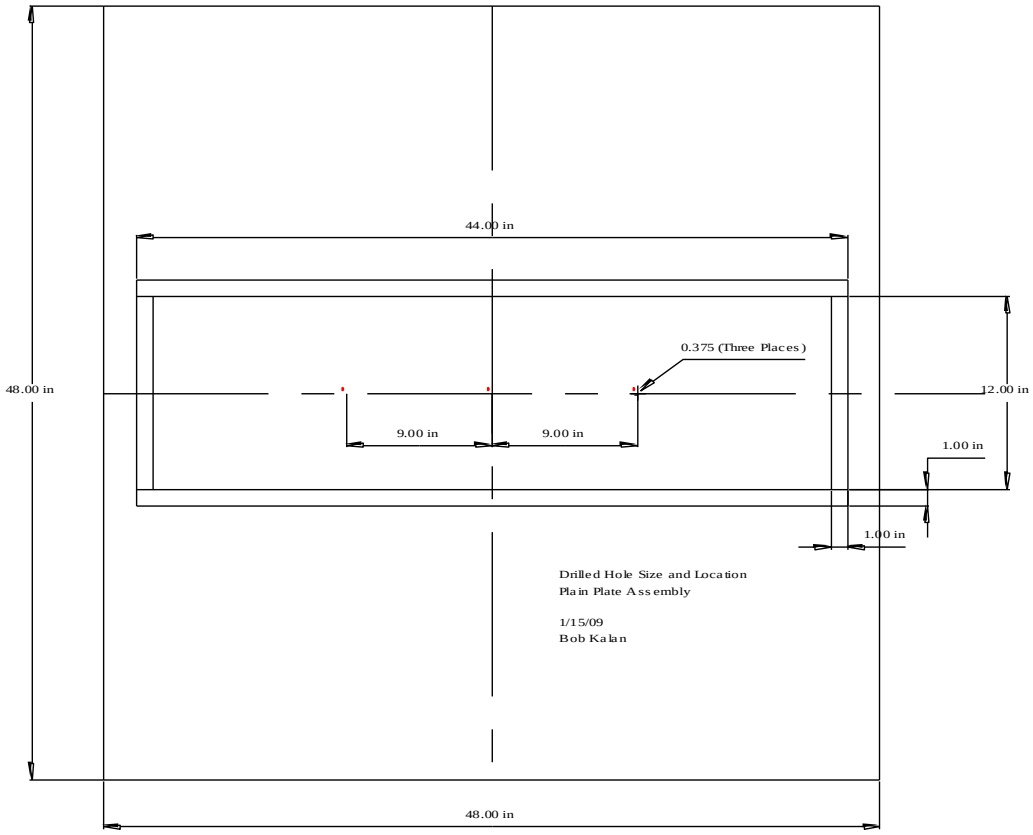

Figure 15. Drilled hole locations Tests 3 and 4

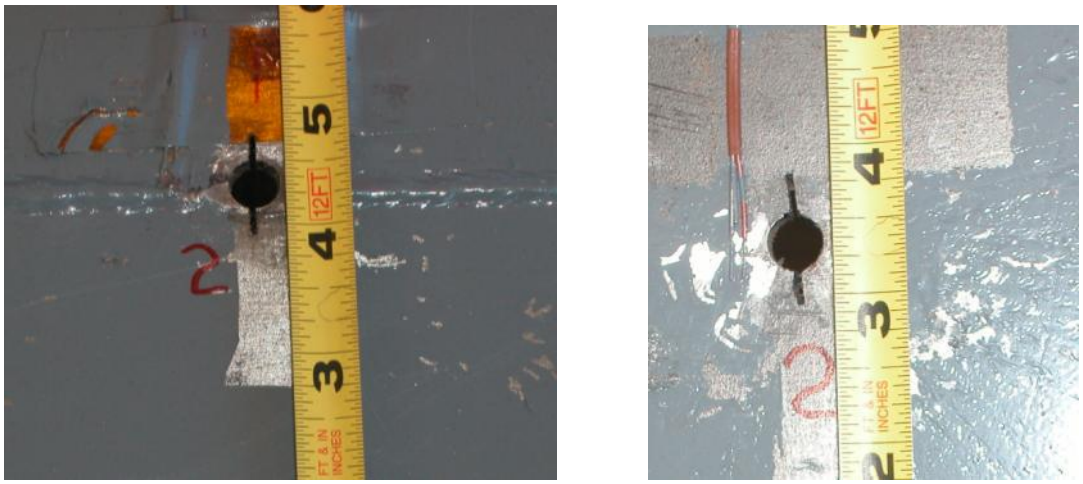

Figure 16. Notched holes for Tests 5 and 6, center hole (hole 2) shown.

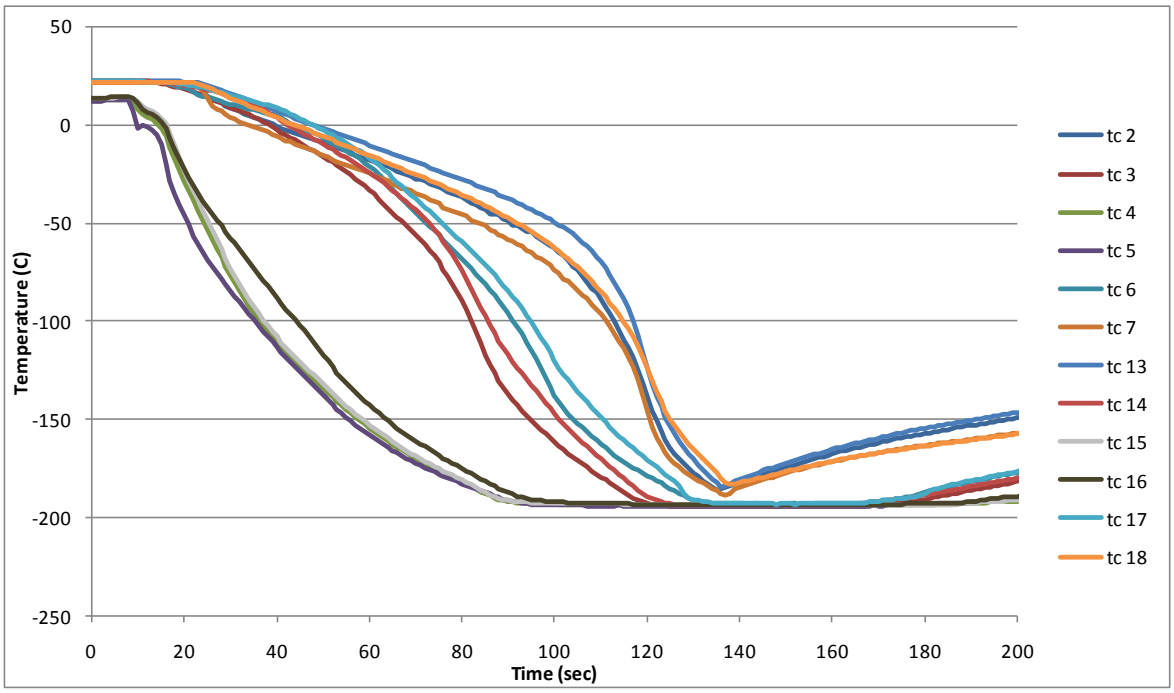

Figure 17. Thermocouple data for Test 5

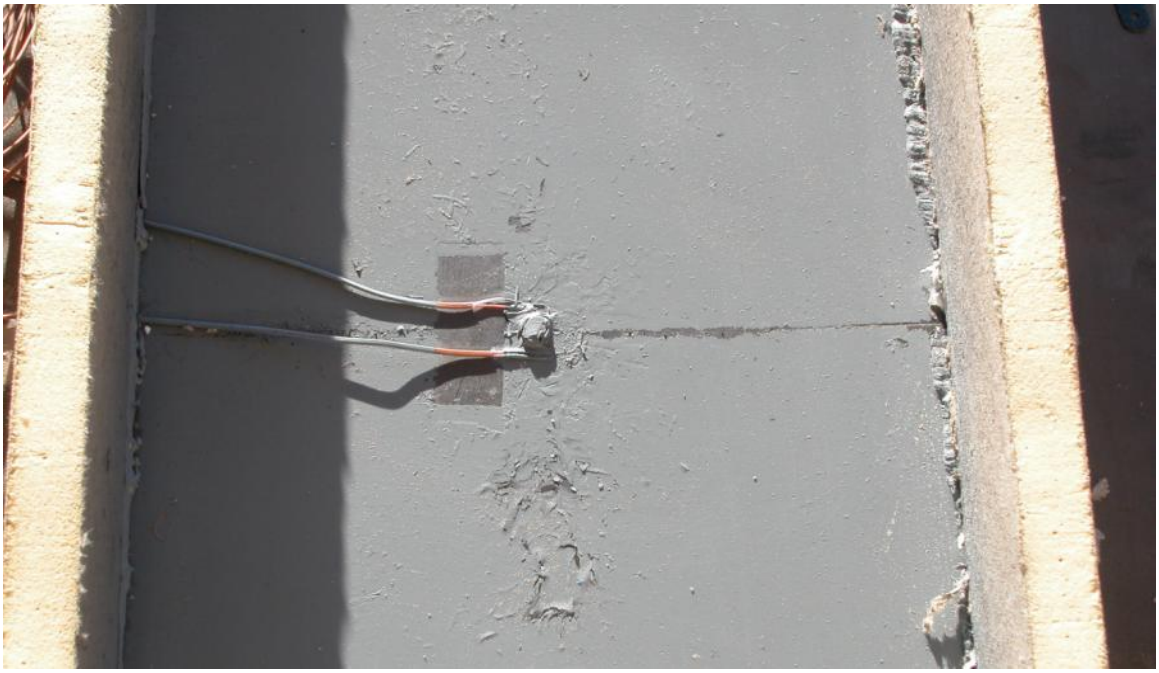

Figure 18. Crack generated in Test 5, 48 in. x 48 in. x ¼ in. plate with notched holes

Figure 19. Crack generated in Test 6, 48 in. x 48in. x ¼ in. welded plate with notched holes

After testing the 48 in. plates, the A36 carbon steel plate with slightly different dimensions, 72 in. x 72 in. x ¾ in. thick, was tested. The thickness of ¾ in. is much closer to the average hull thickness used in most LNG vessels. The plate and trough are shown in Figure 20. The trough dimensions are the same as those used on the 48 in. x 48 in. plates. In place of the steel beams welded around the perimeter of the plate, the extra material and thickness of the plate provided the warm constraining material.

As noted in Table 2, four successive tests were conducted on this plate in order to generate a crack. The plate was first tested with no machining to the plate. Part of this experiment was to investigate the cooling of a thick (¾ in.) plate compared to the 48 in. x 48 in. plates which were only ¼ in. thick. The thermocouple locations for these tests are the same as those for the 48 in. x 48 in. plates. The temperature distribution for the plate (Test 7) is shown in Figure 21. The ¾ in. thick plate used for Test 7 cooled significantly slower than the ¼ in. thick plates in Tests 1 through 6. In addition, the lack of I-beams welded around the perimeter did not prevent the out-of-plane buckling deformation of the plate. The 72 in. plate deformed in a warping, or saddle shape. There was approximately a 1 1/8 in. warping of the plate along the long dimension axis of the trough and approximate 7/8 in. along the short dimension axis of the trough.

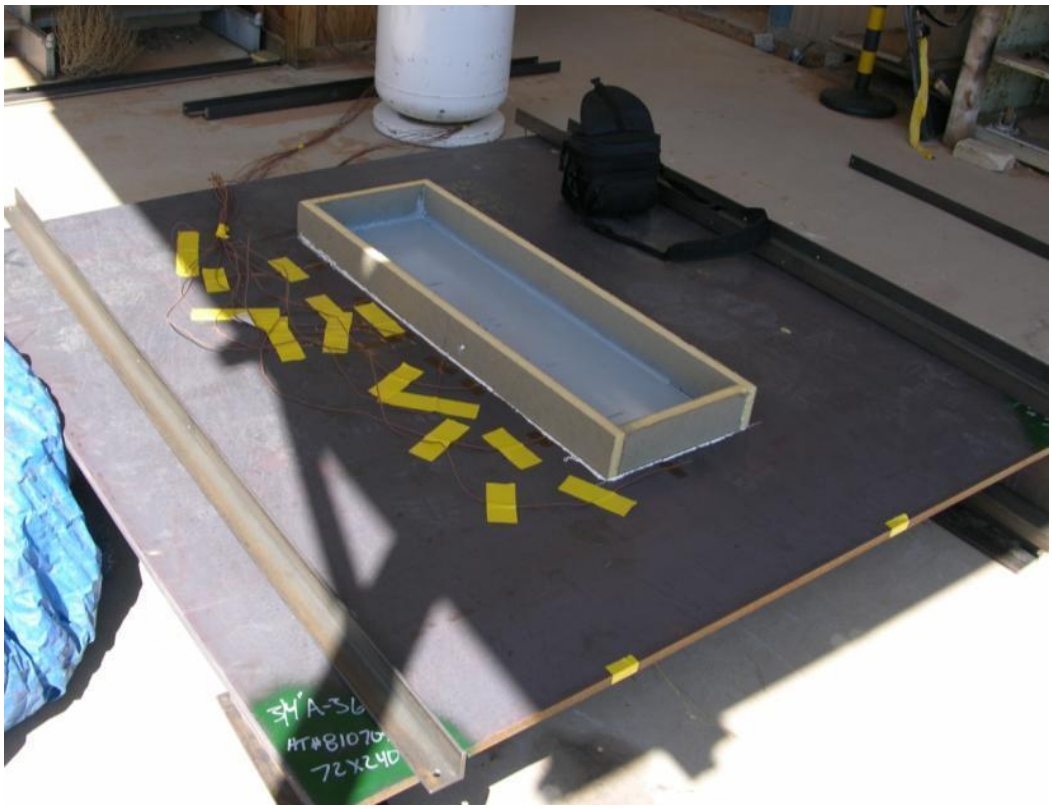

Figure 20. Phase II test plate 72 in. x 72 in. x ¾ in.

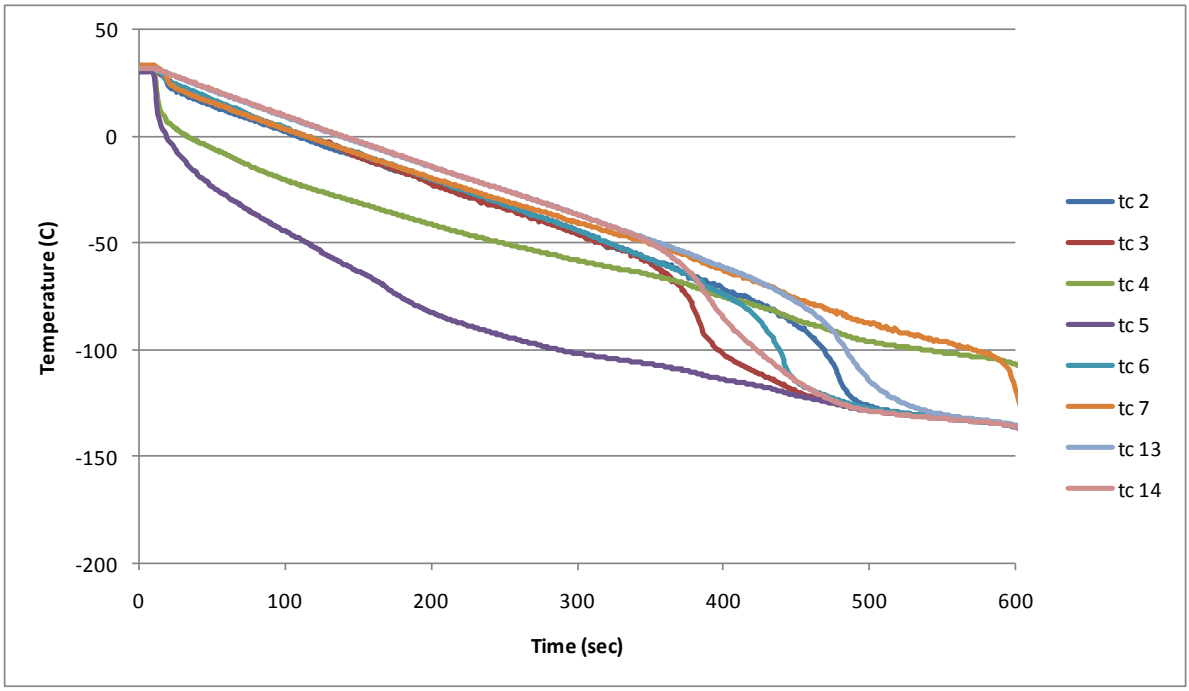

Figure 21. Thermocouple data for Test 7

After the initial test (Test 7) with the 72 in. plate, several additional tests were conducted to study different field techniques for introducing stress concentrations for future tests. All stress concentrations were centered in the trough area with orientations parallel to the short trough dimension. The first attempt introduced a notch cut into the plate using a die grinder. The notch for Test 8 was approximately 2 1/8 in. long by ¼ in. deep at the center as shown in Figure 22(a). This configuration was tested with no crack initiation. Using the die grinder, the notch size was increased to 2 7/8 in. long by 5/8 in. deep by 5/16 in. wide for Test 9 as shown in Figure 22(b). However, the slightly longer and deeper surface notch did not lead to crack initiation for Test 9. From Tests 8 and 9, it was concluded that use of the die grinder to introduce shallow surface notches did not produce sharp enough regions to produce the stress required for fracture. For Test 10, the notch length was increased to 4 inches using the die grinder in addition to cutting completely through the thickness of the plate. In addition, two ¼ in. long thin notches were cut into the ends of the larger die ground notch using a jigsaw. The resulting notch is shown in Figure 22(c). The cooling rates for Test 10 are illustrated in Figure 23. This test resulted in a crack initiated and propagating perpendicular to the long trough dimension as shown in Figure 24. The fracture occurred approximately 4.5 minutes into the test. The crack extended approximately 1.5 inches beyond the outside surface of the trough. This is illustrated in Figure 25. As with Tests 5 and 6, the crack arrested when entering the steep thermal gradient that transitions into warm material. Due to the longer cooling time to fracture, the cooling, and therefore the crack, extended slightly beyond the trough.

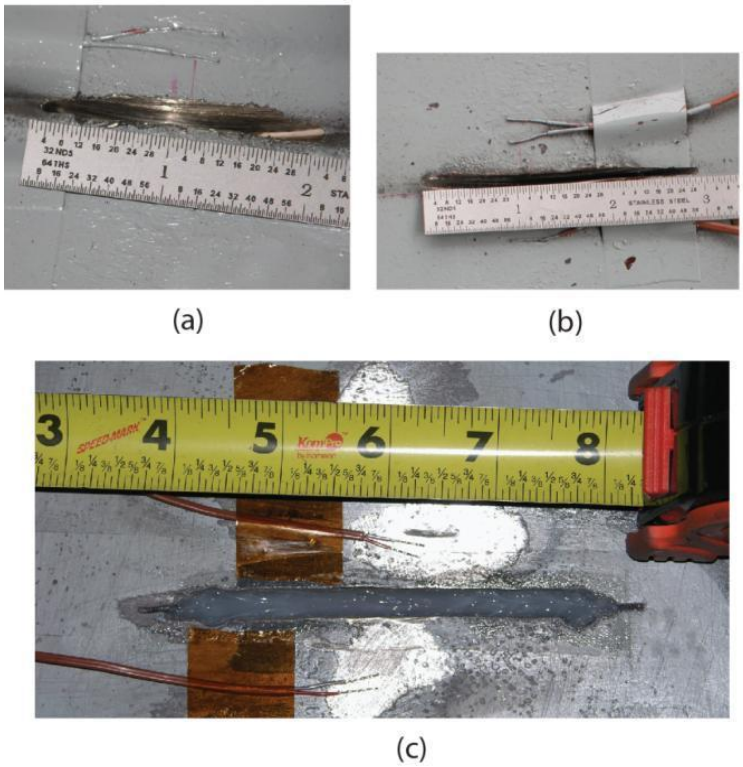

Figure 22. Surface notches cut into 72 in x 72 in plate for (a) Tests 8, (b) Test 9 and (c) Test 10

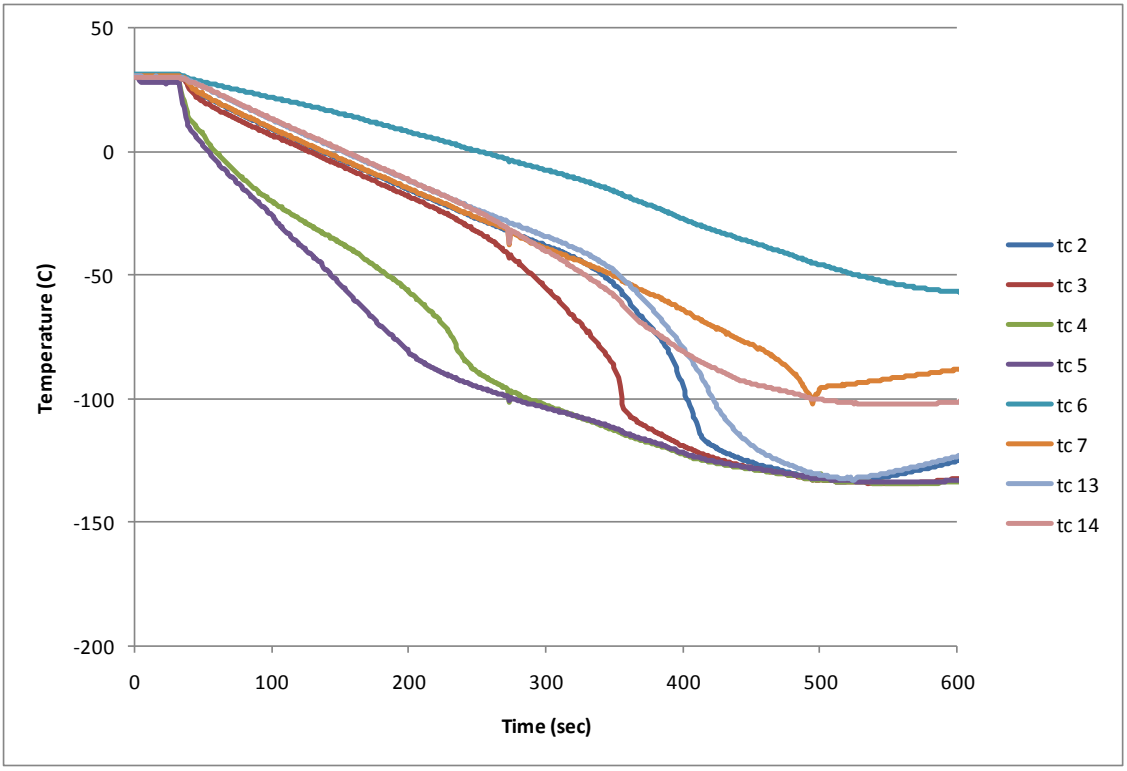

Figure 23. Thermocouple data for Test 10

Figure 24. Cracked formed in 72 in. x 72 in. plate during Test 10

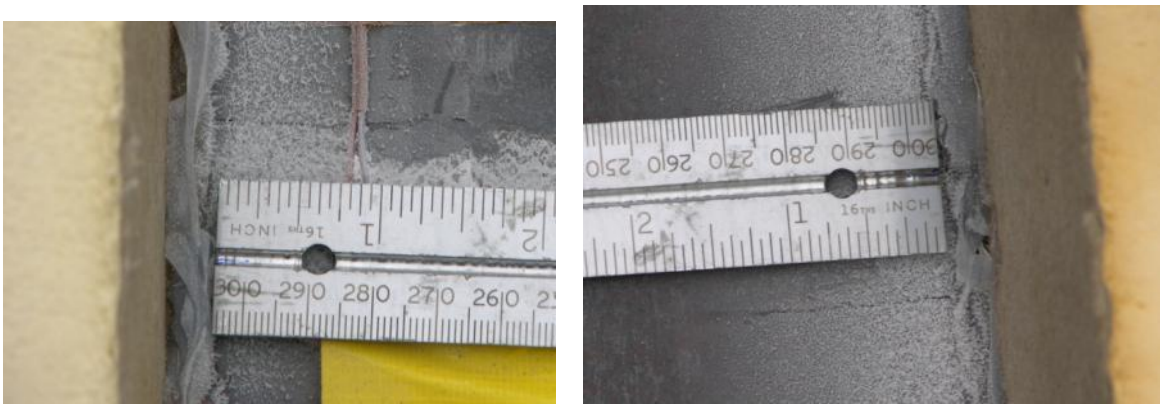

Figure 25. The extension of the crack formed in Test 10 beyond the outside of the cooling trough

4.3 Phase II-B Moderate-Scale Fracture Testing – Marine Grade Steels

Following the initial Phase II-A tests, the Phase II-B series of seven tests were conducted on 4 different test articles using same dimensions and I-beam general configuration as employed in Tests 1 through 6 (48 in. x 48 in.). However, the plate thickness was increased to ¾ in. in addition to the use of marine grade steels. ABS Grade A and ABS Grade EH steels were the two steels chosen for the Phase II-B testing. The ABS Gr. A steel has the lowest stress-strain curve and lowest fracture toughness of the marine grades, while ABS Gr. EH has the highest stress-strain curve and the highest fracture toughness. Therefore, testing of these two materials bounds the different marine grade steels. As with Tests 1 through 6, the test plates were constructed with the W8x40 steel I-beams welded around the perimeter. One test used a 40 in. x 12 in. trough, ABS Gr. A steel, and the same thermal couple layout as in previous tests and shown in Figure 11. The remaining three test articles (one Gr. A and two Gr. EH) employed more significantly modified trough dimensions (24 in. wide by 30 in. long) and a new thermocouple layout. These new trough dimensions cause a significant change to the stress field generated during cooling. The trough dimensions and thermocouple layout are shown in Figure 26 and Figure 27. The wetted area of the trough for this test series was painted using Blue Water Marine AC 70 primer and Marine Urethane.

The Phase II-B tests are listed in Table 3. The initial two tests (Test 11 and 12) were conducted using the same Gr. A test plate with a 40 in. x 12 in. trough. A second Gr. A plate with the 30 in. x 24 in. trough was used in Tests 18 and 19. Finally, two identical Gr EH test plates (both with 30 in. x 24 in. troughs) were constructed for Tests 17 and 20 and Test 21. Tests 13 through 16 identify tests in Phase III and Phase IV conducted in parallel with Phase II-B.

Figure 26. Test layout for the Phase II ABS steel plate tests

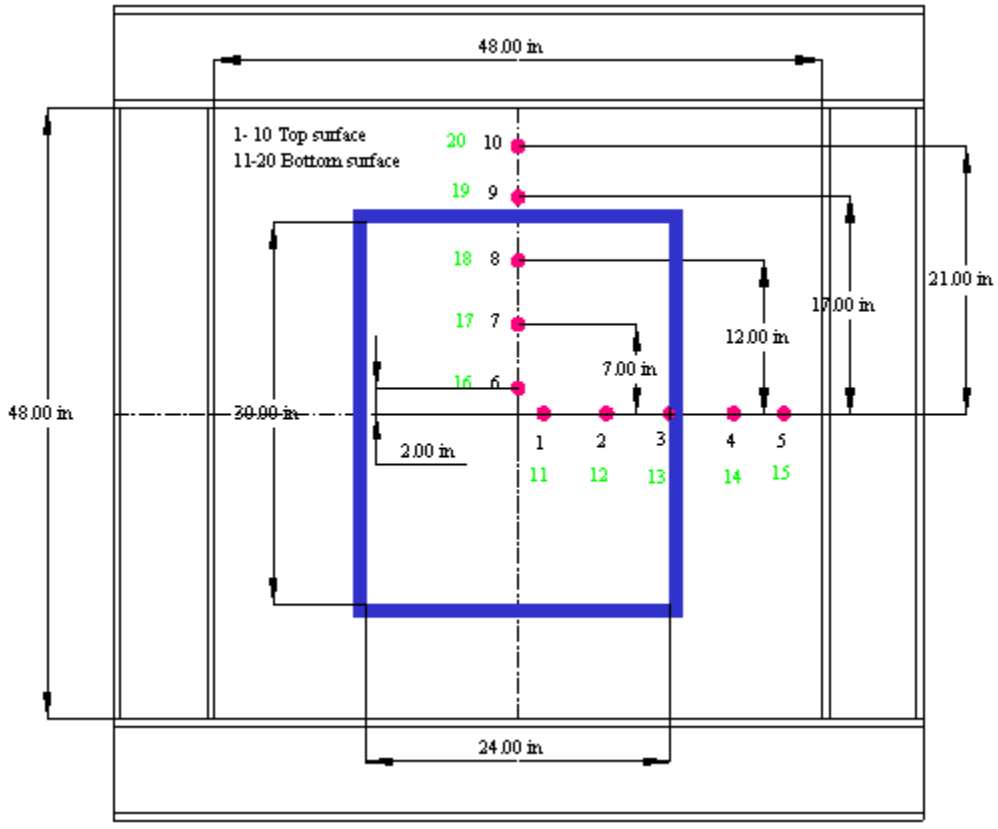

Figure 27. Trough dimensions and thermocouple layout for Phase II ABS steel plate tests

Table 3. Phase II-B Tests with ABS Grade Steel, all with I-Beams

Test Number	**Note**	**Material**	**Plate Size**	**Notch Type**	**Test Results**
11		Grade A	48” x 48”x ¾” 40” x 12” trough	3/8” hole with 1” star slot	Did not crack
12	Same Plate as 11	Grade A	48” x 48”x ¾” 40”x 12” trough	3/8” hole with 2¾” star slot	Plate cracked
17		Grade EH	48” x 48”x ¾” 30” x 24” trough	3/8” hole with 2 ½” slot	Did not crack
18		Grade A	48” x 48”x ¾” 30” x 24” trough	3/8” hole with 2 ½” slot	Did not crack
19	Same Plate as 18	Grade A	48” x 48” x ¾” 30” x 24” trough	3/8” hole with 3 7/8” slot	Plate cracked
20	Same Plate as 17	Grade EH	48” x 48”x ¾” 30” x 24” trough	3/8” hole with 3 7/8” slot	Did not crack
21	Second EH plate	Grade EH	48” x 48”x ¾” 30” x 24” trough	3/8” hole with 3 7/8” slot	Plate cracked

The plate used in Test 11 was tested using Gr. A steel and a stress concentration machined into the center of the trough. The stress concentration was started with a 3/8 in. diameter hole and then extended with 8 notches cut in a 1 in. diameter "star" pattern as shown in Figure 28(a). The 40 in. x 12 in. trough dimensions used for Test 11 is very similar to the dimensions used in the Phase II-A tests. This long but narrow trough severely biases the tensile stress fields within the cooled region of the plate. The stress generated in the direction of the long trough dimension is approximated twice the stress generated in the short dimension of the trough. This would theoretically lead to initiations and crack propagation in direction of the short trough dimension. The star pattern was introduced to determine whether or not a crack would initiate in the direction of the long dimension of the trough in addition to the short dimension, or potentially along the diagonal. The first test (Test 11) on this plate did not generate any cracking. Therefore, the notch length was extended to 2 ¾" in only two directions forming a "cross" shape as shown in Figure 28(b). The test with this configuration resulted in a crack (Test 12) across the trough short dimension as shown in Figure 29 approximately 4 minutes and 45 seconds into the test, but no cracking was generated in the long dimension of the trough. The temperature time histories for Test 12 are illustrated in Figure 30.

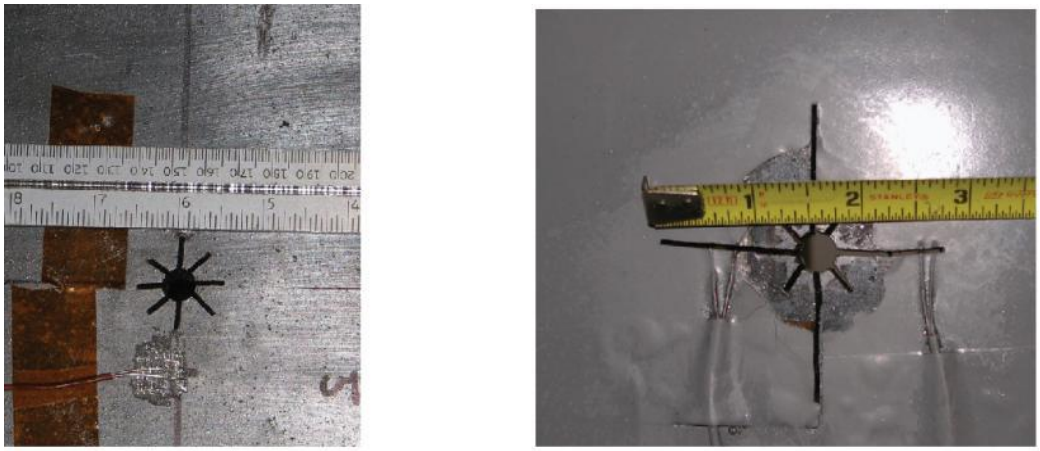

(a) (b)

Figure 28. Notches used in Tests 11 and 12

Figure 29. Crack generated in Test 12

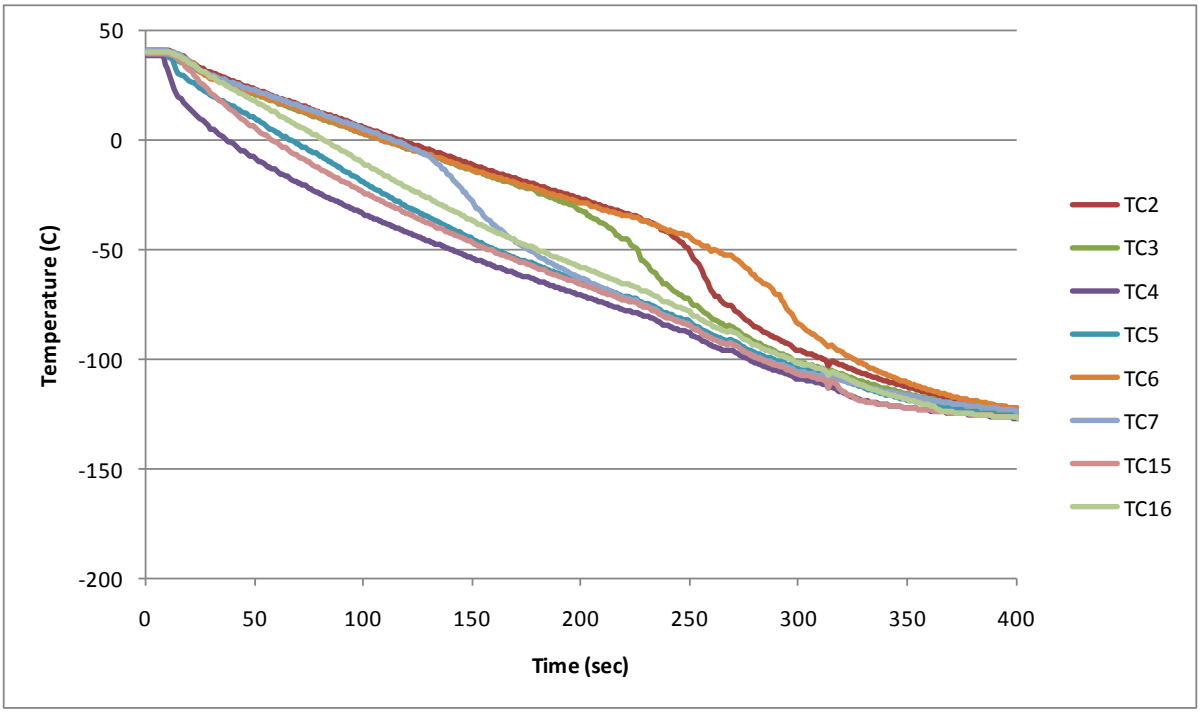

Figure 30. Thermocouple data for Test 12

Tests 17 through 21 were conducted using three tests articles, one Gr. A plate and two Gr. EH plates. Each was tested with a 30 in. x 24 in. trough. Initially, Tests 17 and 18 used 2 ½ in. long notches parallel to the short tough dimension with Gr. EH and Gr. A plates, respectively. Neither of the plates fractured. The notch lengths were increased to 3 7/8 in. as shown in Figure 31. In addition, a second Gr. EH plate was added with the same notch length and is labeled Gr. EH 2 in Figure 31. The Gr. A plate cracked (Test 19) approximately 8 minutes into the test with the resulting crack shown in Figure 32. Note that there were two cracks generated immediately from the one side of the notch. The use of the 30 in. x 24 in. trough dimensions reduces the level of domination of the maximum stress field and enables a higher likelihood of diagonal crack propagation as seen here. The thermocouple data from Test 19 is illustrated in Figure 33. The Gr. EH plate used in Test 17 was retested for Test 20 using the longer notch but no fracture initiated. The thermocouple data for Test 20 is illustrated in Figure 34. A nearly identical Gr. EH plate was tested (Test 21) with a crack initiating approximately 8 minutes into the test and is shown in Figure 35. A second crack propagation was observed in Test 21 approximately 1 minute after the initial cracking due to a slight extension of the first cracks as the cooling in the plate extended outward. The thermocouple data from Test 21 is illustrated in Figure 36. The Gr. EH plate used in Test 20 was not tested again. Since the two Gr. EH test articles were nearly identical, the conclusion was reached that the EH plate that did not fail was extremely close to failing. Slight differences in the material, the construction, and the notch shape could all have contributed to one failing and the other not failing. This very close threshold of failure was taken into account in the computational strain/temperature failure locus calibration process and is described in the computational analysis report in more detail.

Figure 31. Notch geometry used for ABS Grade steel Phase II tests

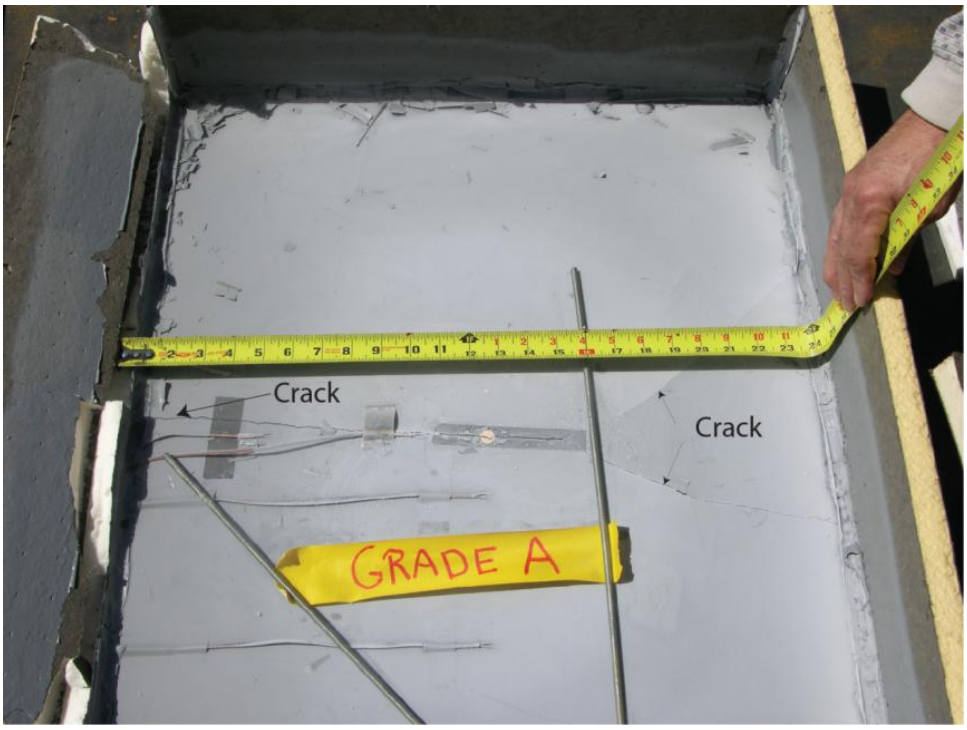

Figure 32. Cracking pattern for Test 19

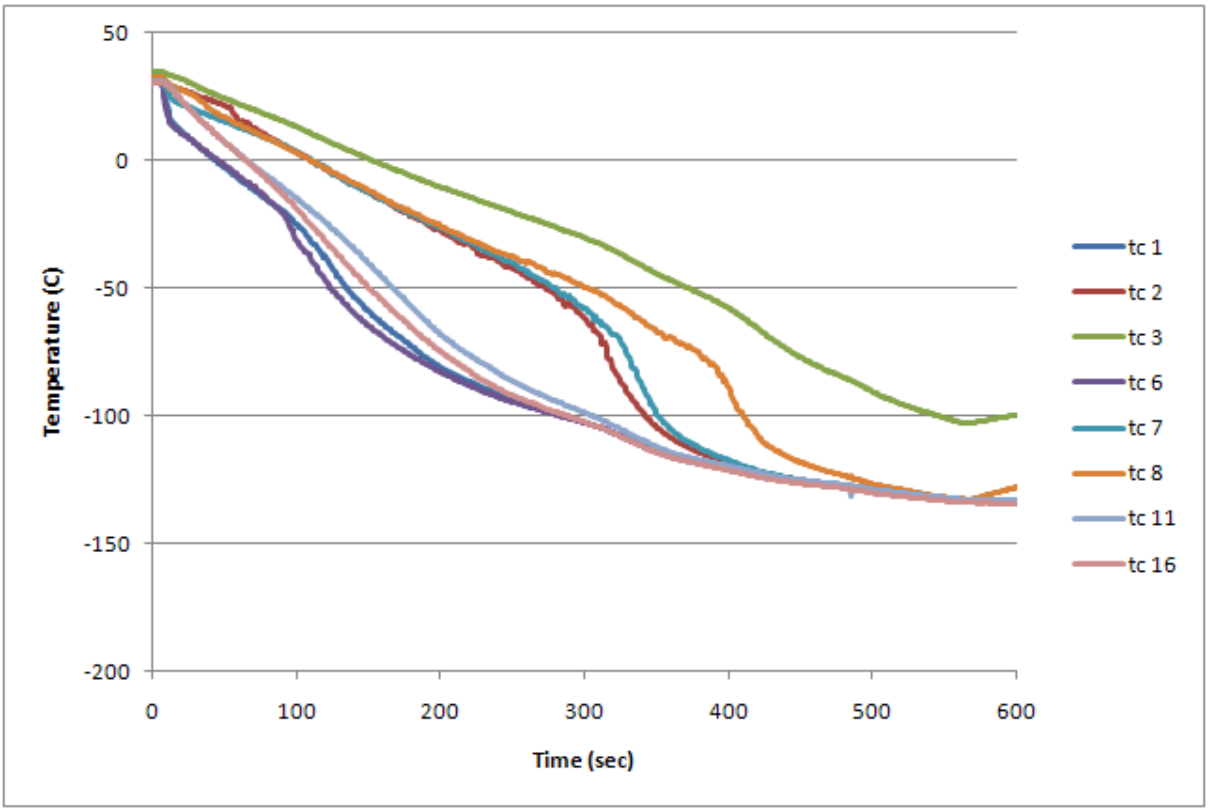

Figure 33. Thermocouple data for Test 19

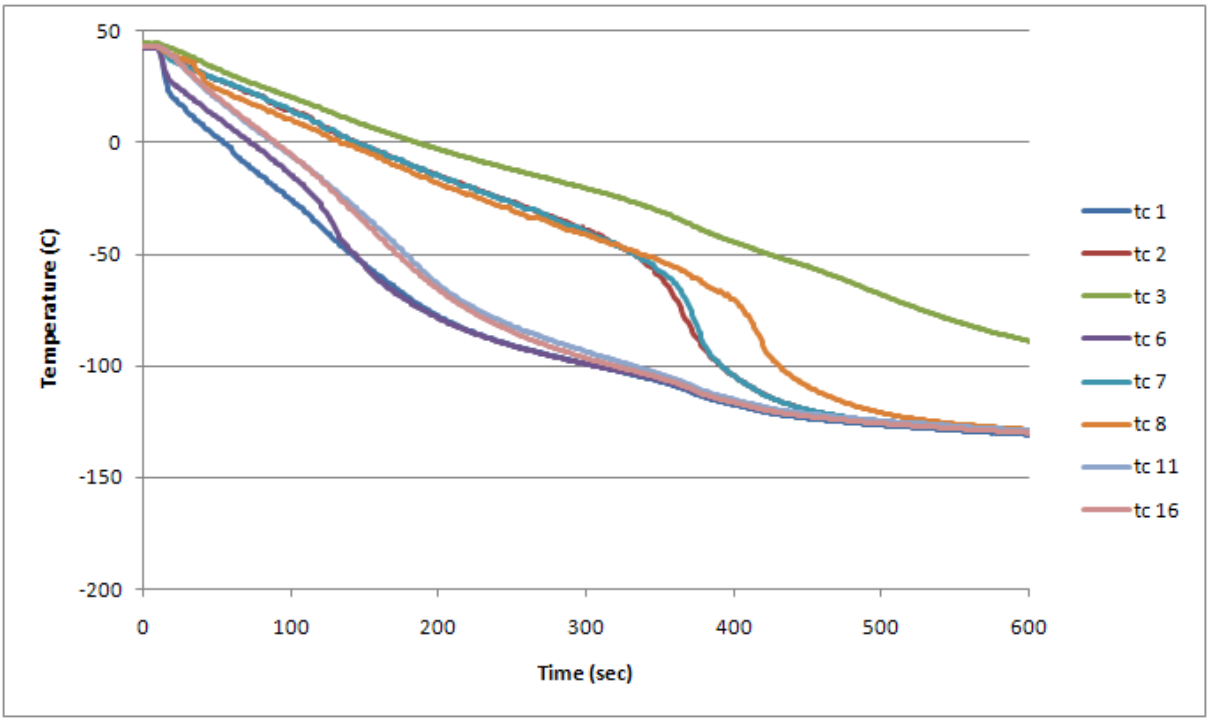

Figure 34. Thermocouple data for Test 20

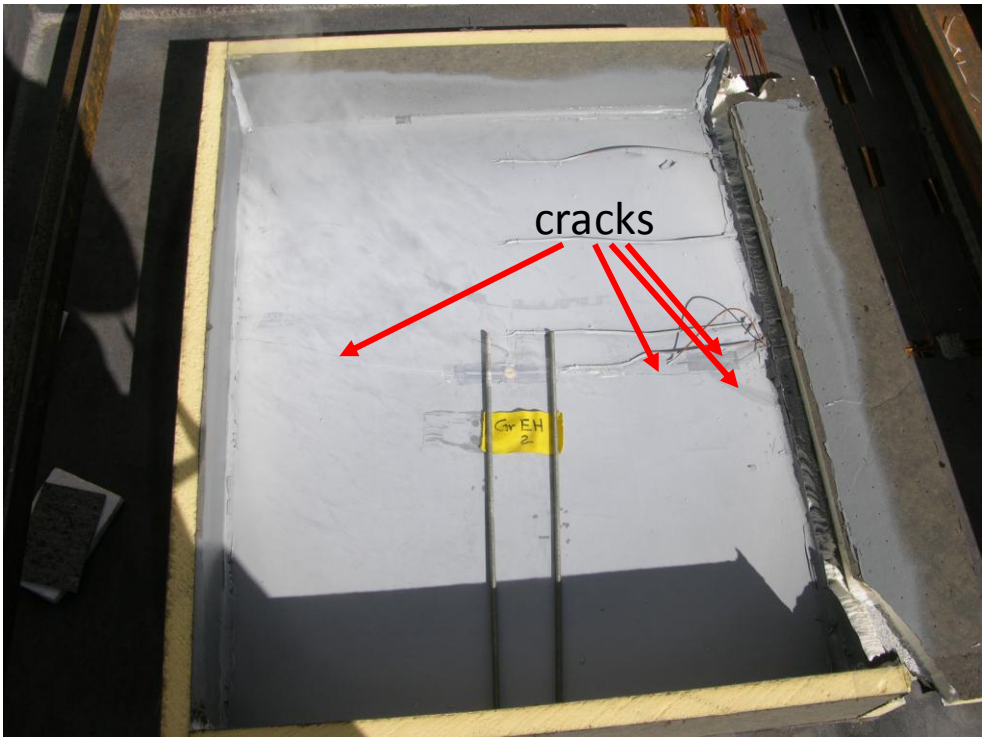

Figure 35. Cracking pattern for Test 21

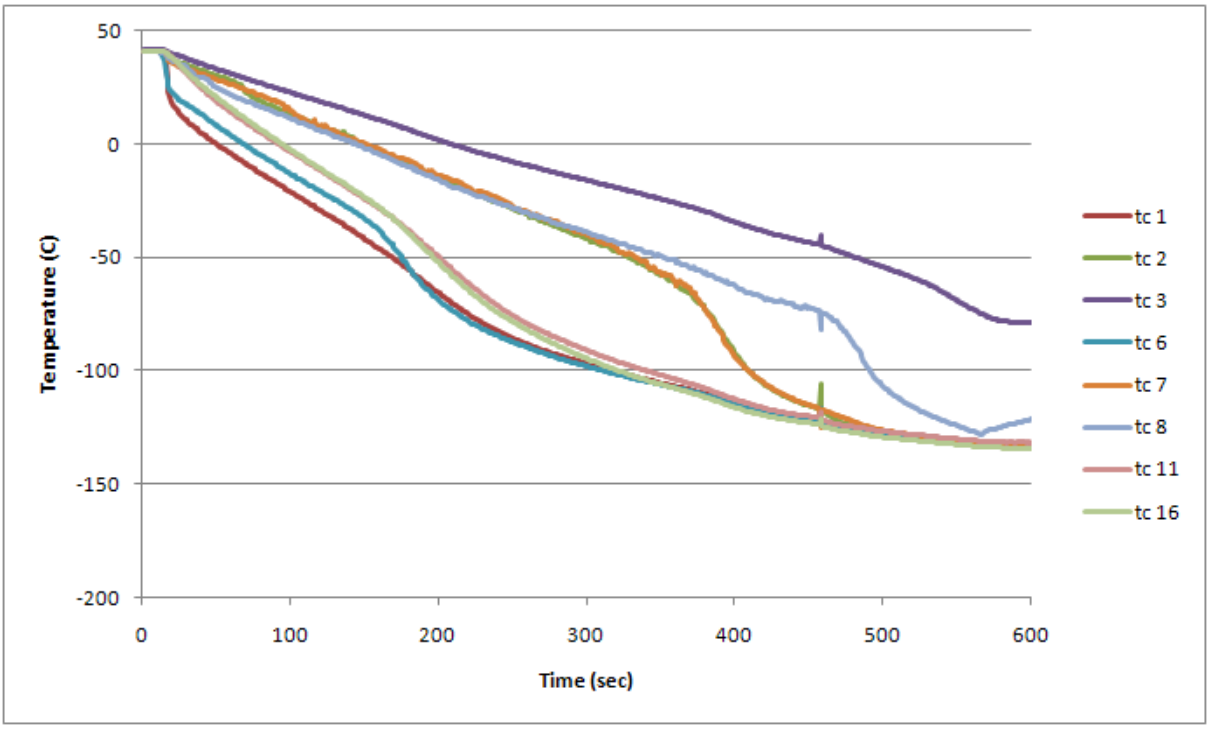

Figure 36. Thermocouple data for Test 21

4.4 Phase III Large-Scale Fracture Testing

In parallel with the construction of the Phase II-B test articles, the Phase III test structures were also assembled. For Phase III of the LNG fracture testing, a larger structure was designed as shown in Figure 37. The structure consists of a combination of ABS Gr. A and EH steel plates. The structure was designed with some of the general features found within a LNG vessel (e.g., intersecting plates, welds, stiffening ribs, etc). The Phase III test structure was not designed as scaled versions of a section of any existing LNG vessel, but rather to study the behavior and general features found in LNG vessels (e.g., intersecting plates, welds, stiffening elements, etc). Referring to Figure 37, the lower plate (blue) is ¾ in. ABS Gr A steel. The vertical walls are ½ in. ABS Gr. EH steel and extend three feet from the surface of the ¾ in. thick Gr. A plate. Three ¼ in. thick by 4 in. high ABS Gr. A stiffening ribs are placed at 2 ft spacings. The ribs were welded perpendicular to the ¾ in. thick Gr. A base plate. Finally, structural W8X40 I-beams were welded to the edges of the plate to add additional constraint. Structural W8X40 I-beams were added (welded) to the bottom of the structure to act as supports. These supports also allowed access to the back surface of the lower plate for attaching thermocouples and insulation material. Three of these large structures were constructed for Phase III testing. A list of the five Phase III tests using those three large test articles is given in Table 4. The first two test structures (Tests 13 and 14 and Test 16) were cooled using multiple dewars of LN_2. This was necessary due to the increased size of the structures and the surface area being cooled. The third large structure (Tests 22

and 23) was identical to the first two, but the test was conducted with water in contact with some of the steel structure. This test was of interest due to the scenarios in actual LNG vessels were a portion of the steel hull may have LNG on one side and have water on the adjacent side. The presence of the water may affect the cooling of the steel plates. The details of all three tests are provided below. Note that Tests 17 through 21 were part of Phase II-B. In addition, Test 15 was part of Phase IV.

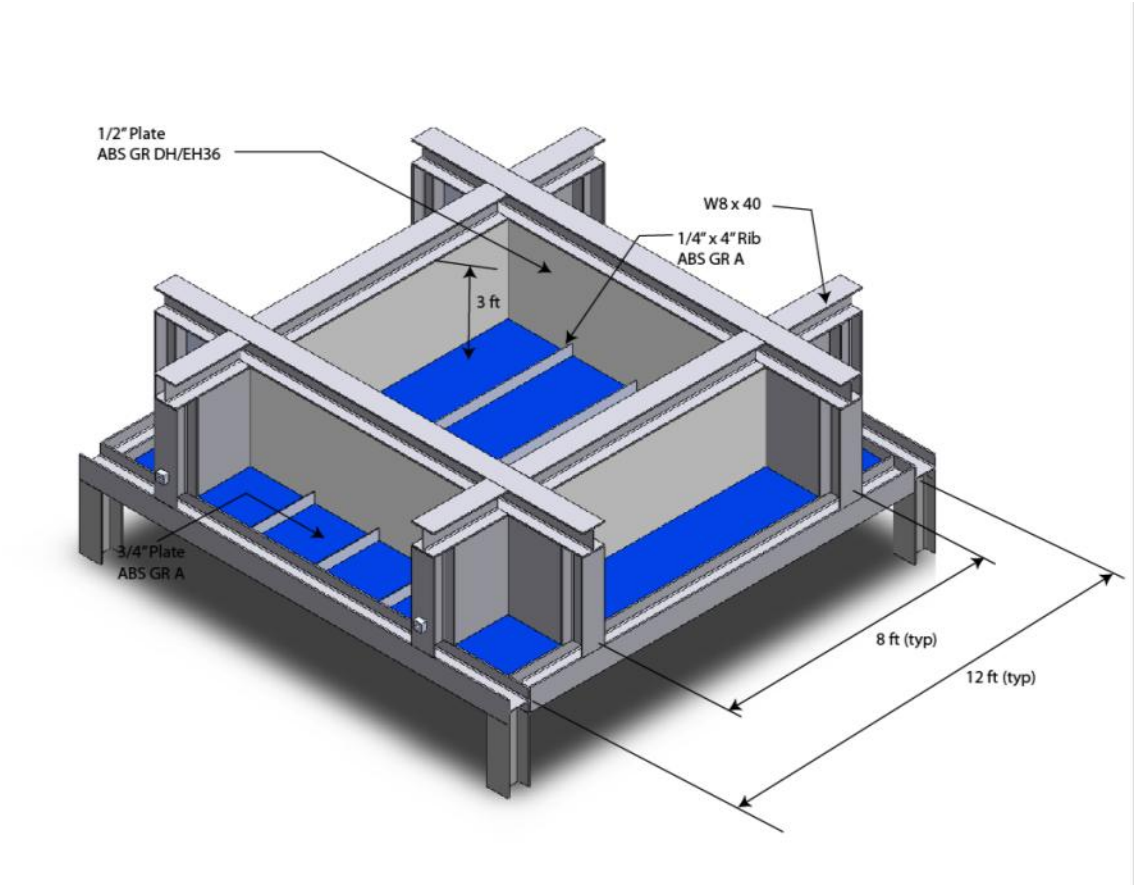

Figure 37. Large Phase III structure layout and materials

Table 4. Large Phase III Structure Tests

Test Number	Note	Steel	Notch Type	Test Result
13	5 valves Dewars open same time	See Figure 37	2 ¾" star notch in Bay A	Did not crack
14	Same structure used in Test 13 Dewars staged	See Figure 37	New Notch 4" cross in Frame B	Cracked
16	6 values Second structure tested	See Figure 37	T-slot 2 ¾"	Cracked
22	6 values First Pool Test	See Figure 37	2 ¾"notch	Did not crack
23	Same structure as Test 22 Second Pool Test	See Figure 37	8" notch	Cracked (after turning off dewars)

4.4.1 Large-Scale Tests without Water

The tests conducted (Test 13 and 14) on the first Phase III structure used a 30 inch wide trough constructed perpendicular to the 4 in. stiffening ribs. The layout of the trough is shown in Figure 39. The trough is separated into two sections. The first section is within the 3 ft vertical Gr. EH plates and is approximately 74 in. long and spans three rib compartments within the structure. The other trough section is approximately 24 in. long and is located

outside of the vertical Gr. EH plate. Photos of the trough are shown in Figure 38. The trough also extends up the first 18 in. of the inside and outside surface of the 3 ft vertical Gr. EH plate.

Fifty-four thermocouples were used during the tests to record temperature data. The layout of the thermocouples is presented in Figure 39. Five low-pressure dewars were used in the two tests (Test 13 and 14) performed on the first large structure. The dewars were connected to five Magnatrol F25M21 solenoid valves to enable remote operation. The layout of the dewar pipes is also shown in Figure 39. One vertical pipe flows into the center of the three inside chambers created by the 4 in. ribs and the foam trough. The other two pipes spray the inside and outside surface of the 3 ft vertical Gr. EH side wall. The flow strikes the 3 ft wall approximately 1 ft above the Gr. A base plate. An eight segment star notch which measure 2 ¾ in. in diameter was machined into the third chamber from the wall (see dark gray spot in Figure 38(a)). This configuration of notches was machined into the structure after the initial painting of the trough area. Therefore, the dark gray spot shows the repainting performed in the notch area. A 4 ft x 8 ft x 2 in. piece of Styrofoam was placed on the underside of the ¾ in. Gr. A plate trough region to act as additional insulation.

The layout of the test structure for Tests 13 and 14 is illustrated in Figure 40. During Tests 13 all five solenoid valves were open simultaneously. The test ran for approximately 30 minutes and no fracturing was generated.

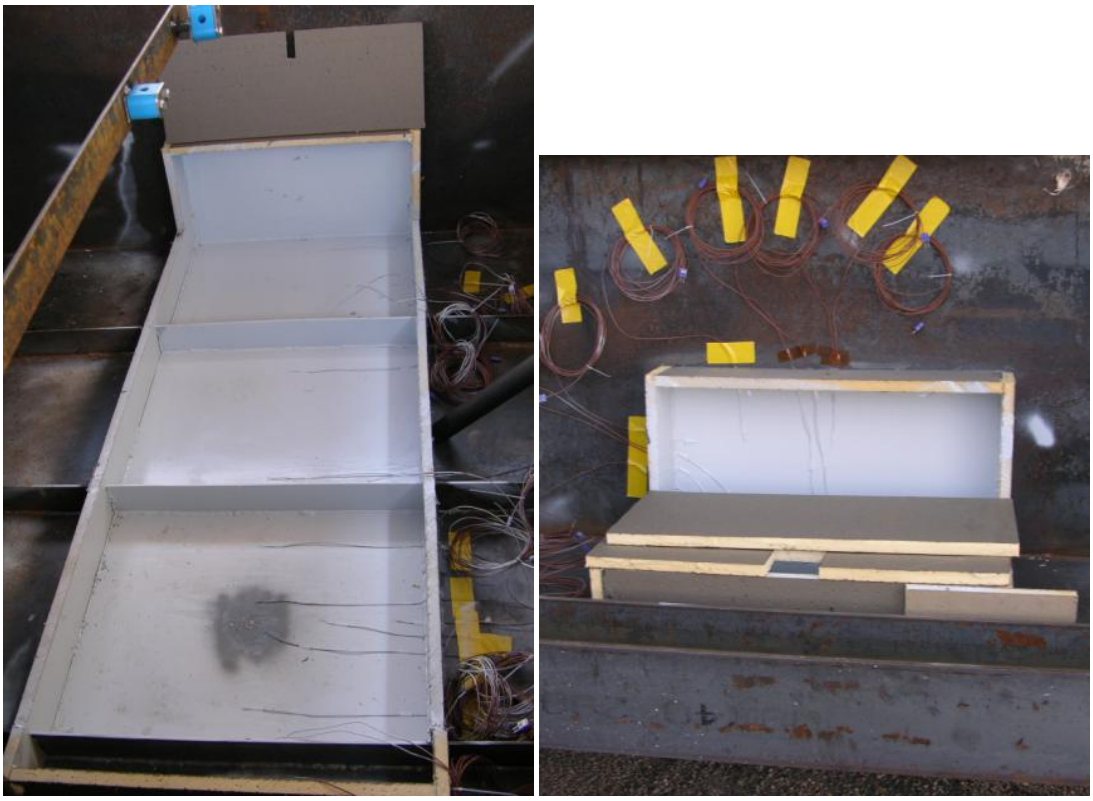

Figure 38. Phase III Test 13 and 14 trough layout, inside the structure (left) and outside the 3 ft vertical Gr. EH plate (right)

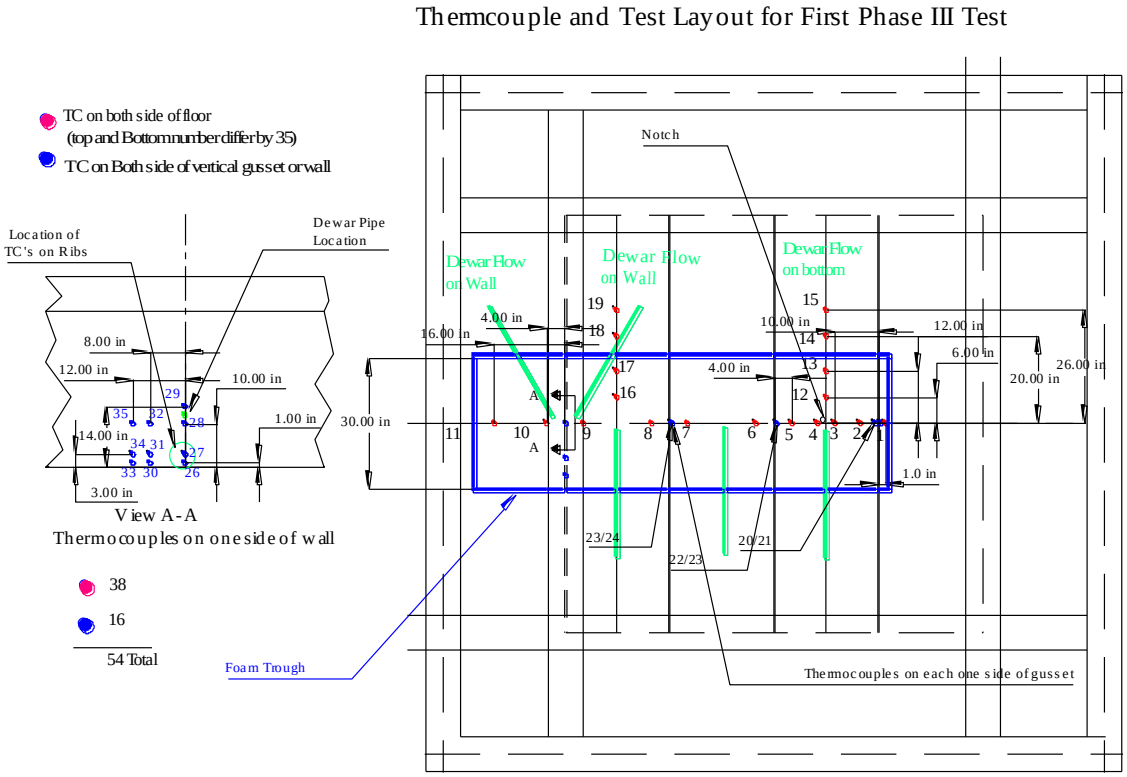

Figure 39. Trough and thermocouple layout for Phase III Test 13 and 14.

Figure 40. Layout of the Phase III tests (Test 13 and 14)

As with many of the Phase II tests, a second Phase III test (Test 14) was performed using the same structure that was used in the first test (Test 13). However, the second test on this structure included a redesign of the notch, notch location, and dewar timing. For Test 14, a 4 in. long cross shaped notch was machined into the middle chamber of the trough as shown in Figure 41 and Figure 42 (brown tape covering cross notches). The dark grey areas in Figure 42 show the repainting performed in areas that experienced paint flaking after Test 13. The original star notches in the far bay remained unrepaired (see Figure 43). Longer notches lead to higher stress concentrations and therefore failure was predicted to occur at the 4 in. cross notches and not to original star notches. Also, timing of the 5 dewar values was introduced so that the entire trough region was not cooled simultaneously. During Test 14, the valves were opened at different times. Referring to Figure 43, valve 2 (Bay B) was opened initially. After 10 minutes and 55 seconds, a crack initiated (audible evidence). Within approximated 15 seconds from this audible sound, valve 3 (Bay C) was opened. At a time of 12 minutes and 23 seconds into the test, a second crack initiation/propagation was heard. Again, within approximately 15 seconds from this sound, valves 1, 4, and 5 were opened. At 15 minutes and 45 seconds into the test, a third crack initiation/propagation occurred. As the test continued, significant quantities of leaking LN_2 fluid was observed passing through the cracked structure. Finally at 16 minutes and 26 seconds into the test, the final crack initiation/propagation occurred. The valves were close 18 minutes and 35 seconds into the test. The fractures that formed during Test 14 are shown in Figure 44 with the thermocouple data illustrated in Figure 45. Note that the thermocouple data for TC7 increases rapidly around 650 seconds. This was due to the thermocouple losing contact with the plate and/or malfunctioning.

The goal of the timed value openings was to learn how it affected the cracks propagated after initiation. The initial region, Bay B, has dimensions 30 in. wide and 24 in. long in the direction of the full trough. As also observed during the Phase II tests, the crack initially propagated in the direction of the short dimension (24 in.), which is the direction of the other sections of the trough (see Figure 44). The second fracture most likely included cracks propagating into Bay C after value 3 was opened. These cracks immediately turned toward the sides of the trough. Note that after the second valve was turned on, the cooling region dimensions were now 48 in. x 30 in. The cooled region now includes Bay C and Bay B, thus the geometry of the cooled region now has the long axis rotated 90 degrees. This rotation of the long dimension therefore rotated the maximum stress direction causing the cracks to turn during propagation. The third observed cracking was most likely the cracks propagating into Bay A and turning toward the sides of the trough after the remaining valves were opened. The final observed crack propagation was likely the extension of multiple existing cracks into material located slightly beyond the borders of the trough. This was observed in the Phase II tests when the cooling continues for some time. Here, the material outside of the direct trough cooling region also begins to cool to the point where crack extension is favorable. Also note that the stiffening ribs were fractured through completely. Since they were nearly as cold as the base plate, they did not provide any type of crack arrestment.

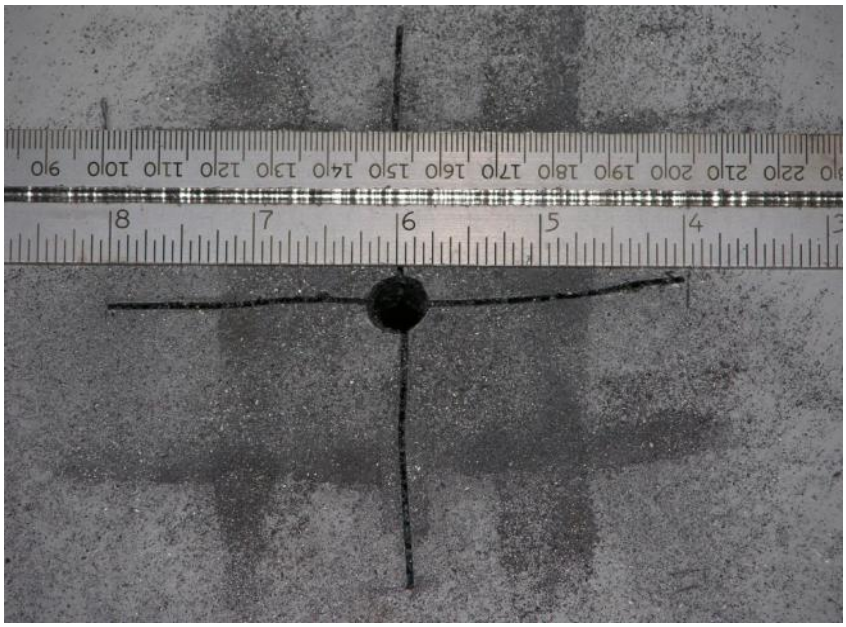

Figure 41. Notch added for use in Test 14

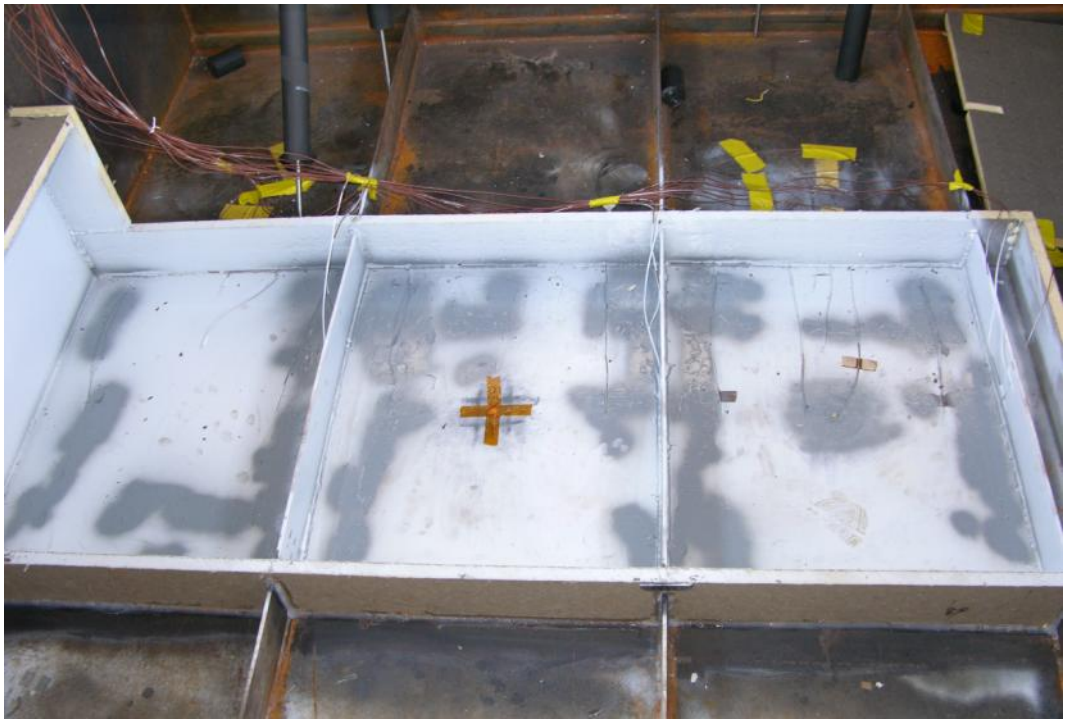

Figure 42. Trough with added notches and paint repair prior to Test 14

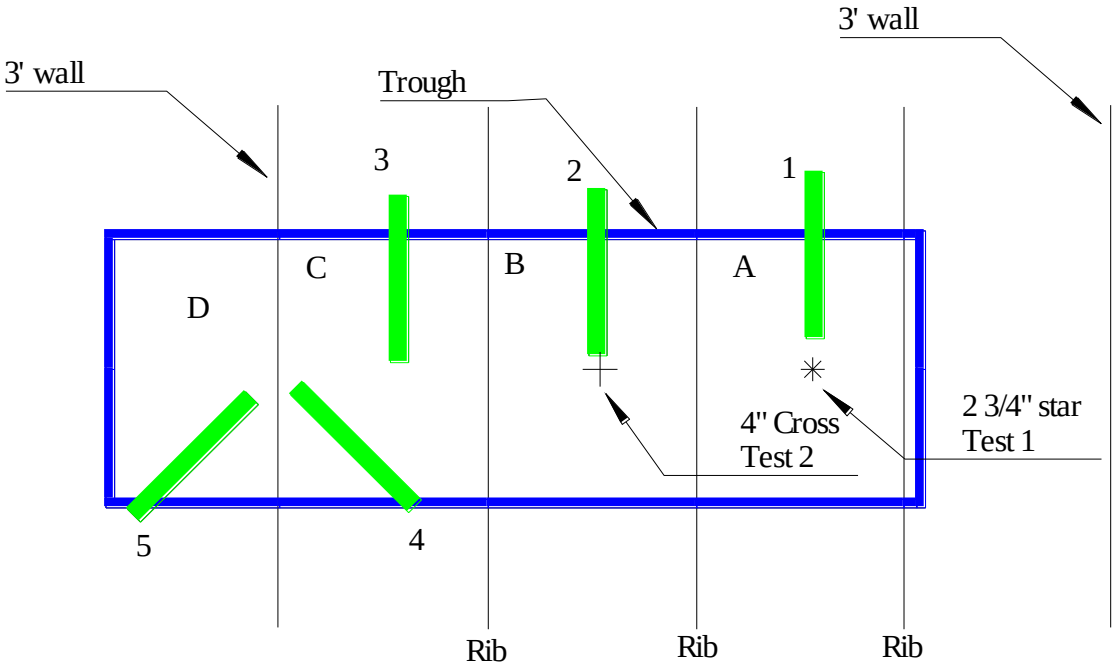

Figure 43. Pipe layouts and Bay/Valve locations for Test 13 and 14 (2 ¾ in. star Test 1 designates in Test 13, 4 in. Cross Test 2 added for Test 14)

Figure 44. Crack formation during Test 14

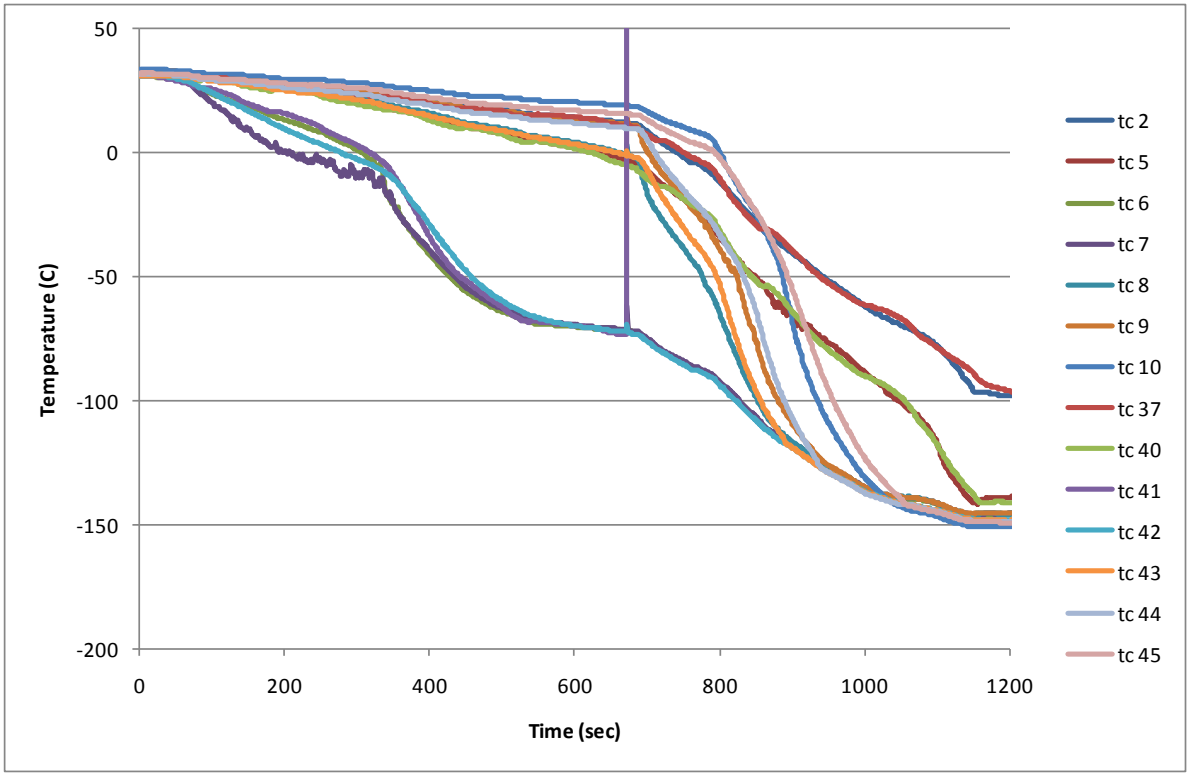

Figure 45. Thermocouple data for Test 14

The next Phase III test (Test 16) used the trough configuration shown in Figure 46, Figure 47, and Figure 48. The trough extended the full width (8 ft.) of the region within the vertical Gr. EH plates and spanned the other direction across two rib sections. The trough ran up the side of the 3 ft vertical Gr. EH wall approximately 18 inches. For the outer region of the structure, the trough extended only approximately 4 in. along the entire 8 ft. span, but also extended up the vertical Gr. EH plate 18 inches along the entire 8 ft. span.

There were filler tubes attached to six low-pressure dewars for Test 16. Four of the tubes filled the inner trough regions. The two remaining tubes sprayed the inside and outside surface of the 3 ft. side wall. Similar to Tests 13 and 14, the tubes spray the side wall approximately 12 in. above the ¾ in. thick Gr. A base plate and centered along the 8 ft. span. The five filler tubes that supplied the inner regions of the structure are clearly show in Figure 47. The wetted surfaces were painted with marine primer that was used in the Phase II-B tests.

Forty–four thermocouples were attached to the structure. The thermocouple layout is presented in Figure 46.

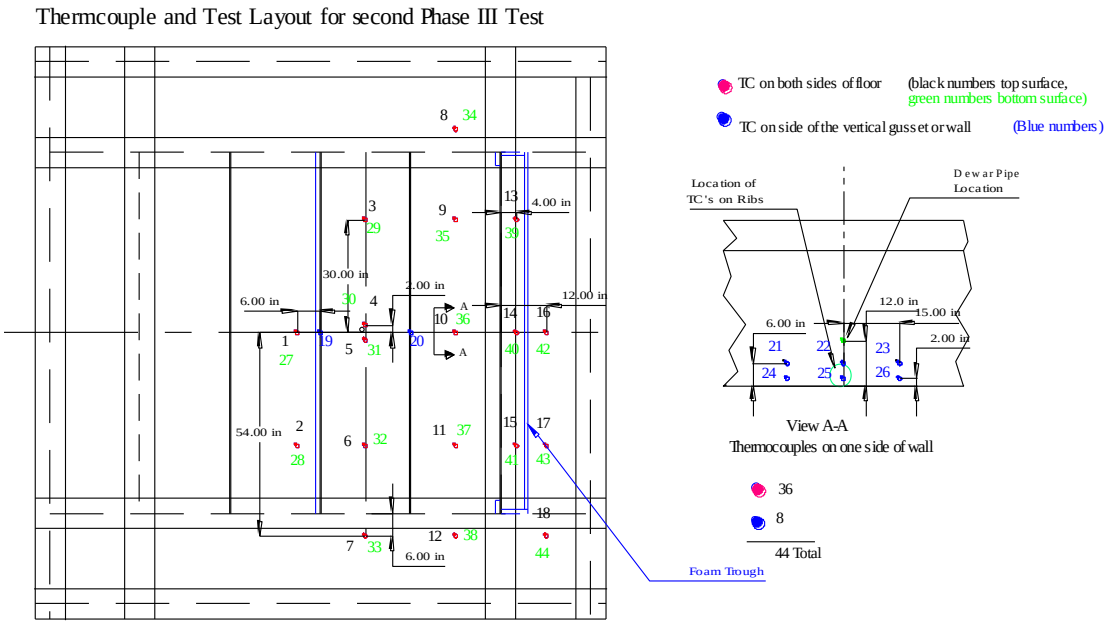

Figure 46. Trough and thermocouple configuration for Test 16

Figure 47. Trough and pipe layout for Test 16

Figure 48. Trough layout outside vertical Gr. EH plate for Test 16

The stress concentration machined into the structure for Test 16 was started with a 3/8 in. diameter hole with notches then extended away from the hole creating a total notch length of 2 ¾ in. The notch was perpendicular to the ribs and was in the second rib chamber as shown in Figure 49. Due the large number of cracks, red dye penetrate was used to highlight the fracture progression. Again, the long dimension of the cooling region for this test was 96 in. (8 ft.) with the short dimension 48 in. (~52 in. if the section outside of the vertical Gr. EH plates is added). This configuration would lead to a crack initiation and propagation mainly in the short cooling dimension; therefore, the notch was machined only in that direction. All six of the valves were open simultaneously at the beginning of the test. At just over 14 minutes into the test, a crack initiated (audible detection). The resulting cracks are shown in Figure 49 and with the thermocouple data provided in Figure 50. The uniform drop in all of the temperature data at about 850 seconds was caused by the vibration that occurred during the fracture. The data after that point is not considered valid.

Examination of the crack pattern suggested there is a high likelihood that the initial crack initiation occurred at the weld "toe" attaching one of the stiffening ribs to the ¾ in. thick Gr. A plate. This rib weld is located adjacent to the "rat hole" near the vertical Gr. EH plate as illustrated in Figure 51. This spot is the intersection of three different plate and weldments resulting in a highly stressed geometry. The resulting stress shock wave propagated through the structure to the machined notches. This was then followed by the subsequent initiation of two additional sites in the weld region between the ¾ in. Gr. A base plate and the vertical Gr. EH plate (upper left of Figure 49). This sequence of initiations is based on a study of the crack propagation and termination pattern. Since only one audible cracking event was observed, all of the initiations occurred nearly instantaneously. It is also clear from Figure 49

that the cracks, for the most part, run in the direction of the short dimension of the cooling region. However, with largest cooling region in terms of area of any test performed in this study, Test 16 exhibited many of the features observed in actual cases of large-scale brittle fracture in steel plating as shown in Figure 52. These include crack branching and semi-random propagation. This semi-random nature is based on the stress wave and the microstructure of the material. Though as mentioned earlier, the direction of the gross path of the cracks was dominated by the maximum stress direction which propagated them in the short cooling dimension. A significant outcome of the test was the propagation of the cracks not only through the stiffening ribs (Figure 53), but also through and up the vertical Gr. EH plate (Figure 54). The larger vertical wall with the higher fracture toughness Gr. EH plate had no effect in arresting a propagating brittle crack since the 3 ft. Gr. EH plate was also cold. Finally, the cracks that propagated through the vertical Gr. EH plate and into the horizontal ¾ in. Gr. A plate turned 90 degrees and joined together to form a crack parallel to the vertical Gr. EH plate. Part of this turning and joining is illustrated in Figure 55. The reason for the crack turning lies in the rotation of the maximum stress direction along the narrow cooled region just outside of the vertical Gr. EH plate. It should also be noted that this crack ran through the base Gr. A plate and not along the weldment joining the Gr. A plate and the Gr. EH plate.

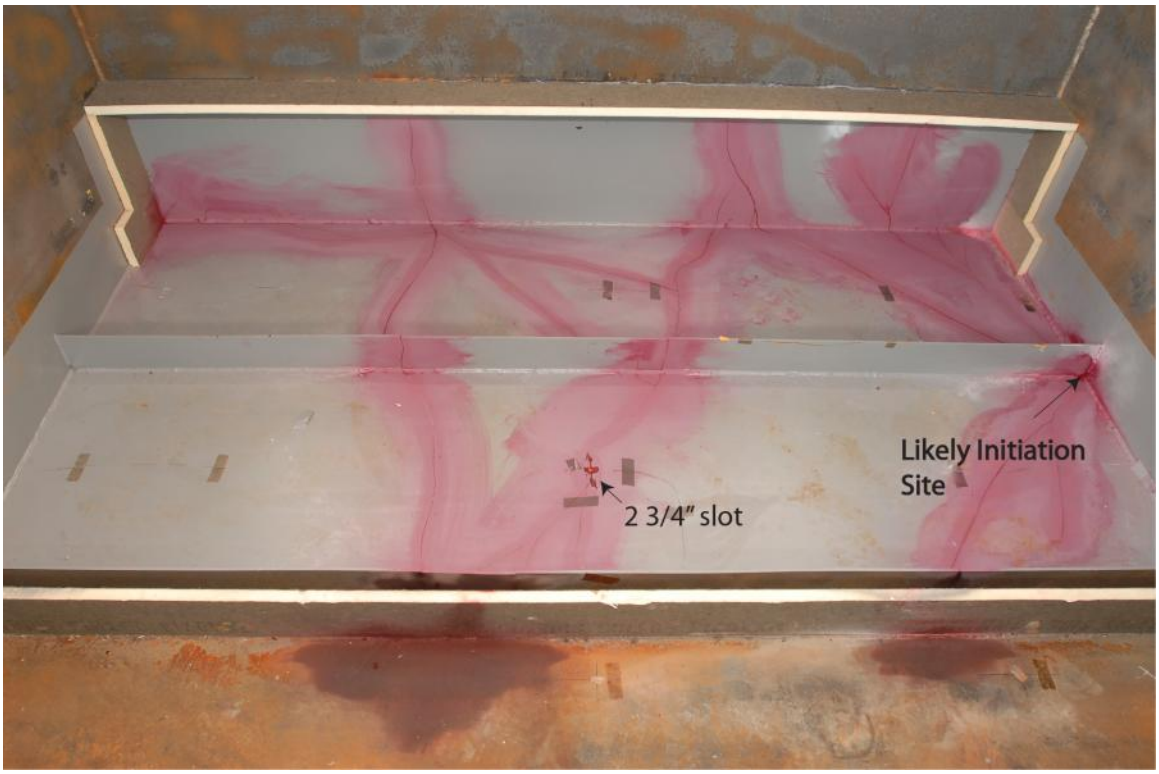

Figure 49. Interior crack formation during Test 16

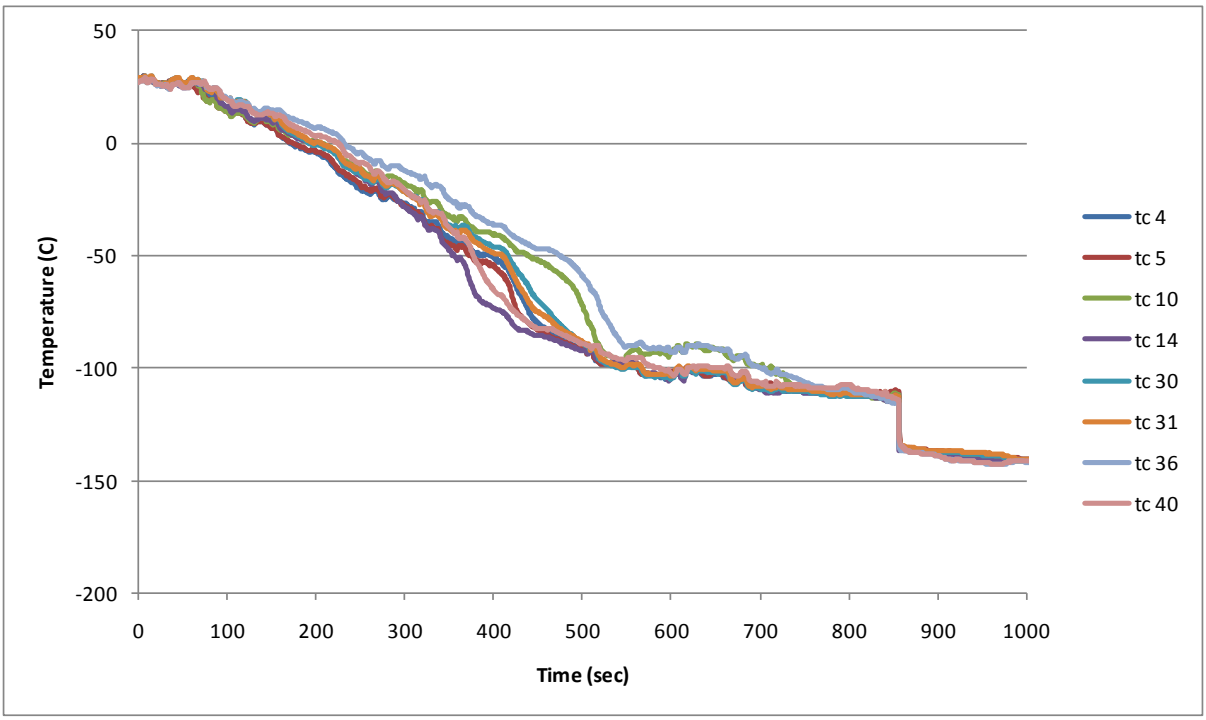

Figure 50. Thermocouple data for Test 16

Figure 51. Close-up of likely initiation site for Test 16

Figure 52. Fractures caused by LNG spills on actual LNG vessels (Roue, 2011)

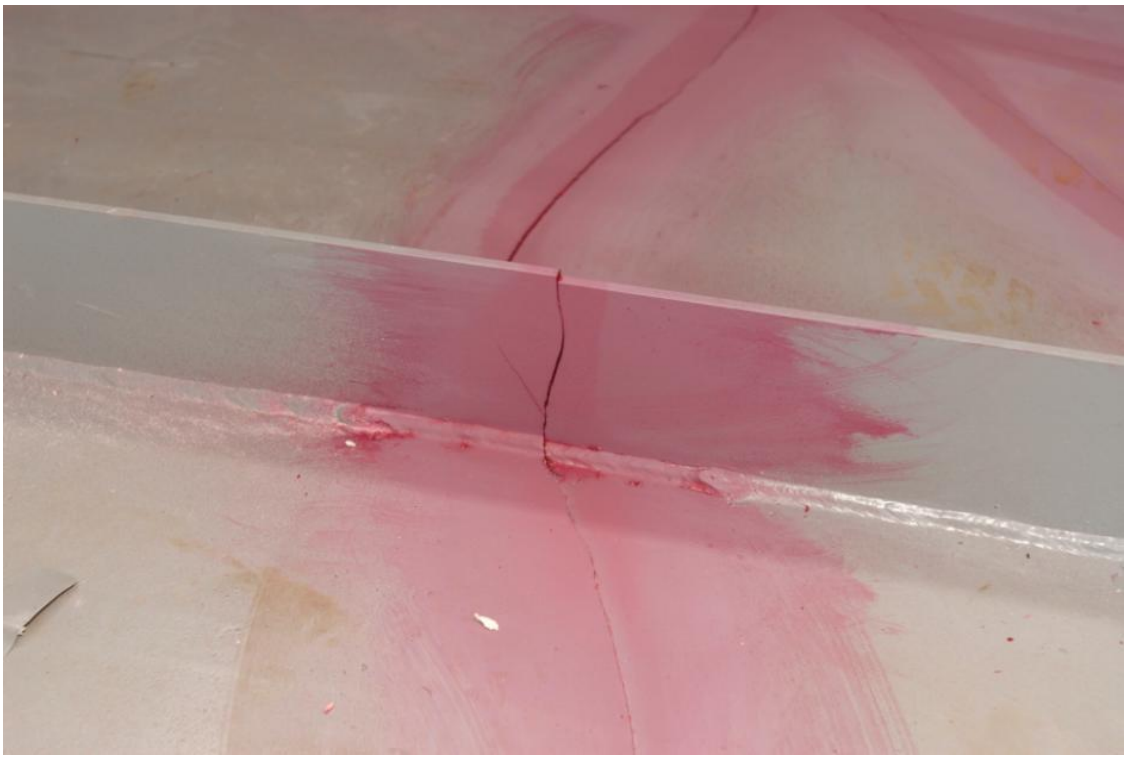

Figure 53. Close-up stiffening rib fracture for Test 16

Figure 54. Outside through-cracks for Test 16

Figure 55. Outside cracking with turning for Test 16

4.4.2 Large-Scale Tests with Water

The last set of tests (Test 22 and 23) conducted using the third and final large structure placed the structure inside a 24 ft diameter pool. The purpose of the tests was to investigate cooling a structure that was in partial contact with water. A schematic of the test configuration is shown in Figure 56. Only a 48 in. wide plate section was in contact with the water as pointed to in Figure 56. Polyurethane foam was used to insulate the remaining portion of the structure from the pool water. The bottom surface was sprayed until forming a 3 in. foam layer as shown in Figure 57. The wetted surfaces were painted with marine paint.

For Test 22, the trough layout, notch dimensions, and the dewar layout were the same as for Test 16. A 2 3/4 in slot was cut perpendicular to the ribs in the second chamber. The backside of this area was insulated from the water by the urethane foam. As with Test 16, six dewars were used during the test and all of the dewar valves were open at the start of the test. The pretest setup of the large structure pool test is shown in Figure 58. Several small holes were drilled into the horizontal plate. Plastic tubes were then attached to the top surface of the holes so that water could be seen rising above the surface of the horizontal plate. These holes/tubes were used to attempt to ensure that water was in contact with the bottom surface of the ¾ in. thick Gr. A plate. The only differences from Test 16 were the water and the Polyurethane foam preventing water from contacting a portion of the ¾ in. Gr. A base plate.

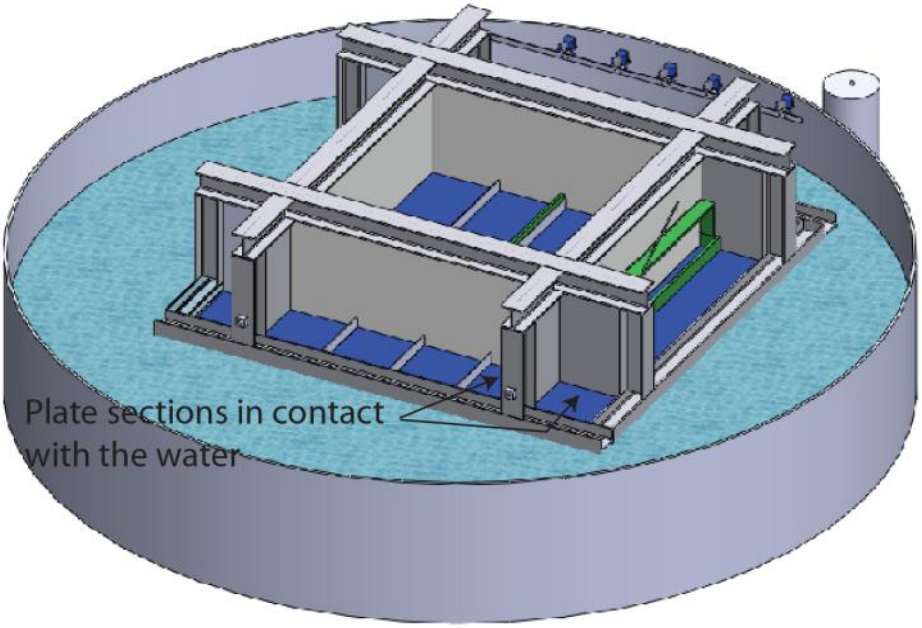

Figure 56. Schematic of the large structure pool tests

Figure 57. Polyurethane foam applied to the bottom of the large structure

Figure 58. Test setup for the large structure pool test

Test 22 ran for approximately 30 minutes (exhausted the supply of LN_2) without cracking the structure. The notch was subsequently enlarged to 8 in. as shown in Figure 59. Using an identical test setup as for Test 22, the second pool test, Test 23, was run for thirty minute and again no cracking was observed. The valves were closed at 30 minutes, the instrumentation was turned off around 42 minutes, and the disassembly of the test setup was then initiated. However, draining of the pool had not been initiated. Approximately 46 minutes after beginning the test (4 minutes after turning off the data acquisition), a crack initiated. The resulting cracks are shown in Figure 60. The crack initiated from the 8 in. long notches and then formed an "X" pattern. The cracks propagated through and up the vertical Gr. EH plate. In addition, the long cooling time caused significant cooling outside of the direct trough region. This led to a propagation of crack well outside of the trough region (right side of Figure 60). Since the crack initiated at a time when no physical contact with the structure was occurring by the test administrators, the most likely reason for crack initiation is that the structure warmed up through a different path than the structure cooled down through. This slightly different path of warming caused the stresses nearest the tips of the machined notches to increase to a level higher than that experienced earlier in the test. Since the data acquisition system was not collecting data, the exact temperature distribution in the structure at crack initiation is not known. However, Figure 61 illustrated the thermocouple data up to approximately 4 minute before fracture. The temperatures are clearly starting to increase at 42 minutes, but the structure was still extremely cold. The warming trend would have continued for the additional 4 minutes until fracture, but not significantly.

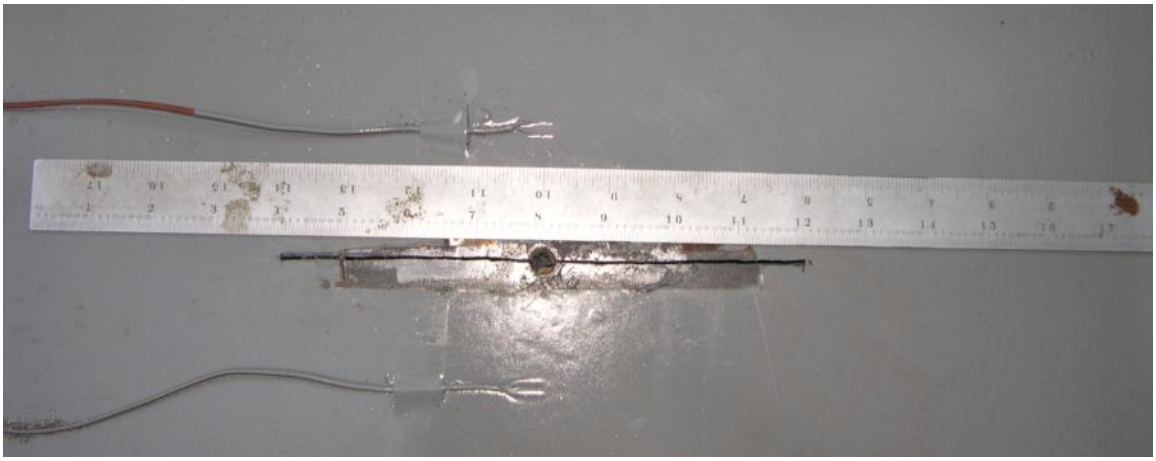

Figure 59. Test 23 notch increased to 8 in.

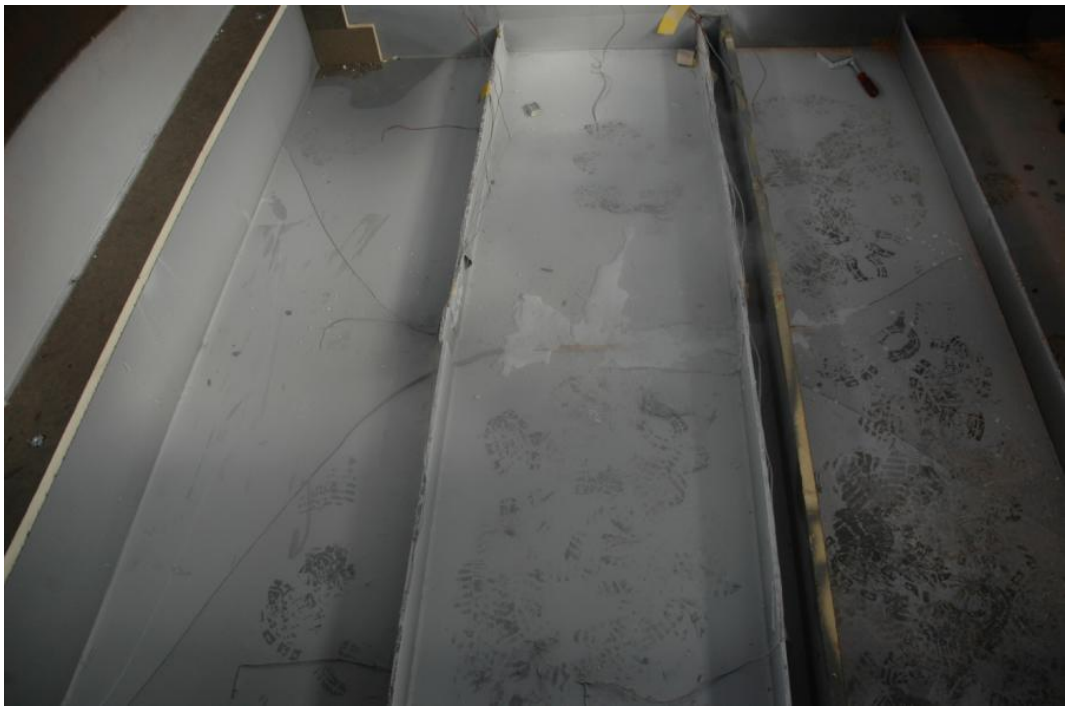

Figure 60. Crack progression for Test 23

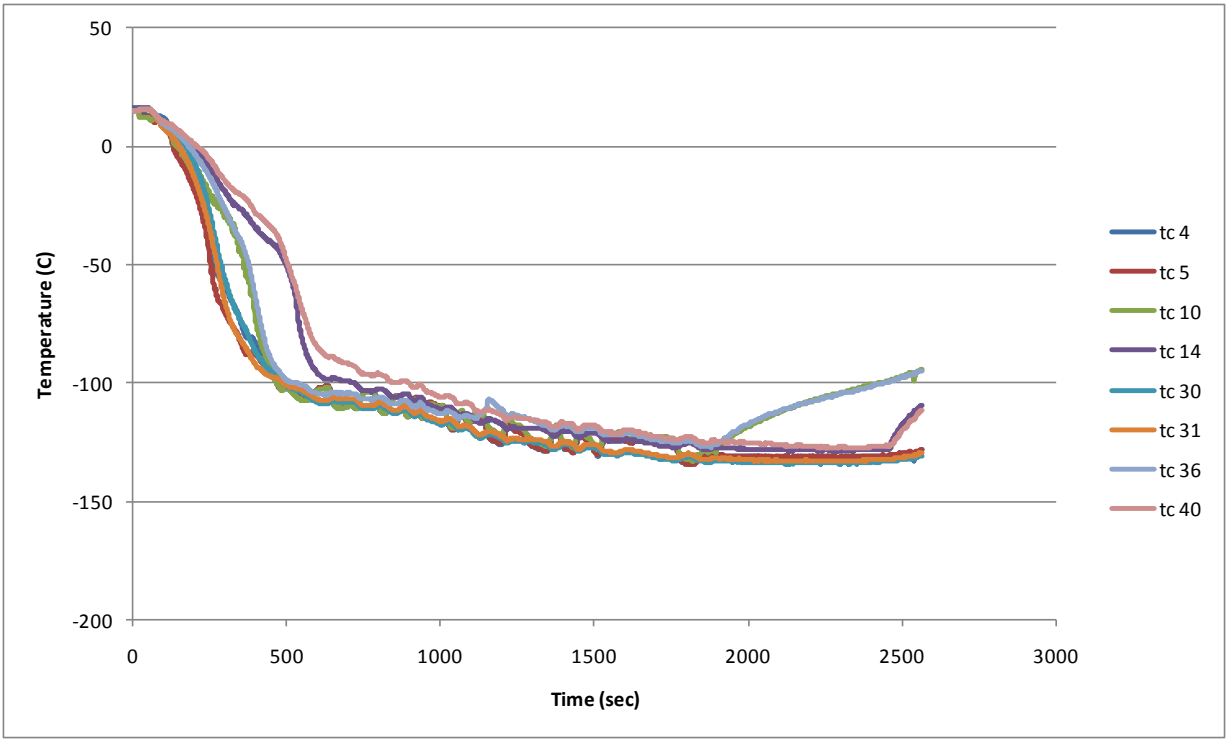

Figure 61. Thermocouple data for Test 23

5. Heat Transfer Testing

The final test series were conducted to collect heat transfer data and to compare cooling rates with LN_2 and LNG. The test plates were 6 in. x 6 in. plates with a 5 in. foam trough caulked around the perimeter as shown in Figure 62. There was also one 18 in x 18 in plate with a centered 6 in. x 6 in. trough caulked in the center. The plate thickness varied from ¼ in. to ¾ in. and the plates were tested bare, painted with a marine epoxy primer, or painted with an epoxy primer and urethane top coat. There were twelve thermocouples on the 6 in. plates and 24 thermocouples on the 18 in. plate. The layout of the thermocouples and the description of the six tests conducted with LNG and LN_2 are presented in Figure 63.

Figure 62. Plate setup used in heat transfer tests

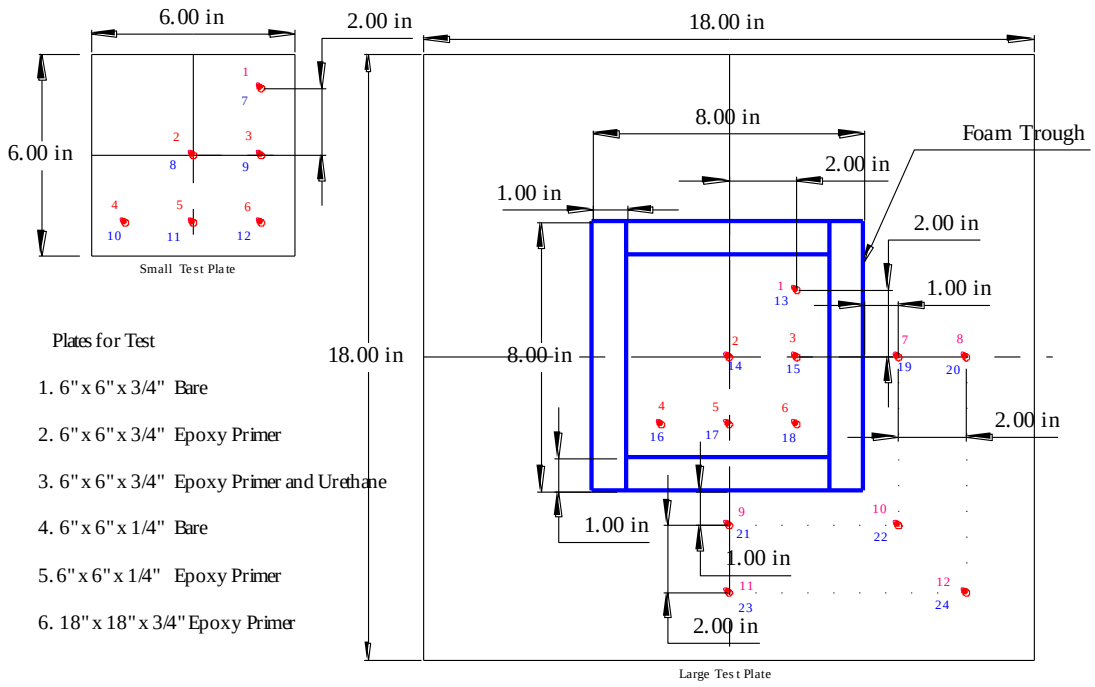

Figure 63. Heat transfer tests dimensions and thermocouple layout

For the LN_2 tests (all six tests collectively designated Test 15), the test plates were filled by pouring in the LN_2 from a small 5 liter dewar. The test plates were placed on a Mettler PC8000 precision balance scale and the trough was filled in about 10 seconds. Hand readings were taken and recorded every 15 seconds as the LN_2 evaporated. The thermocouple data for the six LN_2 heat transfer tests is provided in Figure 64 through Figure 69. A number of thermocouples lost plate contact or malfunctioned and were not plotted. For the ¾ in. thick plates, the surface coatings allow for more efficient cooling as observed in the Phase I tests. However, the differences between the epoxy primer only and epoxy primer with urethane are minimal. The thinner ¼ in. plates cooled much more efficiently than the ¾ in. plates. The addition of the surface coating to the ¼ in. plate did have a noticeable effect, but less than of the ¾ in. plate. For the 18 in. x 18 in. plate tests, only about 200 seconds of data was collected. Due to the increased mass of the plate, the cooling rate to that point was considerably slower than for the 6 in. plates.

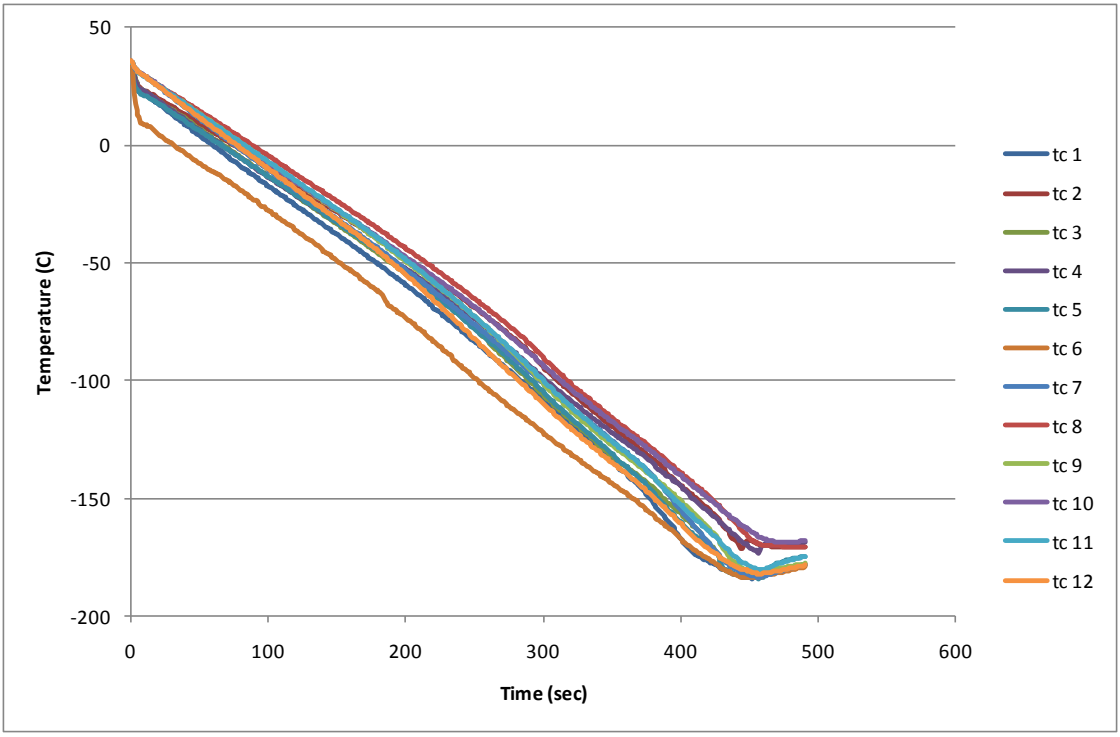

Figure 64. LN_2 heat transfer thermocouple data – 6 in. x 6 in. x ¾ in. Bare

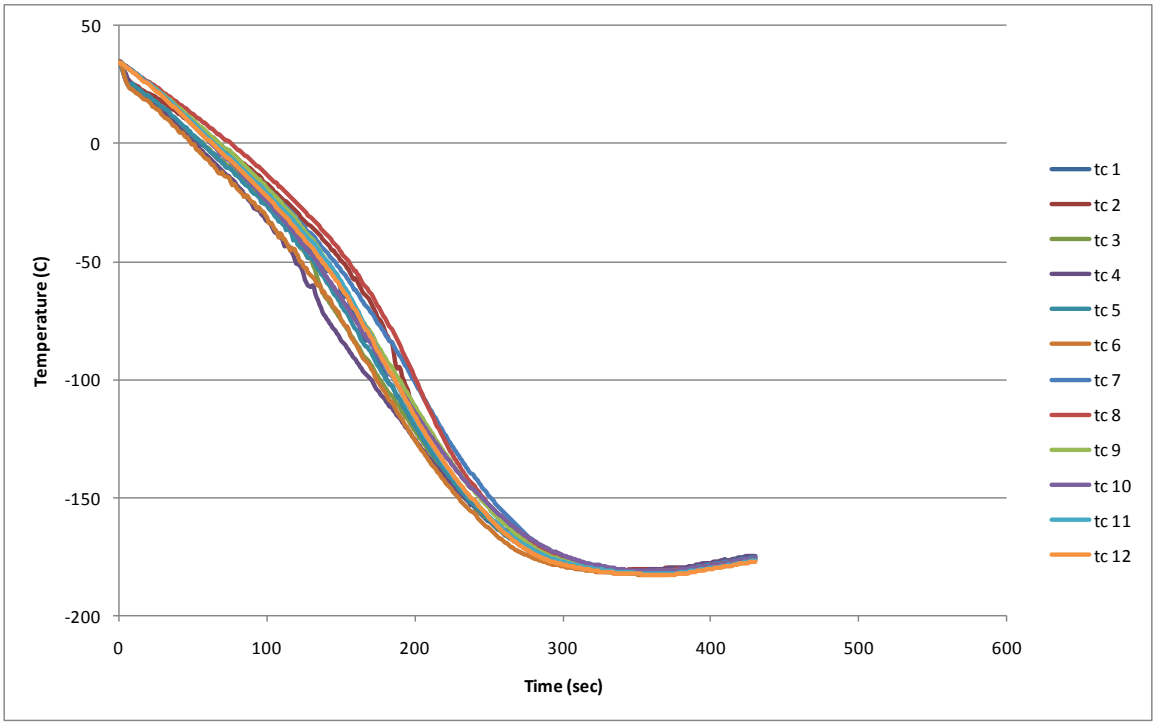

Figure 65. LN_2 heat transfer thermocouple data – 6 in. x 6 in. x ¾ in. Epoxy

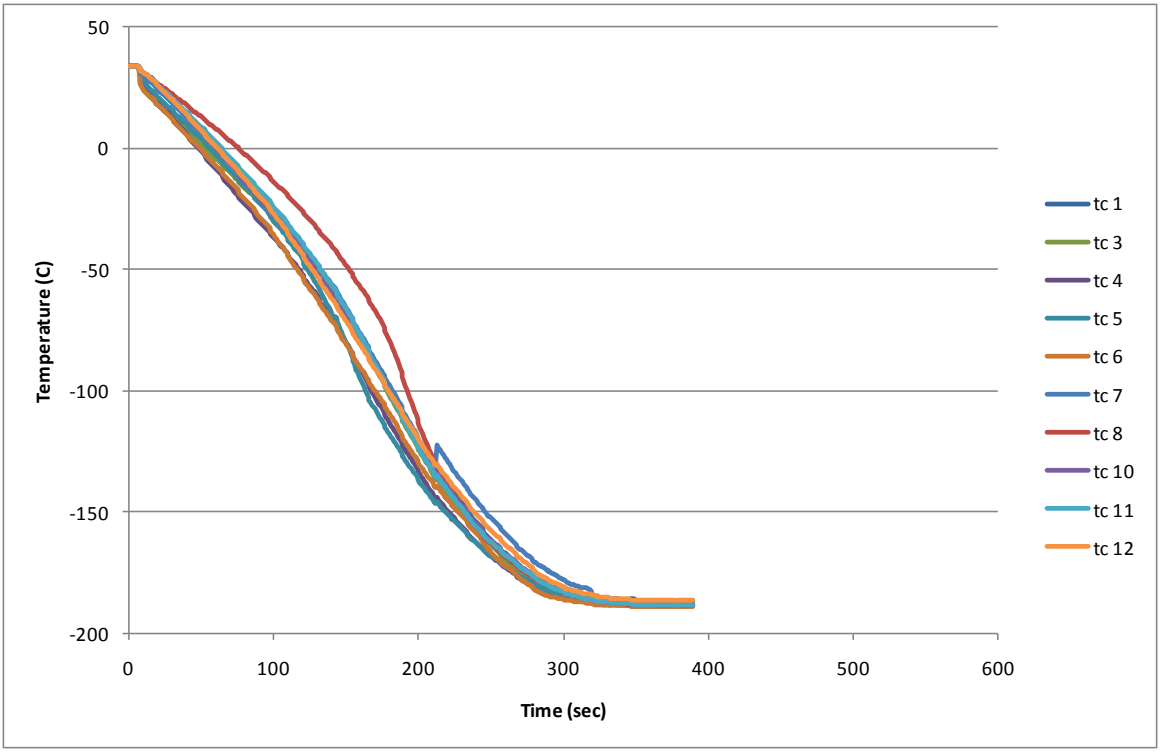

Figure 66. LN_2 heat transfer thermocouple tata – 6 in. x 6 in. x ¾ in. Epoxy Urethane

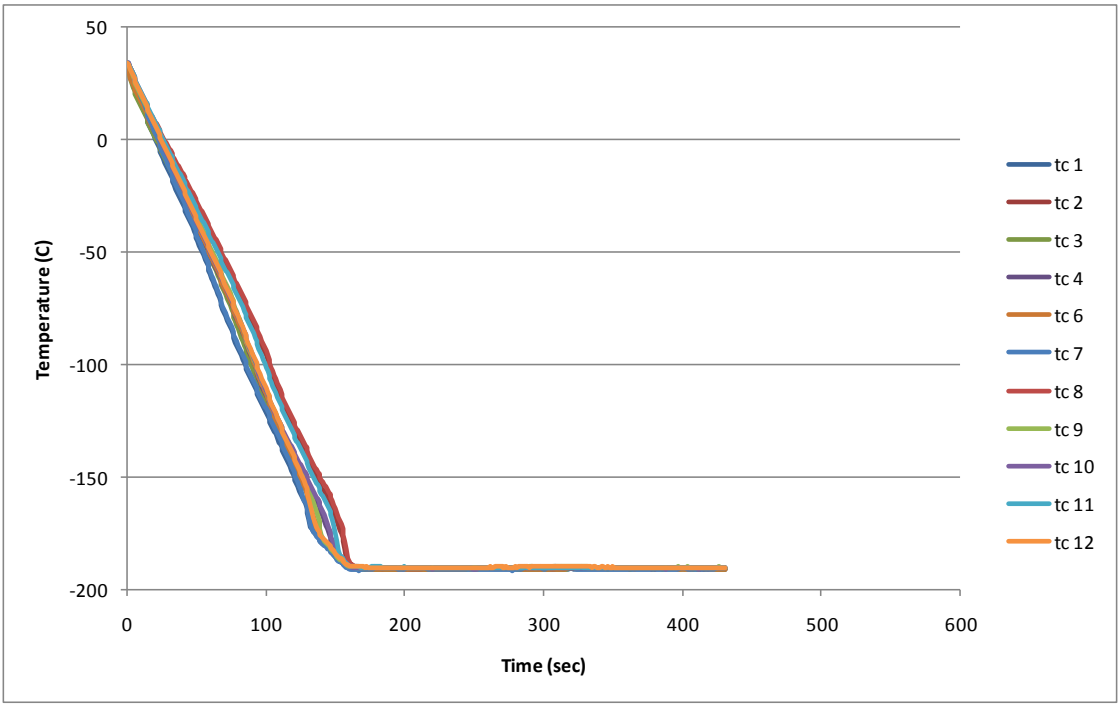

Figure 67. LN_2 heat transfer thermocouple fata – 6 in. x 6 in. x ¼ in. Bare

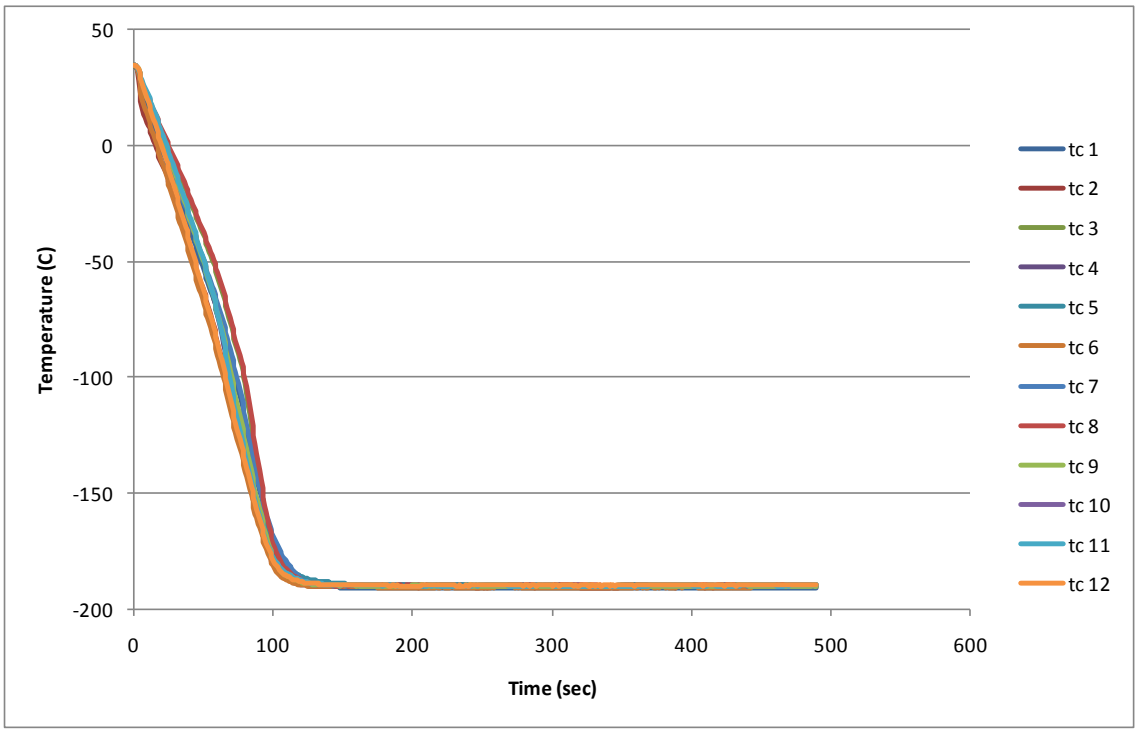

Figure 68. LN_2 heat transfer thermocouple data – 6 in. x 6 in. x ¼ in. Epoxy

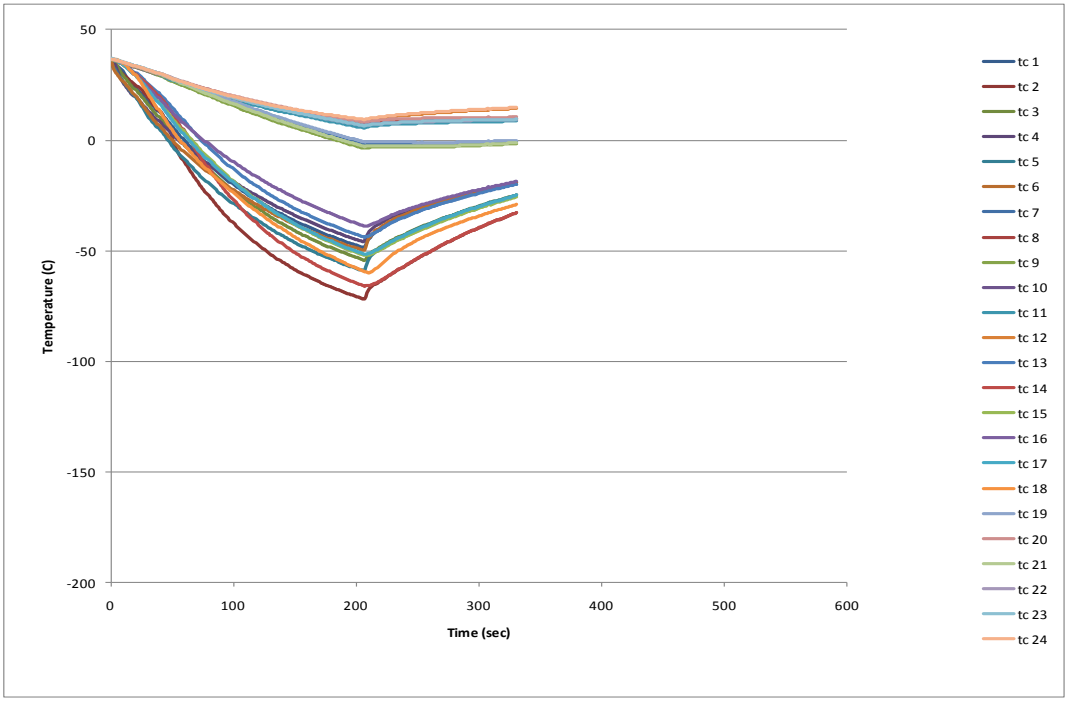

Figure 69. LN_2 heat transfer thermocouple data – 18 in. x 18 in. x ¾ in. Epoxy

The LNG heat transfer coefficient tests (all six tests collectively designated Test 24) were conducted remotely as illustrated with the schematic in Figure 70. The low pressure CRYO-CYL 180 dewar in Figure 71 was purchased from Chart Industries. The dewar was filled using an LNG tanker brought on site for the LNG fire tests, using a standard truck hose coupling mounted to the dewar support rack. A Magnatrol F25M21 solenoid valve was used to control the flow from the dewar during the test plate filling process.

During the tests, the trough filling was monitored by remote camera. A flow deflector, shown in Figure 72 was use to keep the flow from impinging directly on the bottom surface of the plate during filling. The fill pipe and deflector were held approximately 1" above the bottom surface of the test plate.

An Interface SM-25 load cell was used to measure the weight of the LNG as a function of time. The thermocouple data and the load cell data were coupled in time by using the timing of the Magnatrol solenoid valve actuation. The thermocouple data for the six LNG heat transfer tests is provided in Figure 73 through Figure 79. For the ¾ in. thick plates, the surface coatings allow for only slightly more efficient cooling. As with the LN_2, the differences between the epoxy primer only and epoxy primer with urethane are minimal. The thinner ¼ in. plates cooled much more efficiently than the ¾ in. plates. The addition of the surface coating to the ¼ in. plate again did have a slight effect. For the 18 in. x 18 in. plate tests, approximately 1 hour of data was collected. Due to the increased mass of the plate, the cooling rate to that point was considerably slower than for the 6 in. plates. Figure 79 provides the cooling for the 18 in. plate over the first 600 seconds (10 minutes) only.

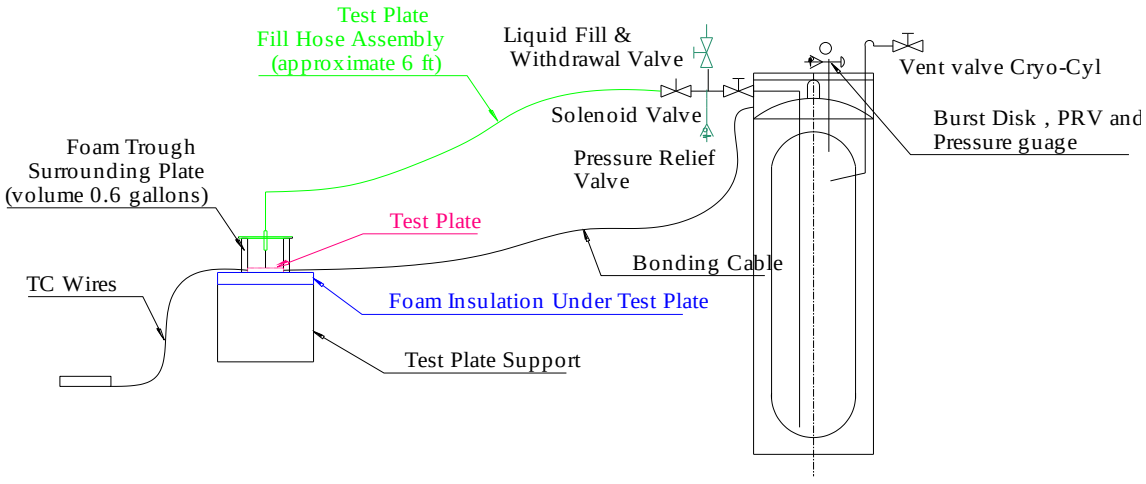

Figure 70. Schematic of the LNG heat transfer tests

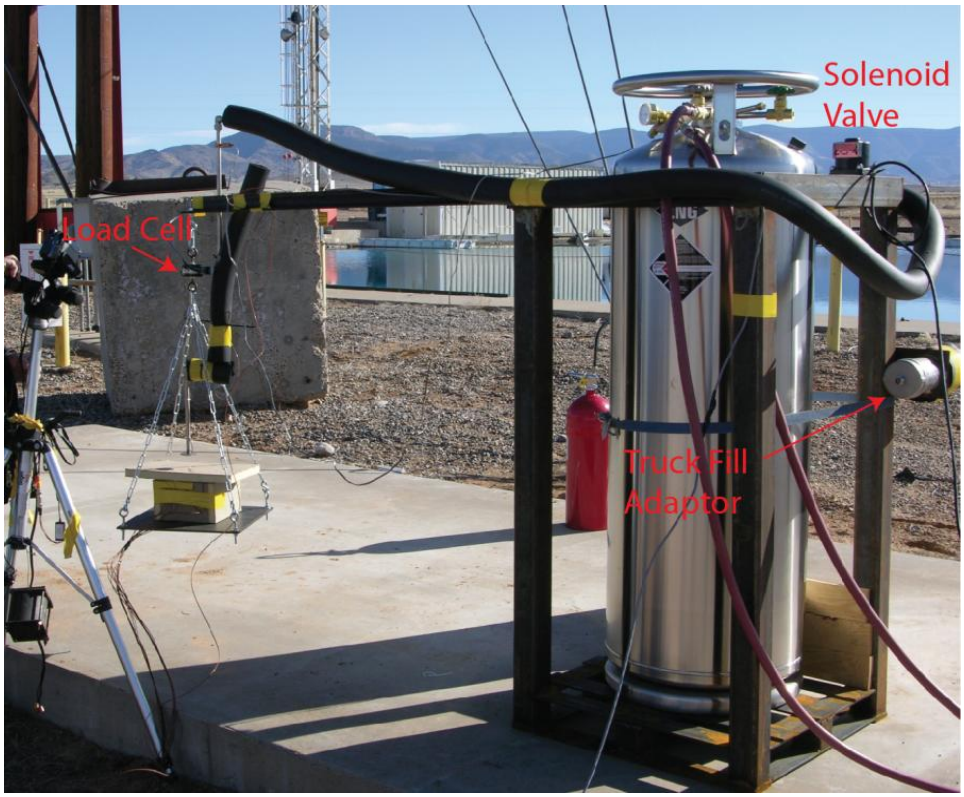

Figure 71. LNG heat transfer test configuration

Figure 72. Test plate and flow deflector

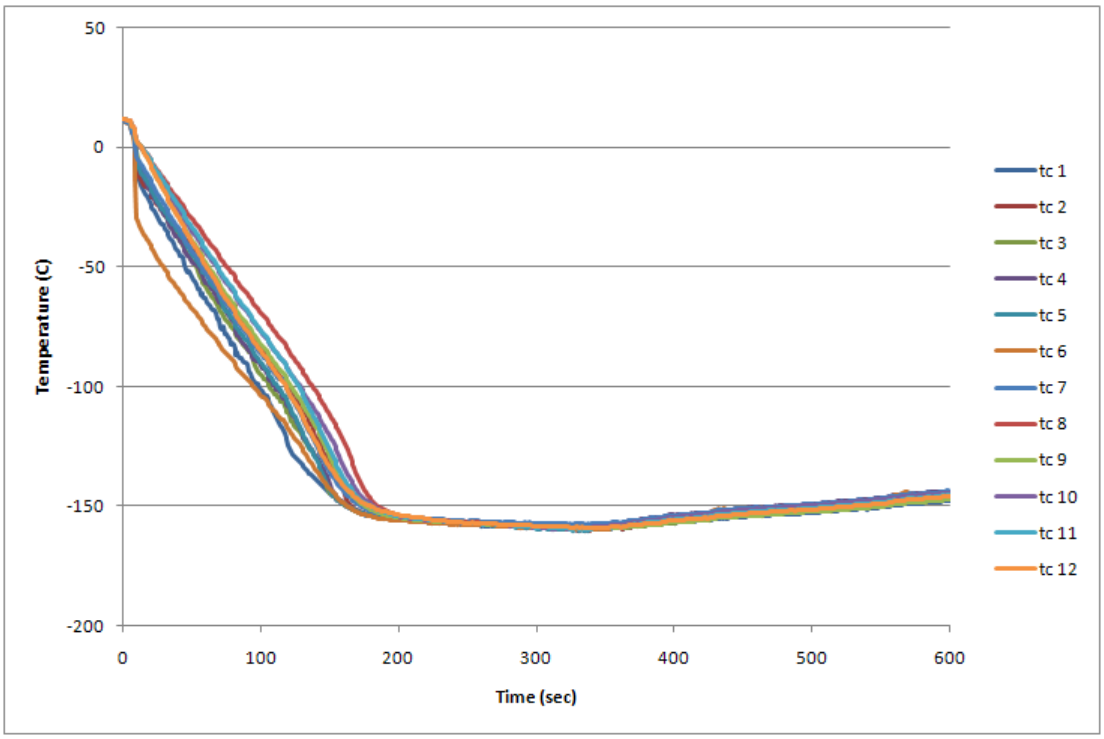

Figure 73. LNG heat transfer thermocouple data – 6 in. x 6 in. x ¾ in. Bare

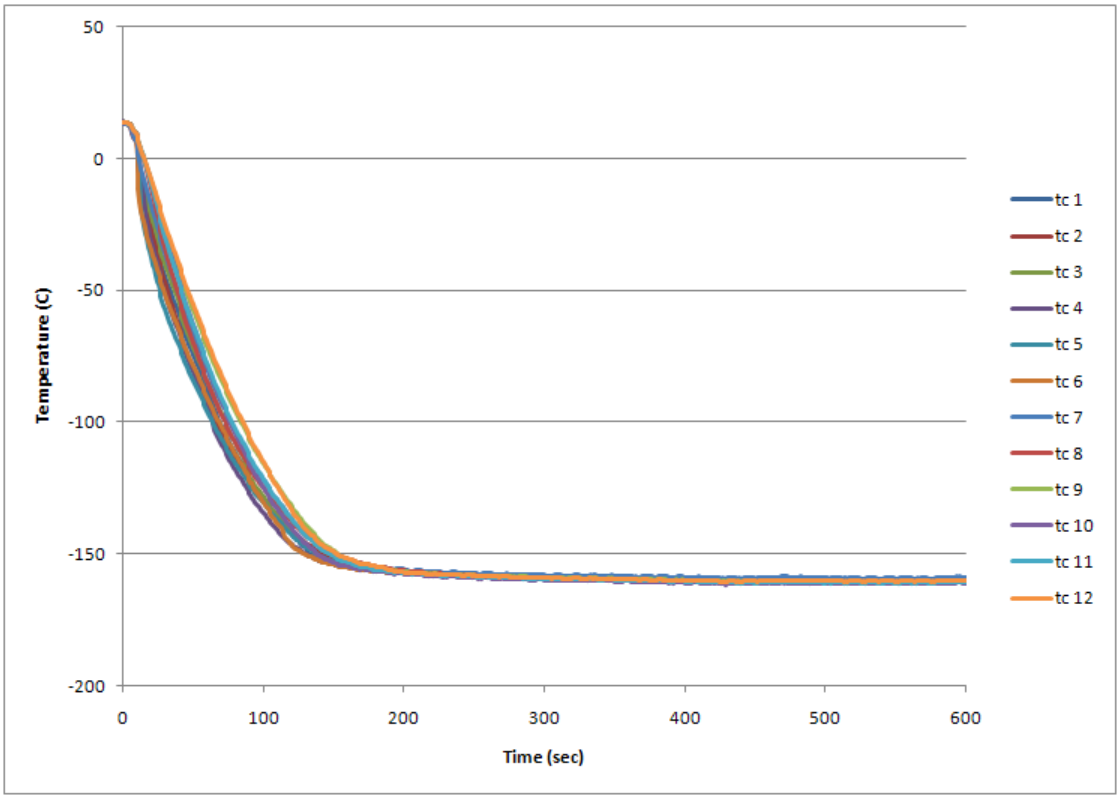

Figure 74. LNG heat transfer thermocouple data – 6 in. x 6 in. x ¾ in. Epoxy

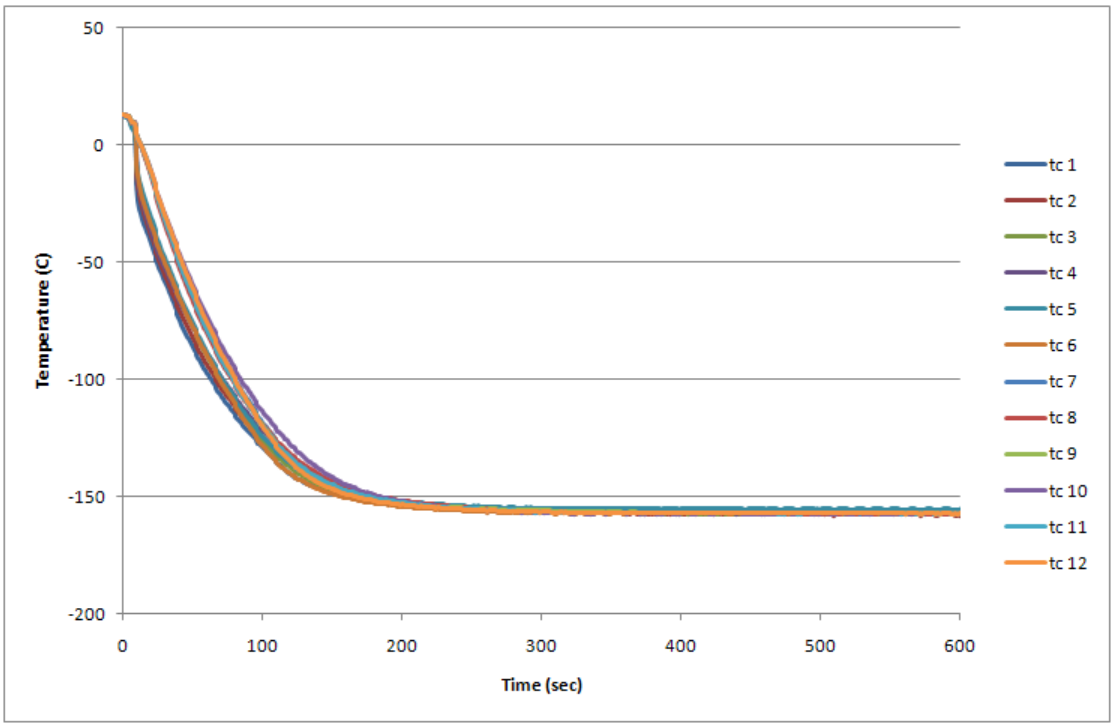

Figure 75. LNG heat transfer thermocouple data – 6 in. x 6 in. x ¾ in. Epoxy Urethane

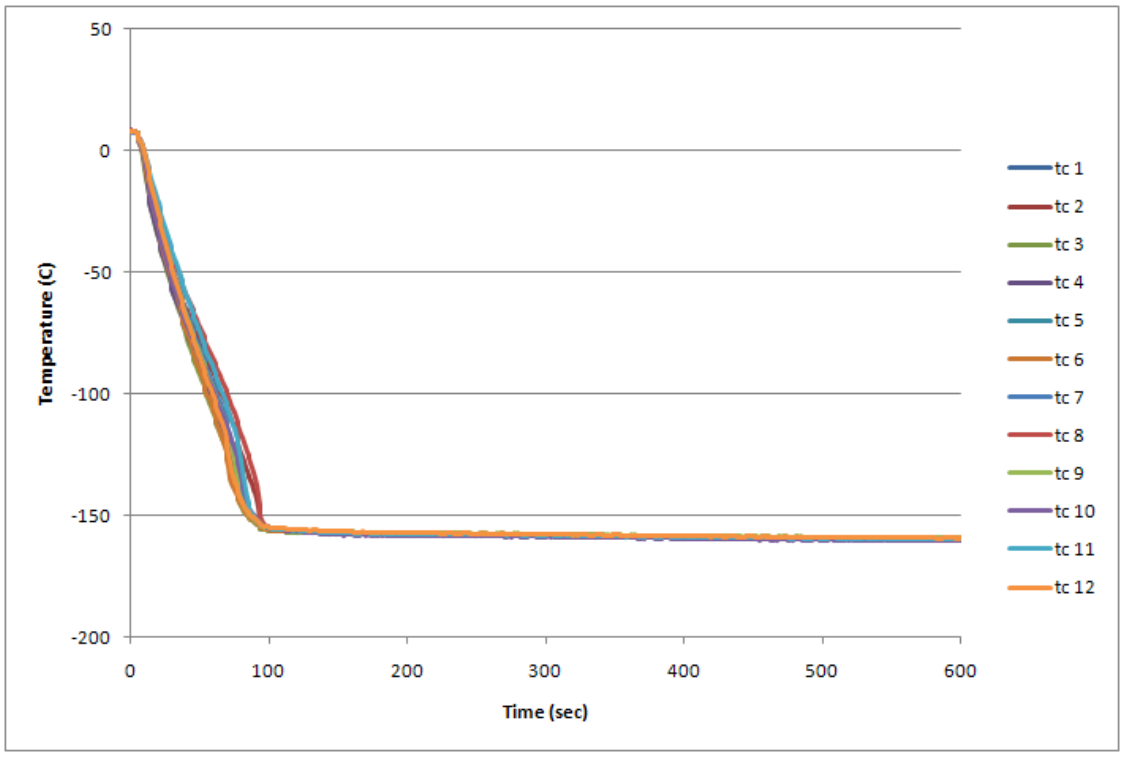

Figure 76. LNG heat transfer thermocouple data – 6 in. x 6 in. x ¼ in. Bare

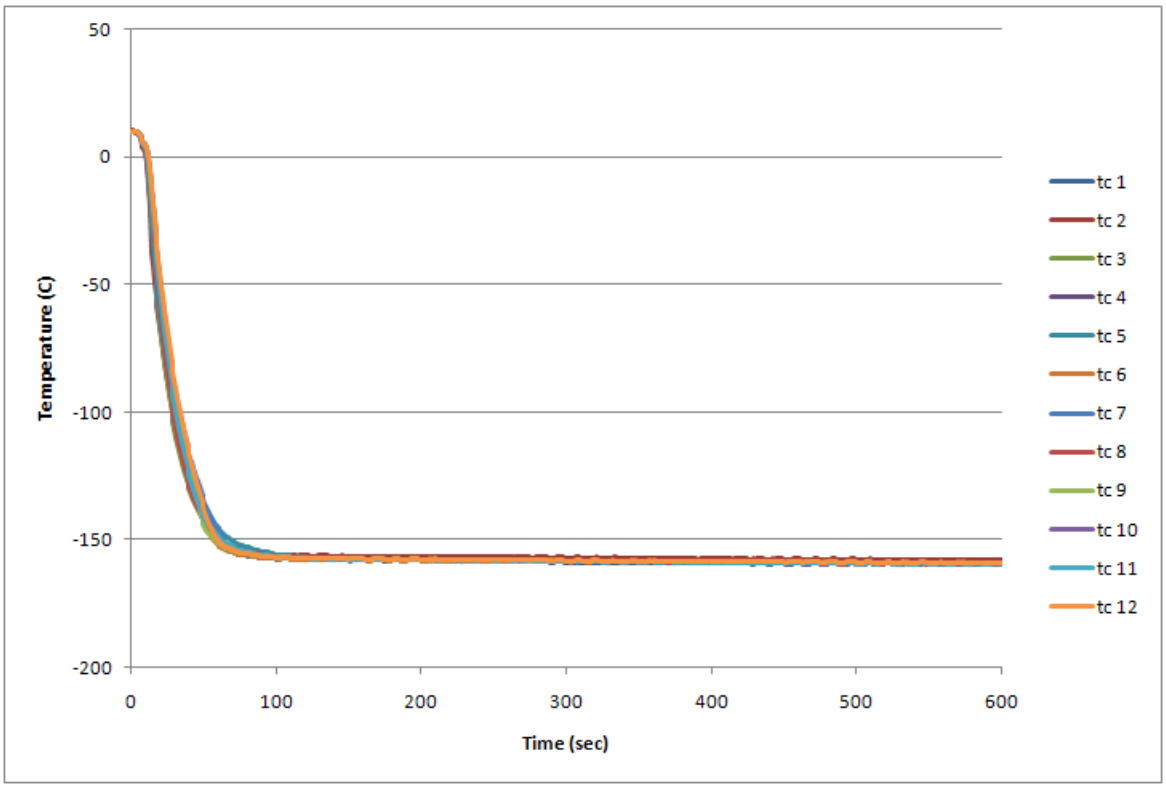

Figure 77. LNG heat transfer thermocouple data – 6 in. x 6 in. x ¼ in. Epoxy

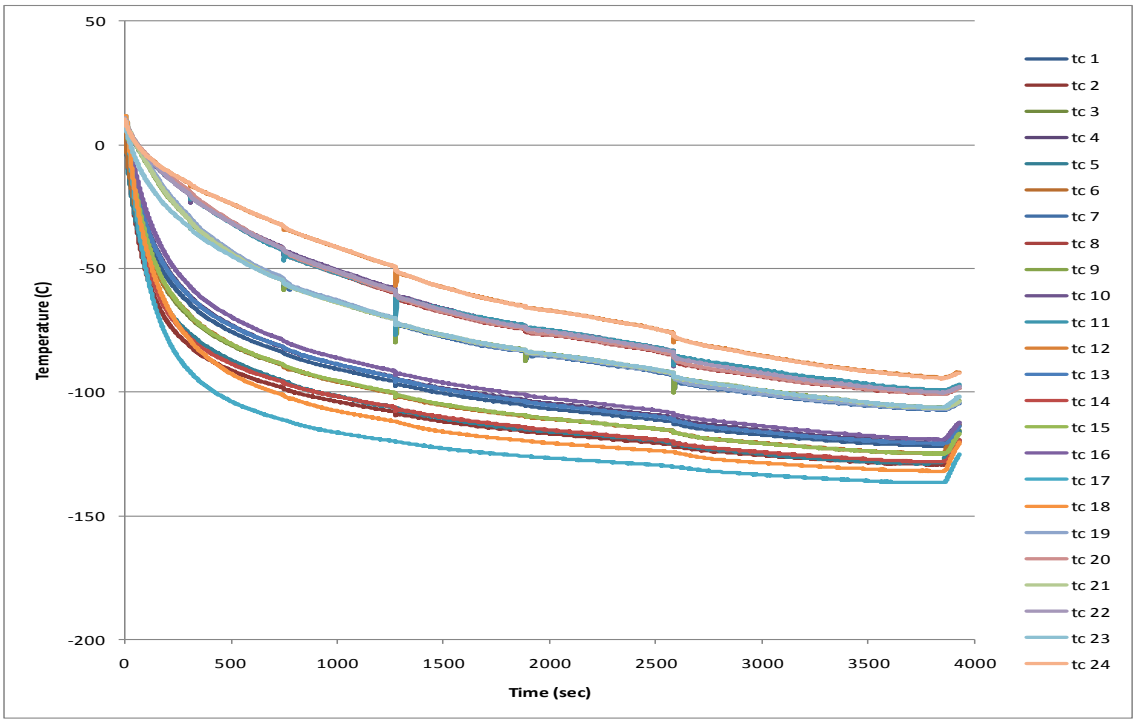

Figure 78. LNG heat transfer thermocouple data – 18 in. x 18 in. x ¾ in. Epoxy

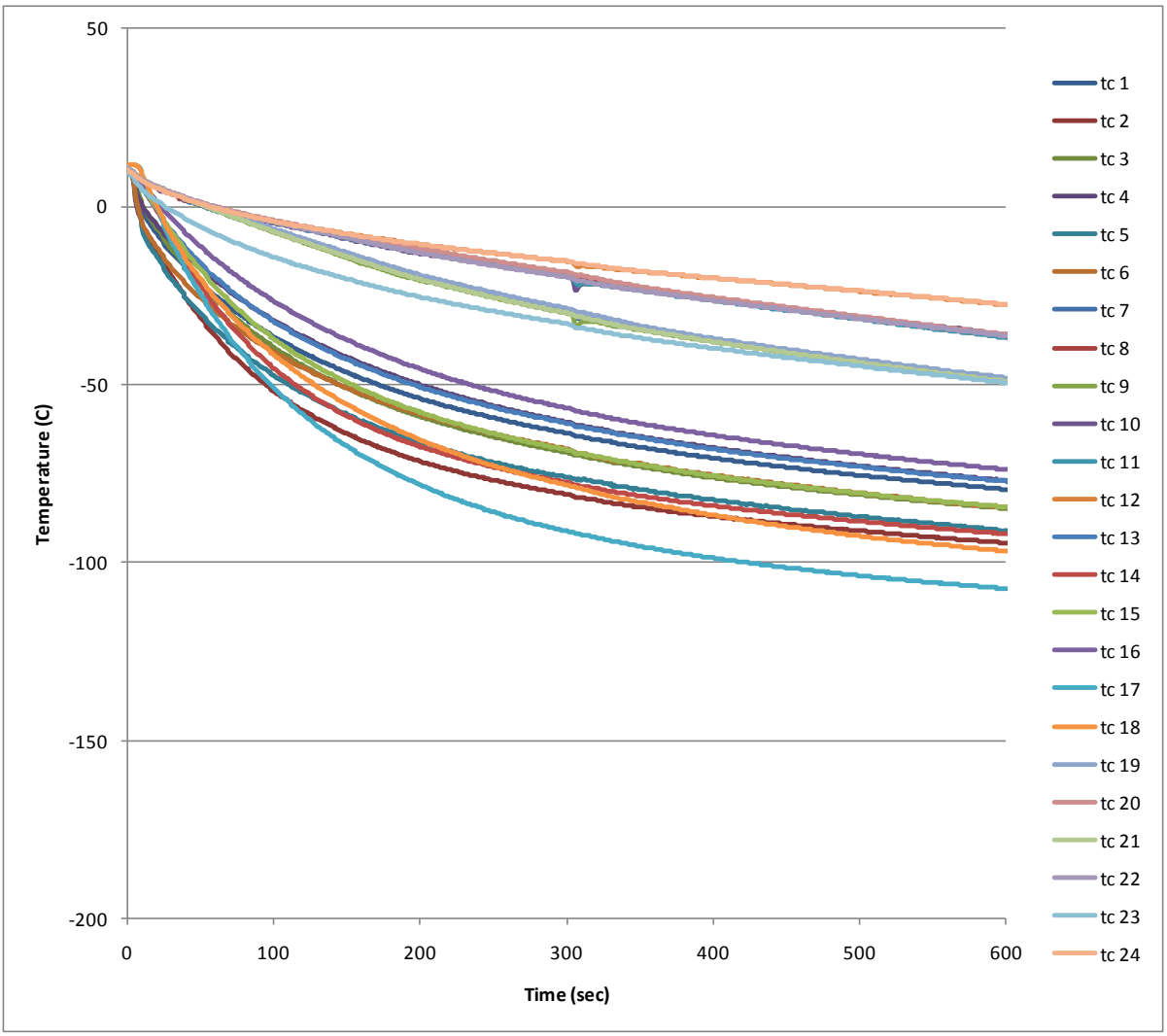

Figure 79. LNG heat transfer thermocouple data – 18 in. x 18 in. x ¾ in. Epoxy (zoom)

Comparisons of the LNG and the LN_2 cooling rates in Figure 82 and Figure 83 show more efficient cooling for the LNG for the ¾ in. bare and epoxy urethane plates, respectively. The LNG tests were conducted with an initial temperature approximately 20°C cooler than the LN_2 tests. However, even when adjusting for this difference, the LNG cooling rates are still higher than the LN_2 rates. Finally, the lowest achieved temperatures in the plates are lower for the LN_2 since it is -191°C and LNG is only -161°C. This difference is not significant since the steel will enter the lower shelf fracture toughness regime well above either of these temperatures. The fracture toughness of the materials used in these tests is discussed in Volume III (Petti et al., 2011) of this study.

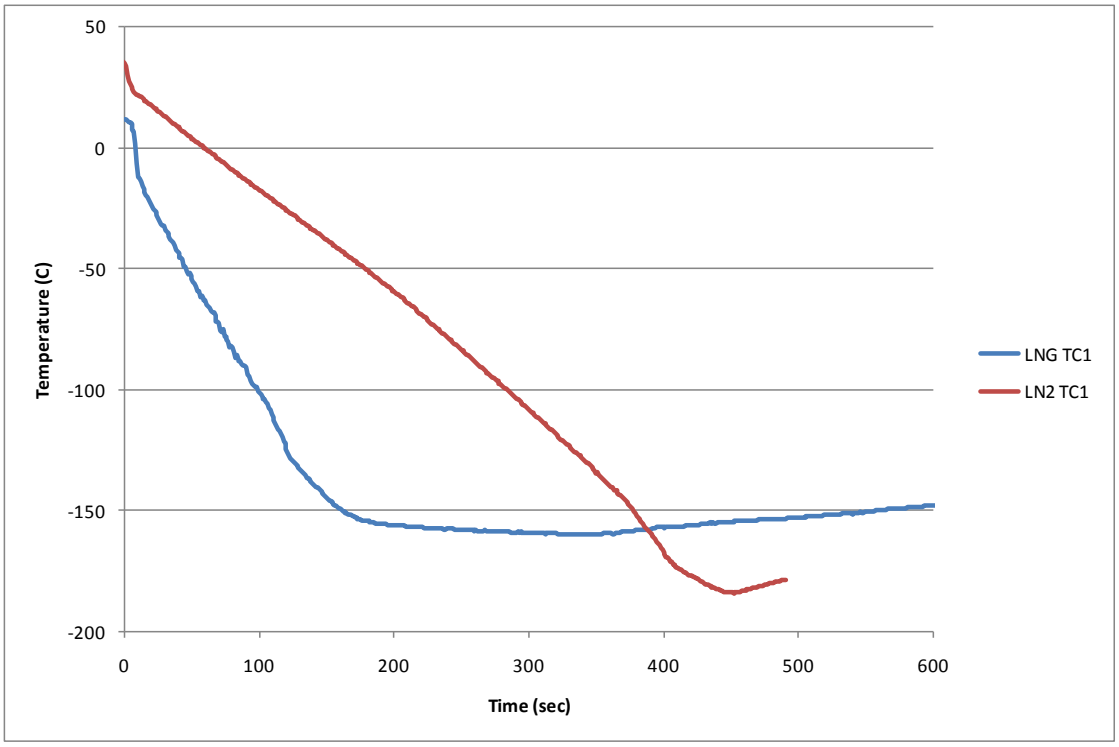

Figure 80. LNG vs. LN_2 heat transfer thermocouple data for TC1 – 6 in. x 6 in. x ¾ in. Bare

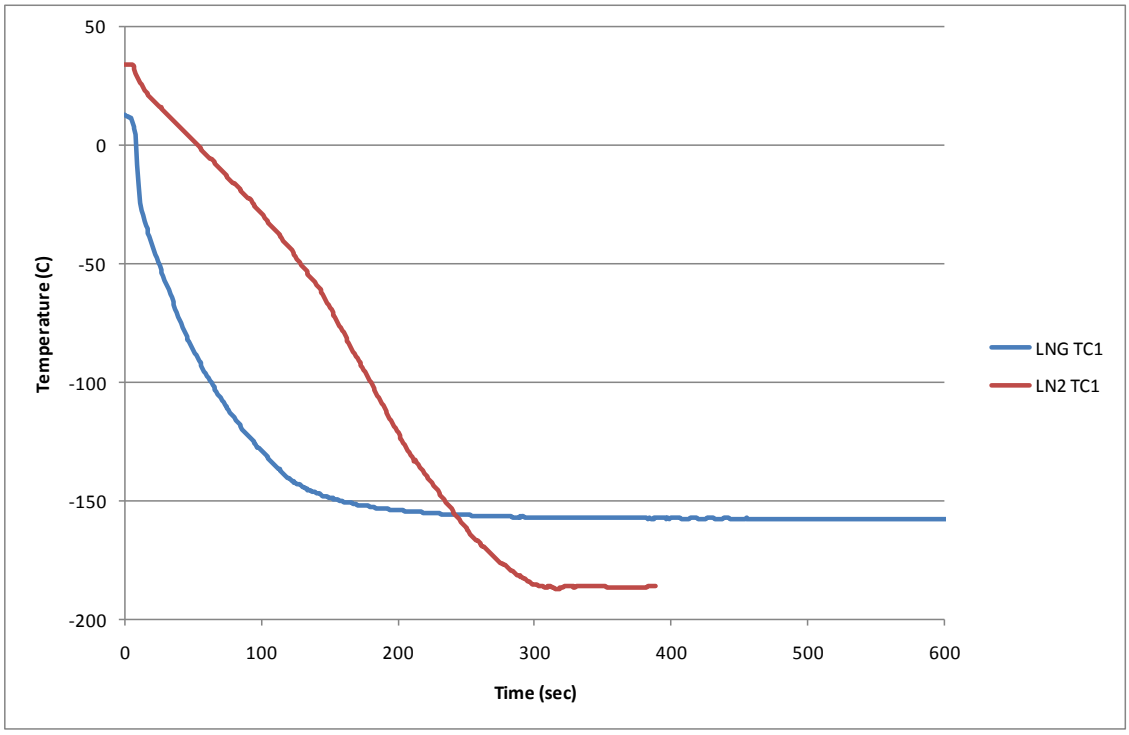

Figure 81. LNG vs. LN_2 heat transfer thermocouple data for TC1 – 6 in. x 6 in. x ¾ in. Epoxy Urethane

6. Summary and Conclusions

This report summarizes the four phases of large-scale testing conducted as part of the Cascading Damage Study to investigate the effect of cryogenic liquids contacting steel plates. The purpose of these tests were to investigate the cooling of steel plates subjected to cryogenic liquids and to study the development and propagation of cracks in the plates due to the induced thermal stresses and lowering fracture toughness. The plate sizes ranged from simple 4 ft square plates in Phase II to 12 ft x 3ft structures with more complex geometry in Phase III. Twenty-two structural tests were conducted in Phases II and III, nine of which resulted in cracking. In order to generate thermally induced fracturing, stress concentration were introduced with varying degrees of severity and typically in stages. In one instance (Test 16), the crack initiated from the weld toe near the connection of a stiffening plate to the main base plate and vertical intersecting plate. Two tests (Test 15 and 24) were each a collection of 6 individual heat transfer tests.

The tests performed in the study are used in the validation of the failure model applied in the computational analysis portion of the project. The details of those analyses are provided in a separate report. Beyond their use in the computational analyses, the test results have provided the following observations and insights:

- The steel plate cracking observed in these tests is representative of brittle cracking observed in steel hull sections of commercial LNG tankers subjected to accidental LNG spills.
- Crack initiation requires a sufficient stress concentration given the temperature of the steel; however, LNG vessels are complex and aged structures containing a large population of crack initiators.
- Fracture propagation generally follows the flow path with the stress fields and microstructure influencing the local fracture patterns.
- Intersecting plates and stiffening elements do not restrict crack propagation along with the larger base plates if also subjected to the cryogenic temperatures.
- Crack propagation is arrested when the crack leaves the low-temperature material region and propagates into the warmer region where the metal is ductile. At this point, load redistribution of the structure/tanker could cause the brittle cracks to extend under ductile tearing. However, since these structures only experienced initial gravitational loads, no noticeable ductile tearing extension was observed in these tests. In actual structures, including LNG tankers, other stresses will be imposed that could theoretically lead to further crack extension by ductile tearing.
- Cooling rates on steel plate sections rely on many factors including the size of the structure, the size of the spill (trough), the plate thickness, the specific cryogenic liquid (LNG vs. LN_2), the presence of water at or near the spill, and the presence of a surface coating. The cooling rate observations and data from these tests are used in the computational analyses.

References

American Society of Testing and Materials (ASTM), (1993) Manual on the Use of Thermocouples in Temperature Measurement: 4th Edition, Manual Series MNL 12.

Anderson, T.L., (1995), Fracture Mechanics Fundamentals and Applications, Second Edition.

Figueroa, V.G., Lopez, C., O'Rourke, K.K., (2011), LNG Cascading Damage Study Volume II: Flow Analysis for Spills from Moss and Membrane LNG Cargo Tanks, SAND2011-9464, Sandia National Laboratories, New Mexico.

Hightower, M., et al. (2004). *Guidance on Risk Analysis and Safety Implications of a Large Liquefied Natural (LNG) Spill Over Water*, SAND2004-6258. Albuquerque, NM: Sandia National Laboratories.

Hightower, M., Luketa-Hanlin, A., Gritzo, L.A., Covan, J.M. (2006). Review of Independent Risk Assessment of the Proposed Cabrillo Liquefied Natural Gas Deepwater Port Project, SAND2005-7339. Albuquerque, NM: Sandia National Laboratories.

Hertzburg, R.W., (1996), Deformation and Fracture Mechanics of Engineering Materials, Fourth Edition.

Petti, J.P., Wellman, G.W., Villa, D., Lopex, C., Figueroa, V.G., Heinstein, M., (2011), LNG Cascading Damage Study Volume III: Vessel Structural and Thermal Analysis Report, SAND2011-6226, Sandia National Laboratories, New Mexico.

Roue, Roger, (2011), Personal communication between Roger Roue, SIGTTO (Society of International Gas Tanker & Terminal Operators Ltd) and M. Hightower (Sandia National Laboratories).

Appendix A – Stress Concentrations

In order to explain the effects of stress concentrations, a simple example is provided here. Equation 1 and 2 along with Figure 82 illustrate a stress concentration at the edge of a circular or elliptical hole in a plate (Hertzberg, 1996). For a circular hole, the major (a) and minor (b) axes are equal, $a = b$, and therefore, $\sigma_{max} = 3\sigma_{applied}$. For an elliptical flaw, Eq. 1 can be modified to be a function of the radius of curvature (ρ) of the end of the ellipse resulting in Eq. 2. Equation 2 also includes the assumption that the length of the ellipse is much larger than the radius of curvature. Equation 2 illustrates that as the length of the ellipse increases, or notch in our cases, the stress at the edge of the ellipse also increases. In addition, a reduction of ρ also increases the edge stress. The introduction of the machined notches to the drilled holes in our tests increased the stress significantly.

$$\sigma_{max} = \sigma_{applied}\left(1 + \frac{2a}{b}\right) \quad \text{Eq. 1}$$

$$\sigma_{max} = 2\sigma_{applied}\sqrt{a/\rho} \quad \text{Eq.2}$$

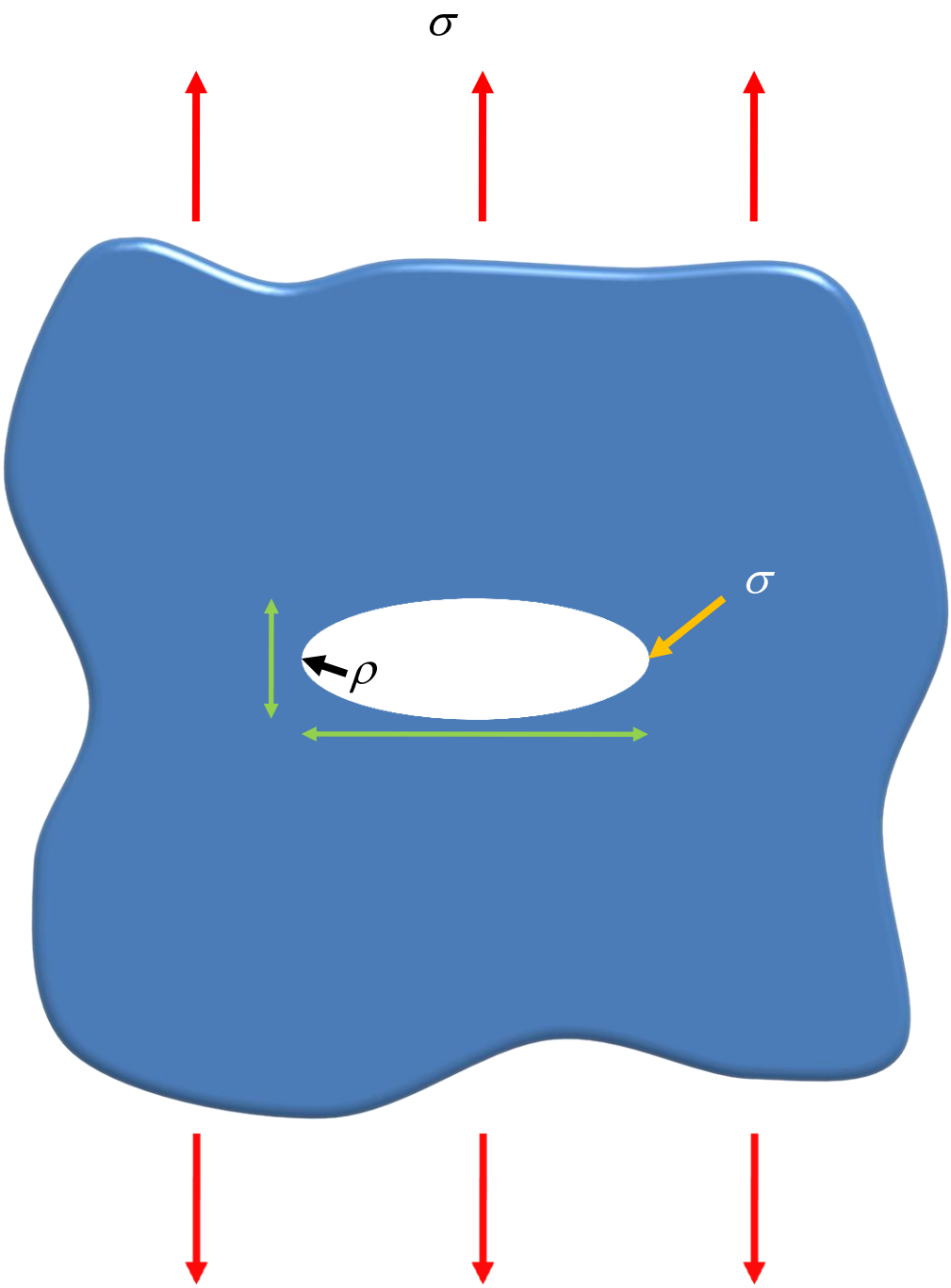

Figure 82. Stress Concentration at Circular and Elliptical holes in Plates

As ρ continues to decrease toward 0, the ellipse transitions into a "crack" in which the tip theoretically becomes perfectly sharp. Cracks of prefect sharpness, ρ = 0, do not actually exist, some small blunting is always present. In addition, material yielding prevents the stresses from increasing beyond the material strength. Using Linear Elastic Fracture Mechanics (LEFM) (Anderson, 1995), this mathematically sharp crack tip region is commonly referred to as a "singularity". The amplitude of the singularity is defined with the stress intensity factor, $K_{I\text{-}applied}$. Equation 3 is used to compute the stress intensity factor for a through crack in an infinite plate as show in Figure 83. The fracture toughness of the structural steels used in LNG construction decreases with temperature. At LNG temperature (-161^{o}C), these steels are extremely brittle and have reached their "lower shelf" fracture toughness. This makes LEFM appropriate in predicting fracture when the applied stress intensity, $K_{I\text{-}applied}$, exceeds the fracture toughness of the material for a given temperature and flaw size (a).

$$K_{I-applied} = \sigma_{applied}\sqrt{\pi a} \qquad \text{Eq. 3}$$

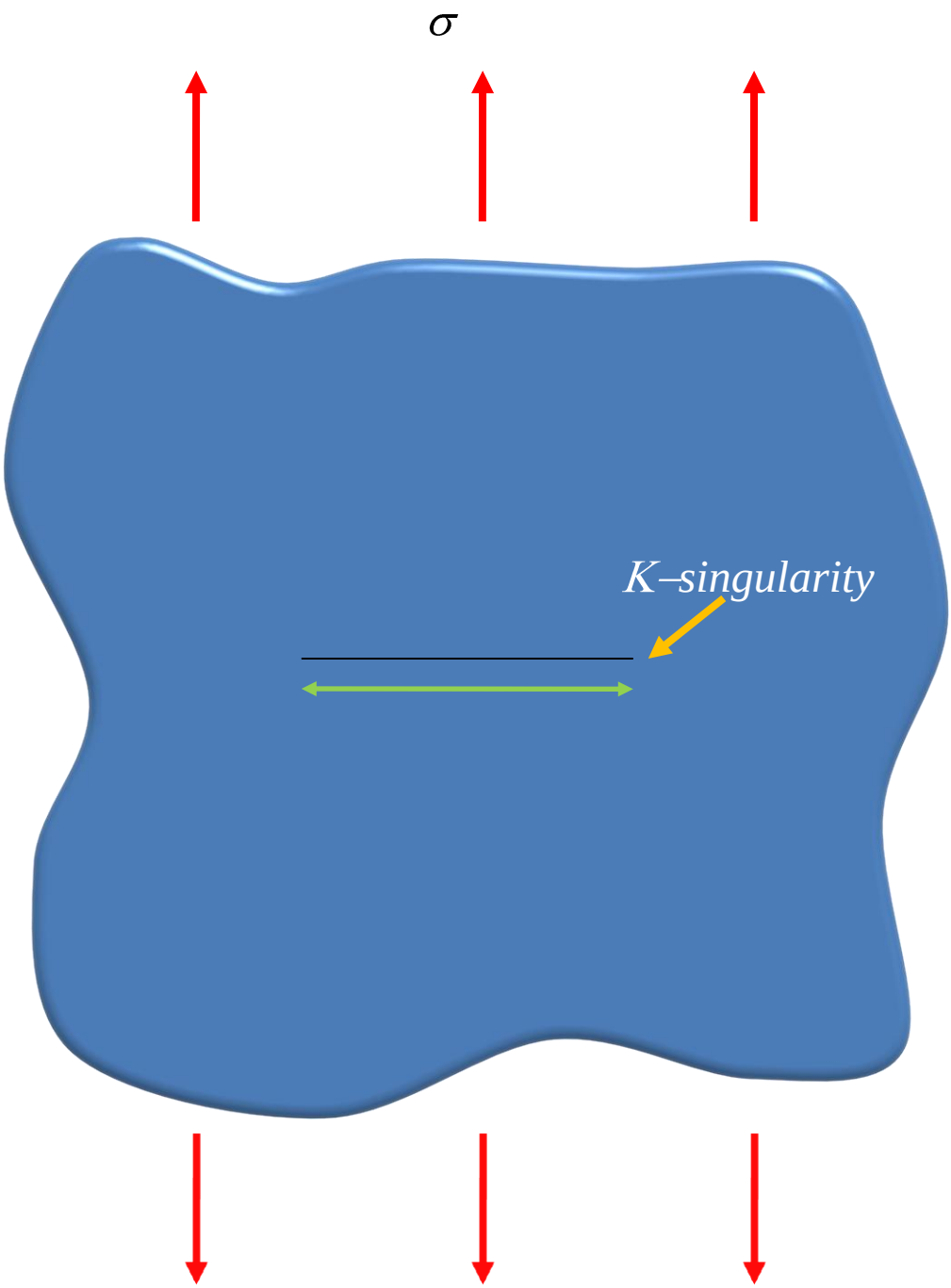

Figure 83. Crack Tip Stresses in Plates

Appendix B – Test Data

The complete set of thermocouple data are provided in this Appendix for the Phase II and III tests. For Tests 1 through 12, Figure 11 shows the thermocouple locations. For Tests 17 through 21, Figure 27 illustrates the thermocouple locations, For Tests 13 and 14, Figure 39 shows the thermocouple locations. Finally, for Tests 16, 22, and 23, Figure 46 provides the thermocouple locations.

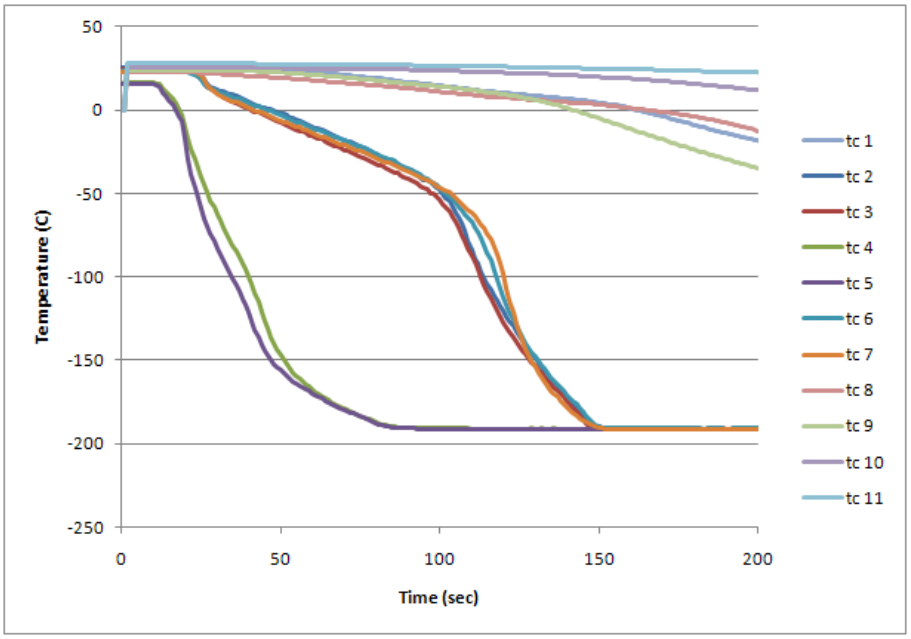

Figure 84. Test 1 – TCs 1-11

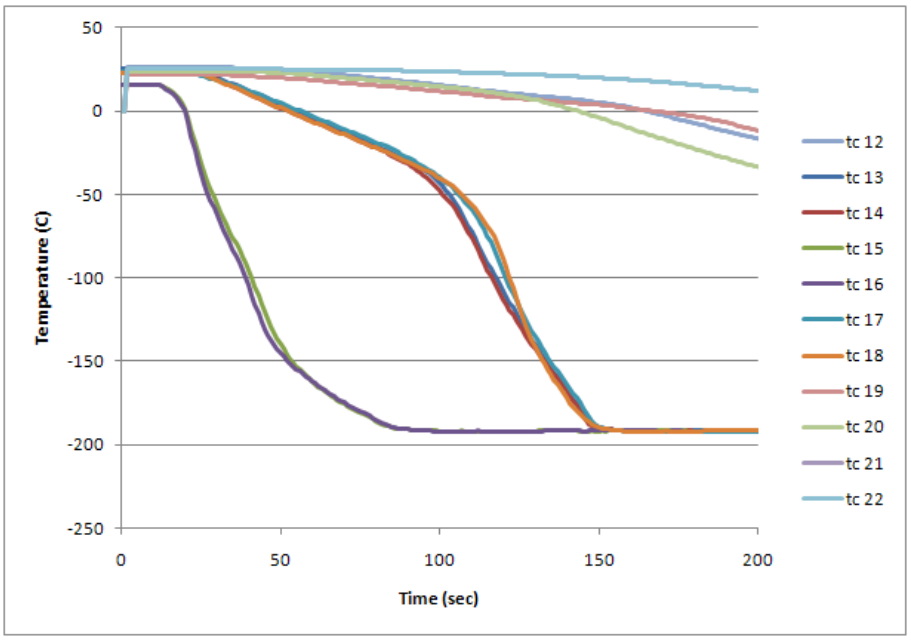

Figure 85. Test 1 – TCs 12-22

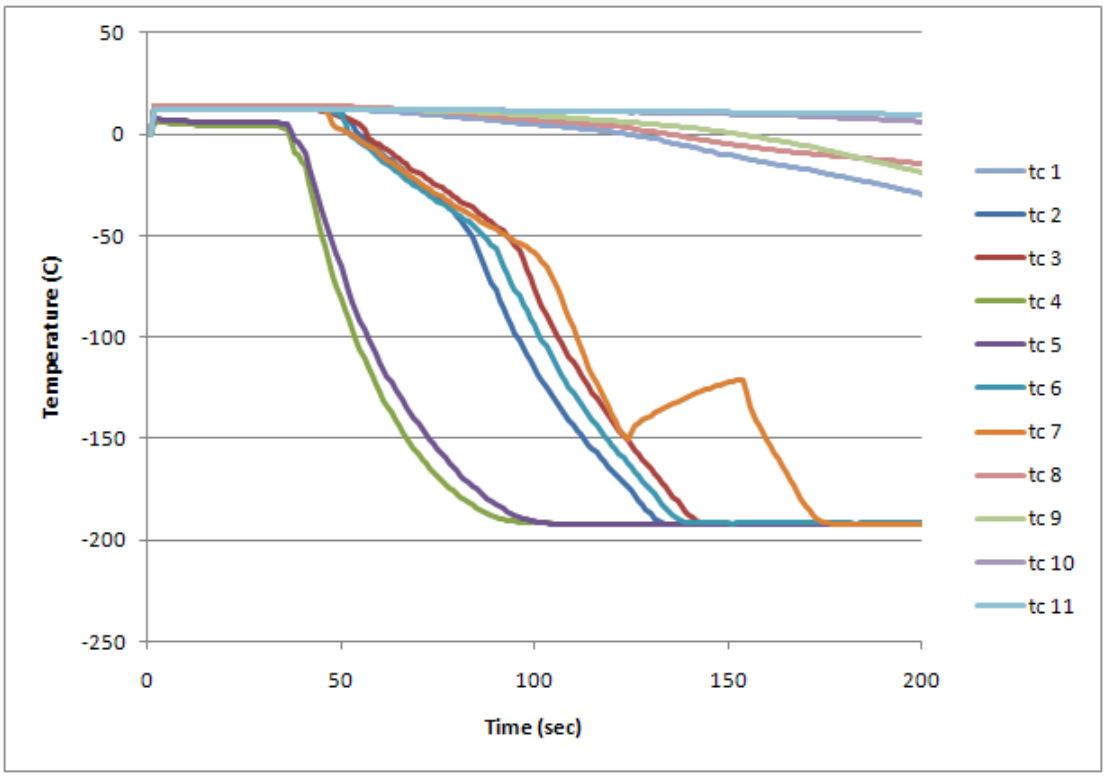

Figure 86. Test 2 – TCs 1-11

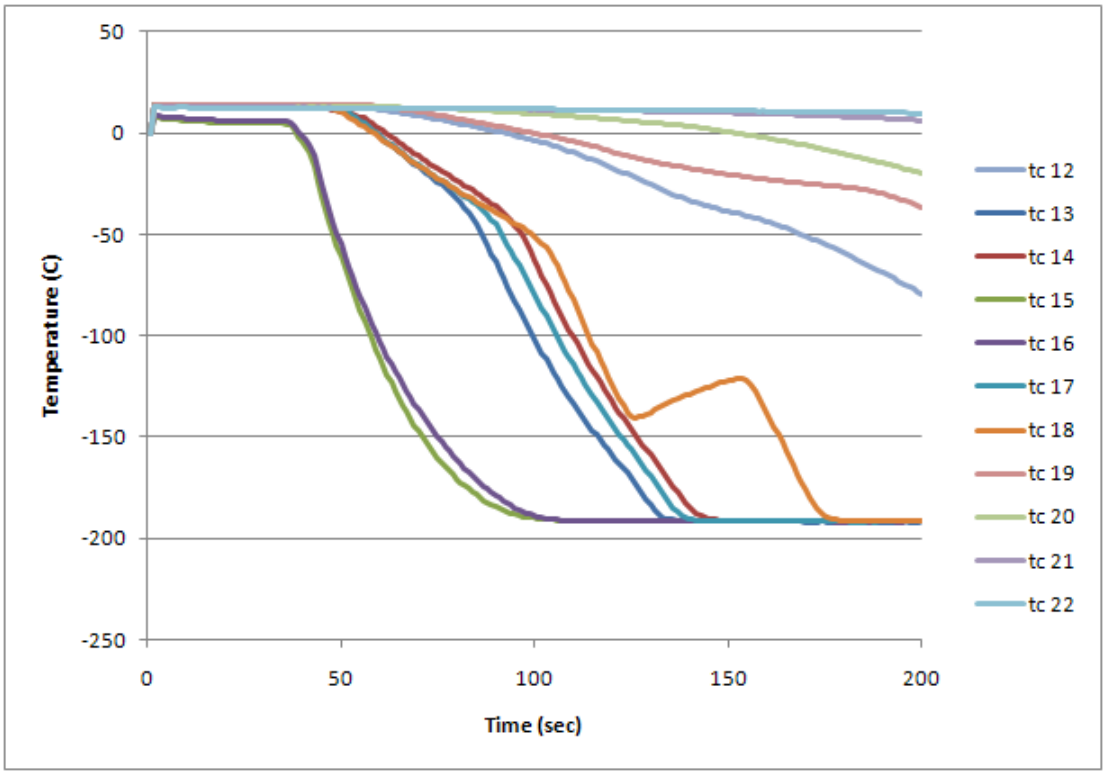

Figure 87. Test 2 – TCs 12-22

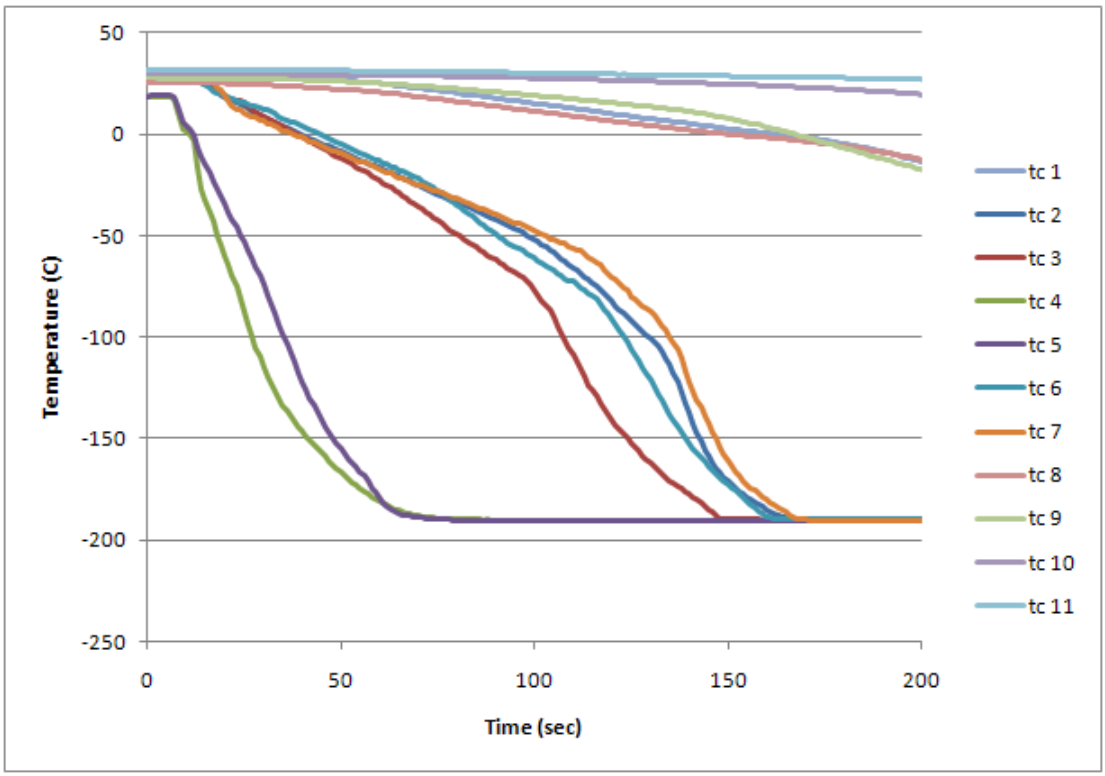

Figure 88. Test 3 – TCs 1-11

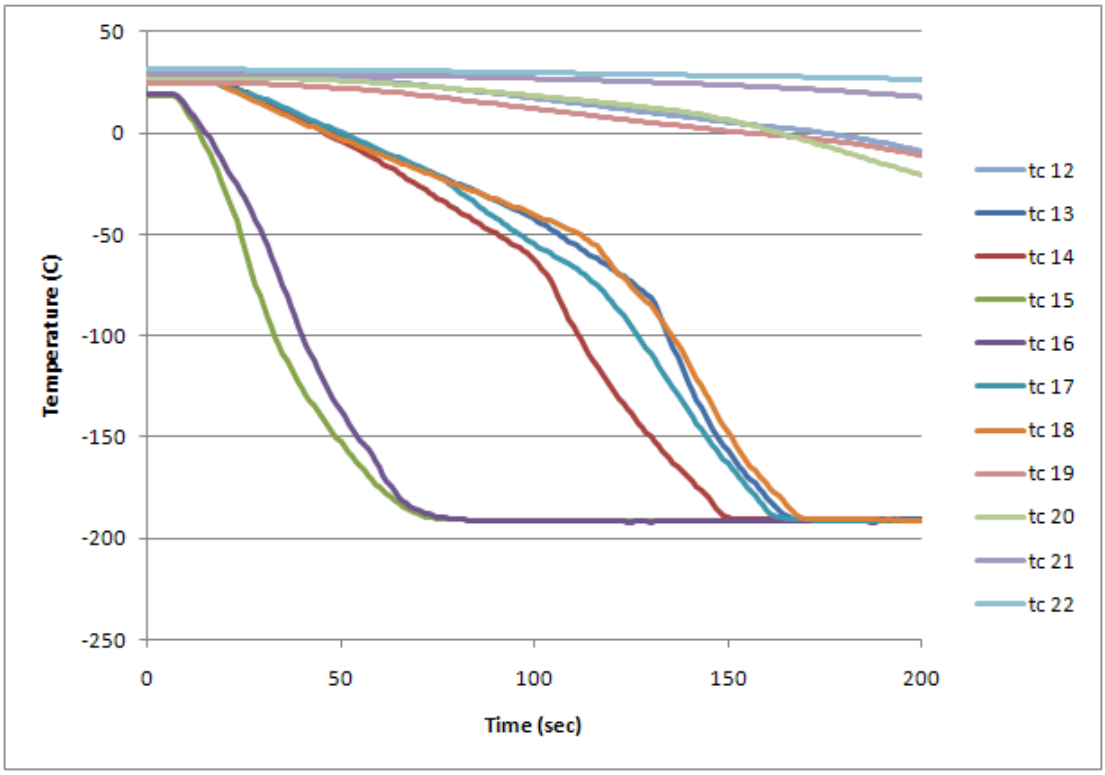

Figure 89. Test 3 – TCs 12-22

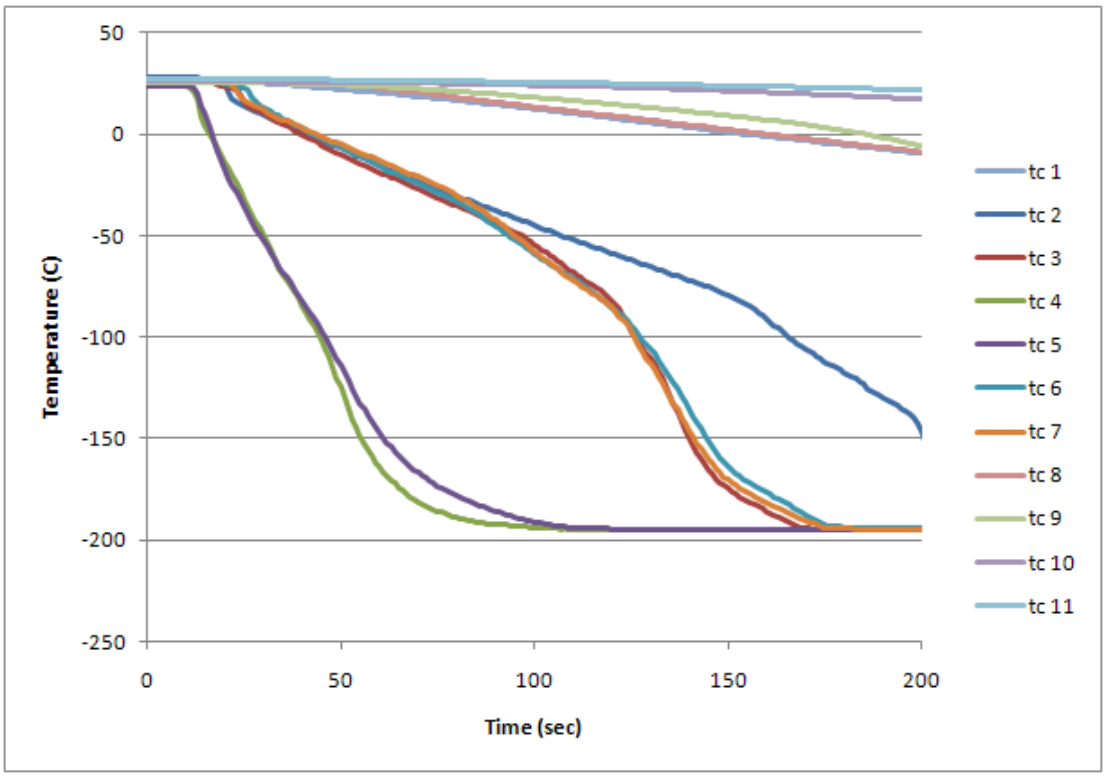

Figure 90. Test 4 – TCs 1-11

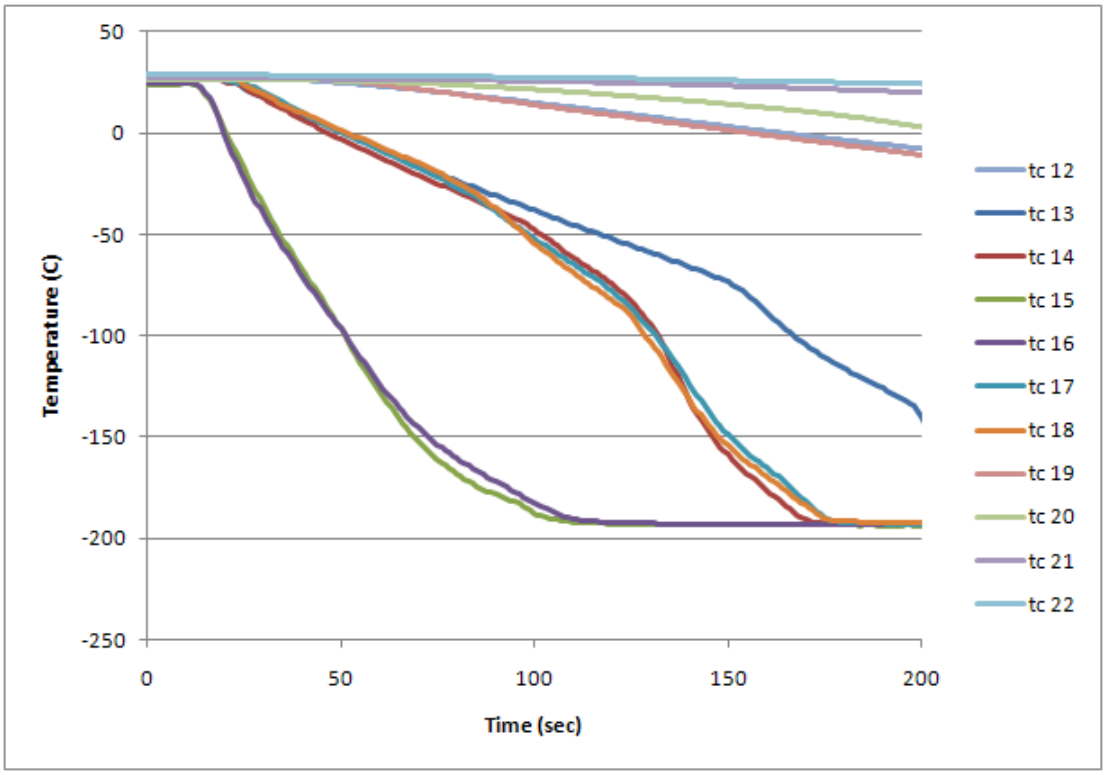

Figure 91. Test 4 – TCs 12-22

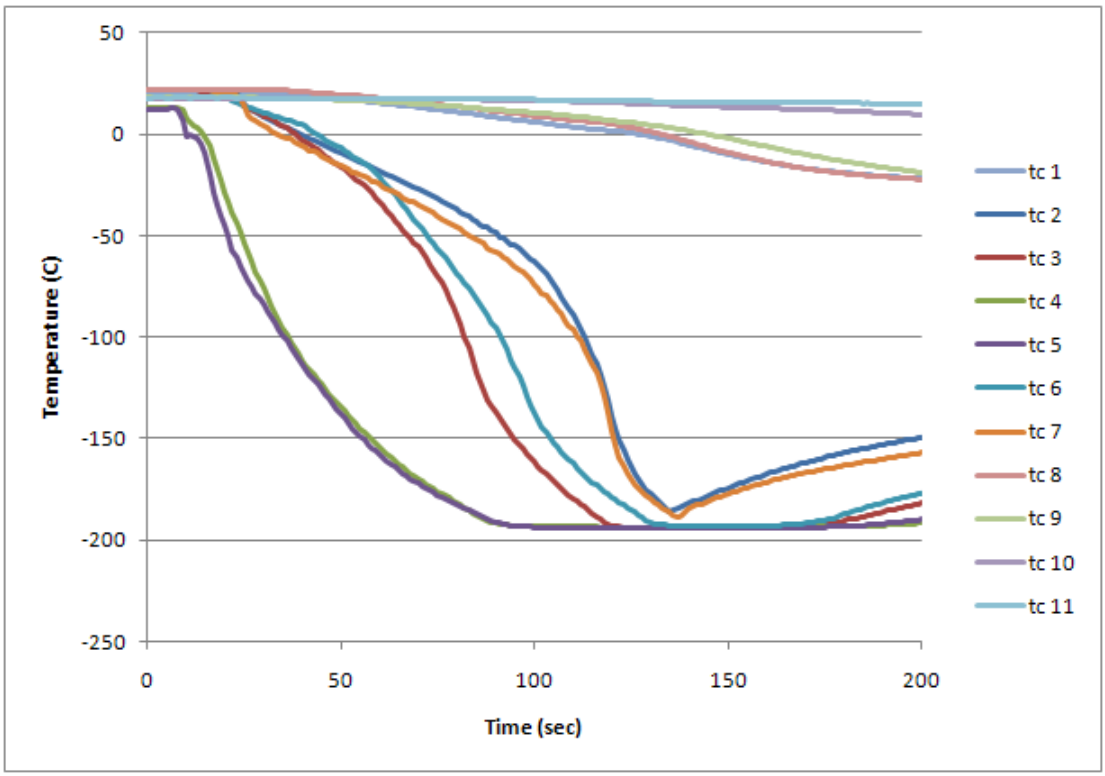

Figure 92. Test 5 – TCs 1-11

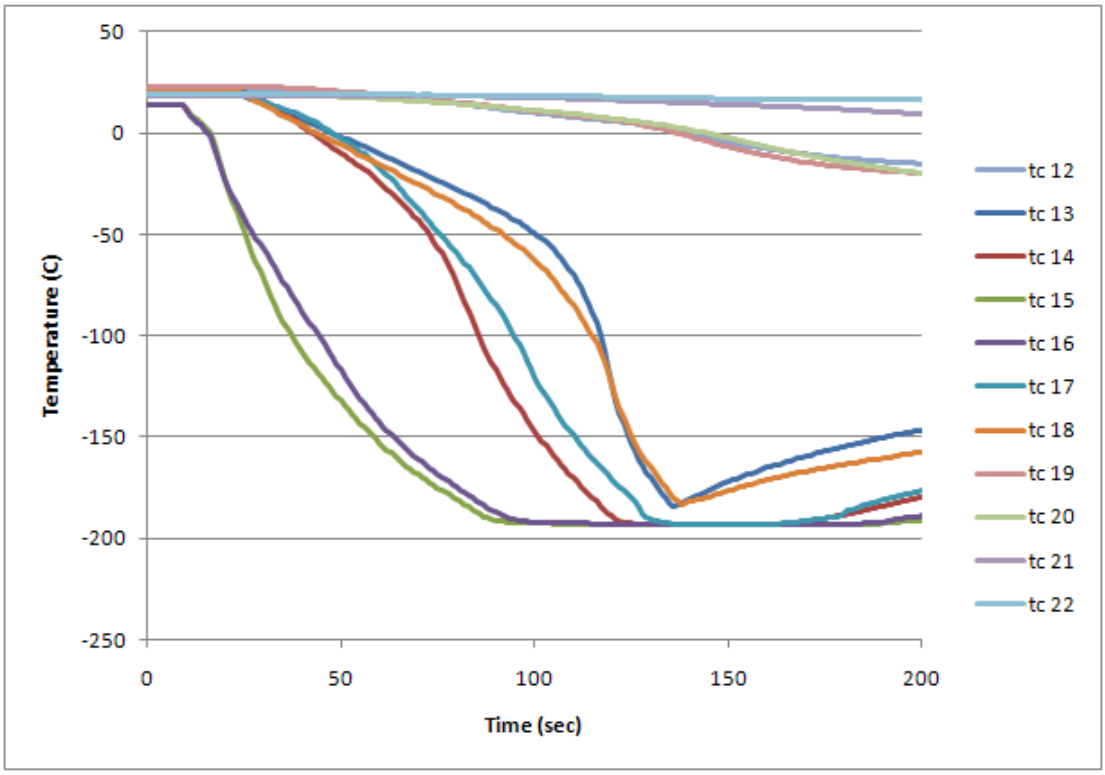

Figure 93. Test 5 – TCs 12-22

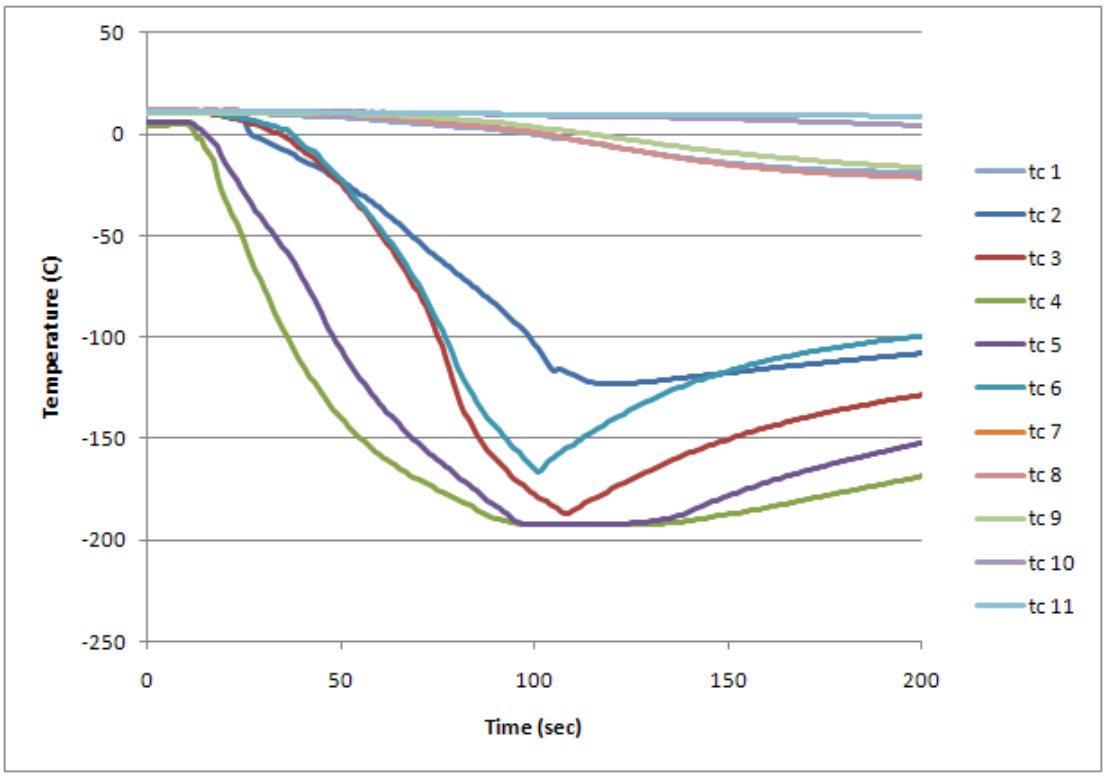

Figure 94. Test 6 – TCs 1-11

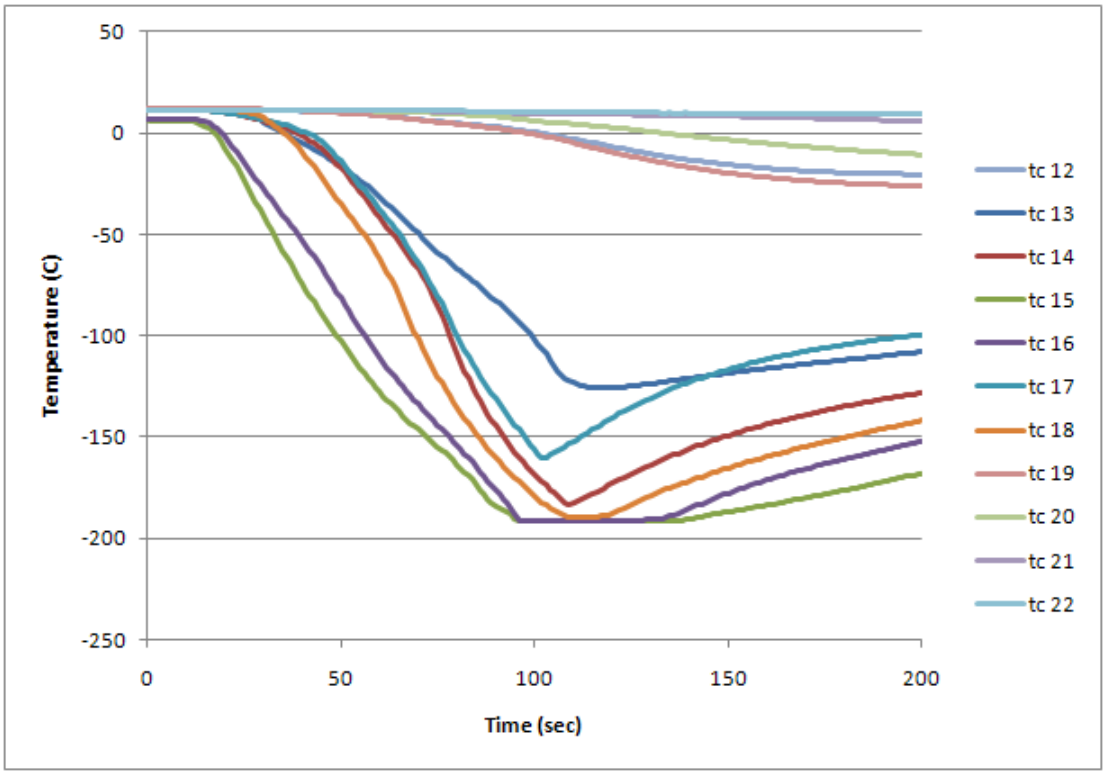

Figure 95. Test 6 – TCs 12-22

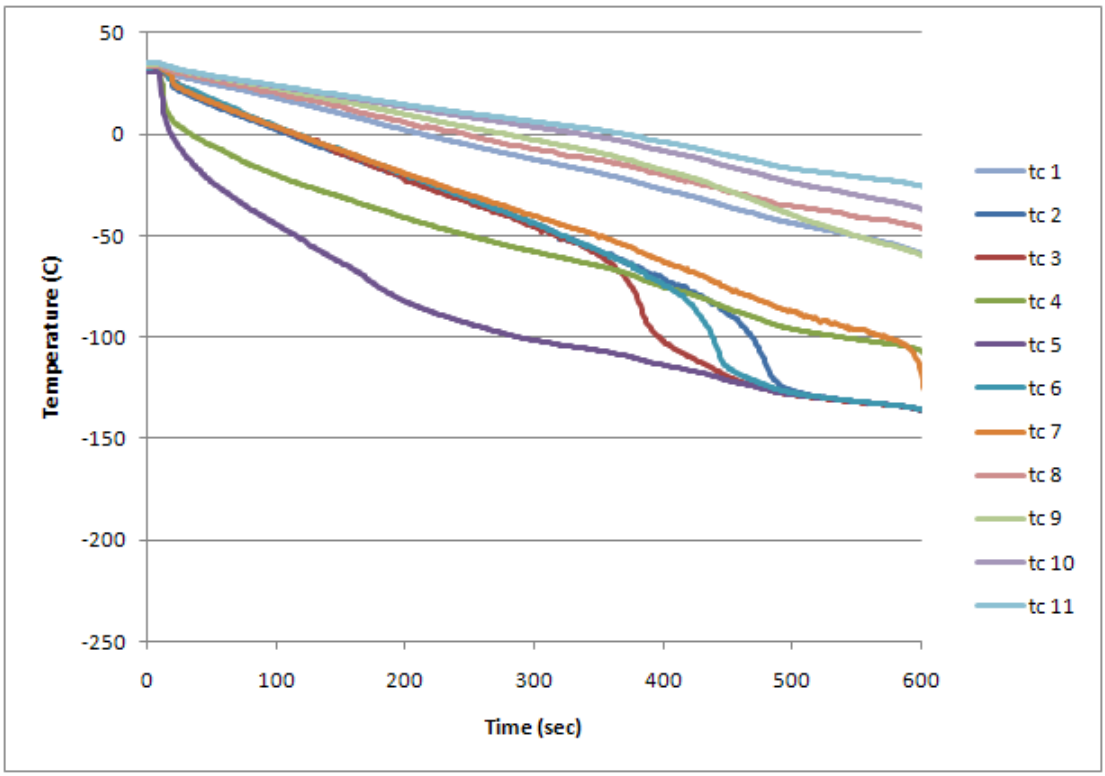

Figure 96. Test 7 – TCs 1-11

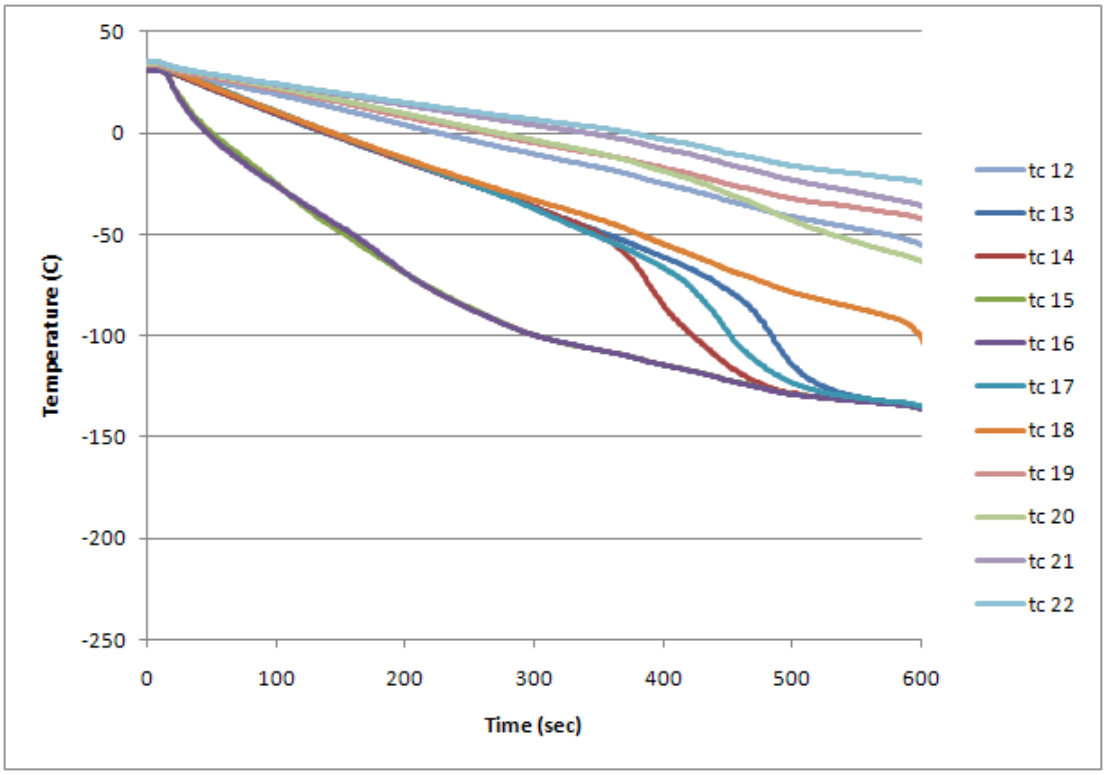

Figure 97. Test 7 – TCs 12-22

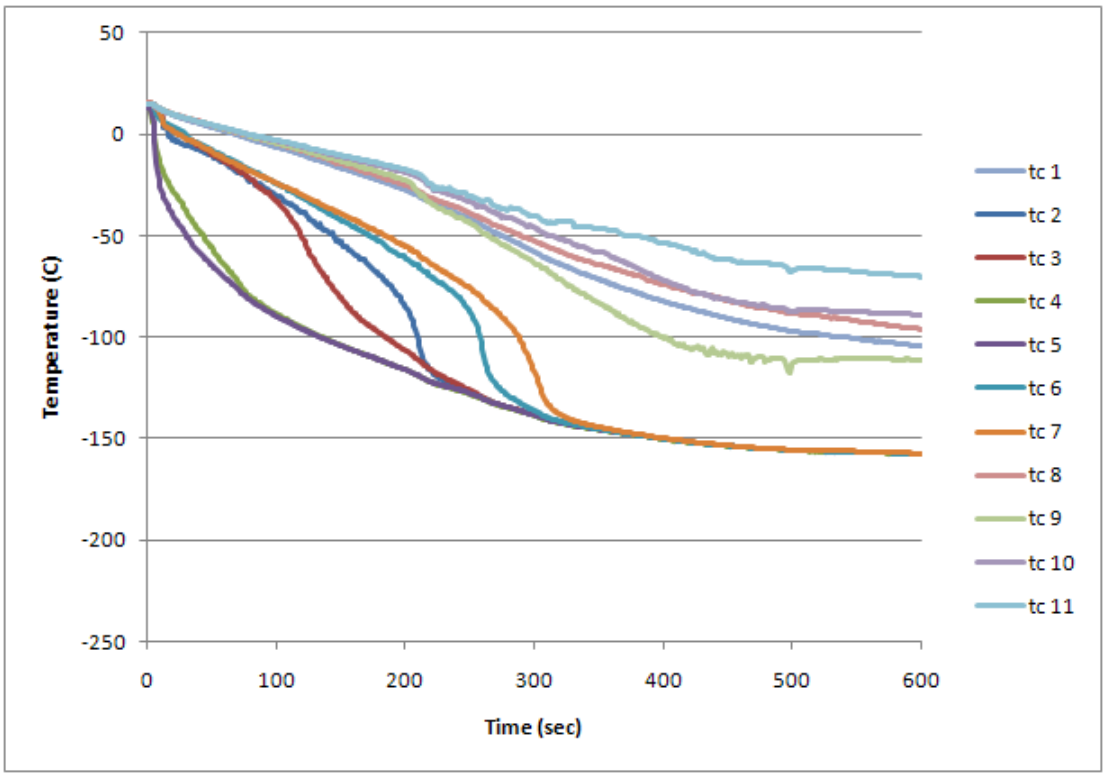

Figure 98. Test 8 – TCs 1-11

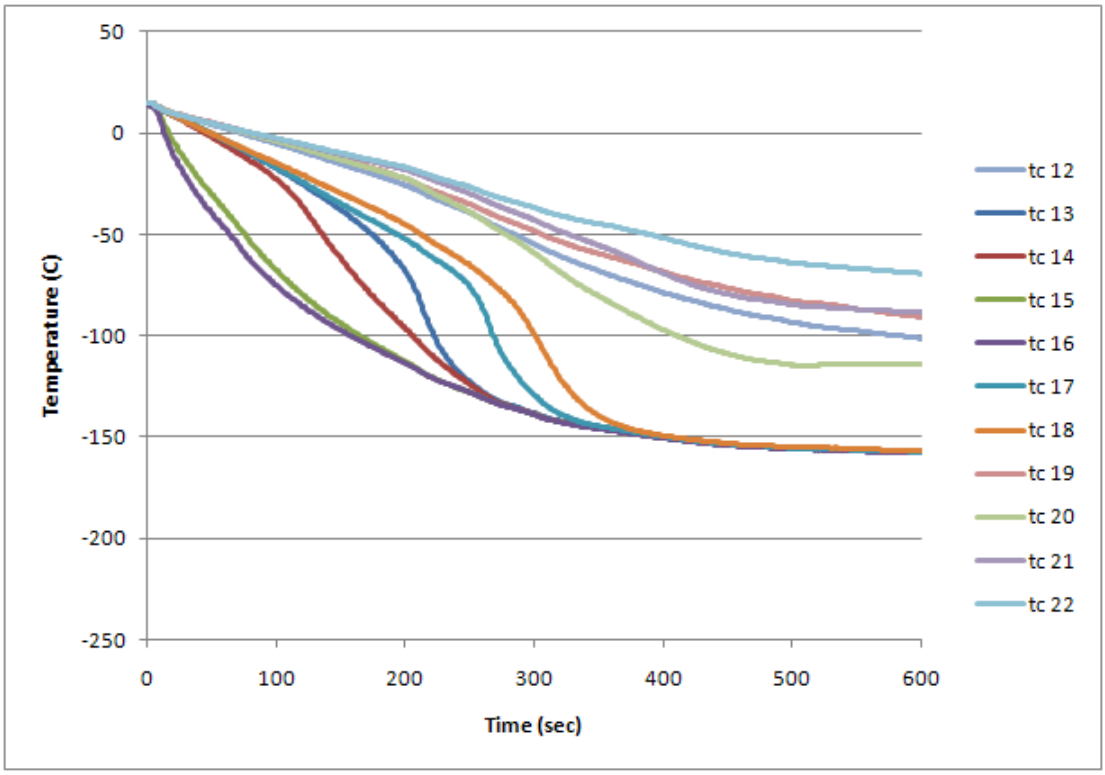

Figure 99. Test 8 – TCs 12-22

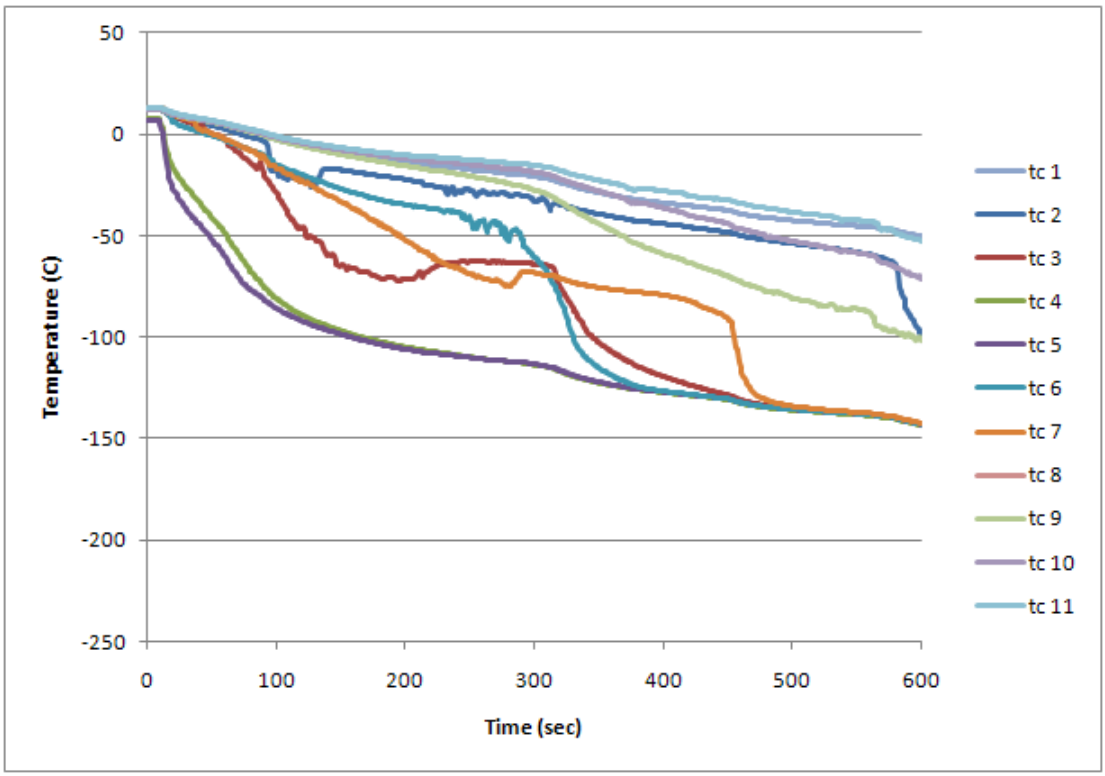

Figure 100. Test 9 – TCs 1-11

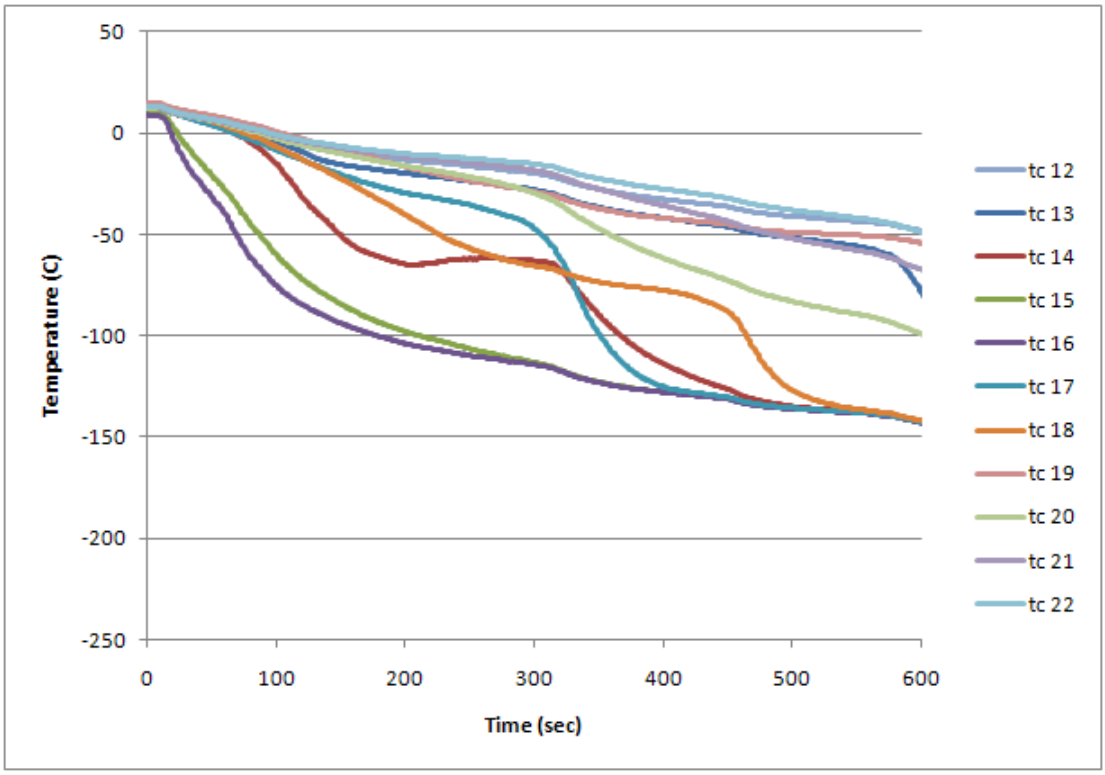

Figure 101. Test 9 – TCs 12-22

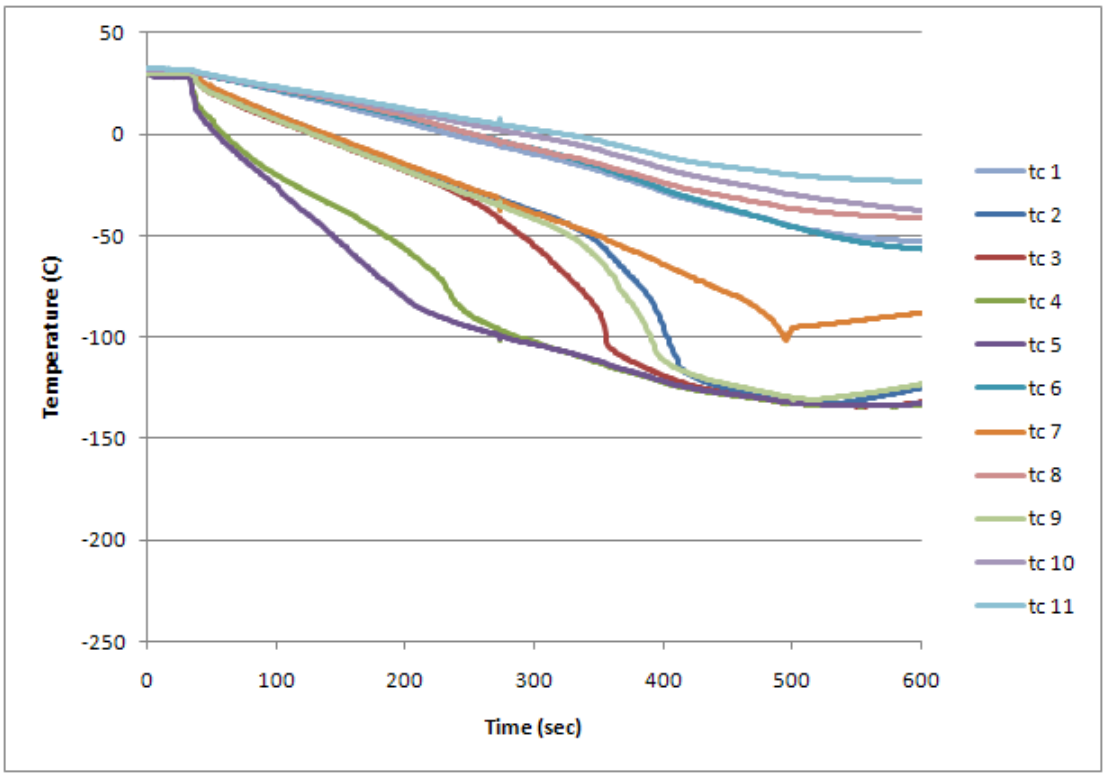

Figure 102. Test 10 – TCs 1-11

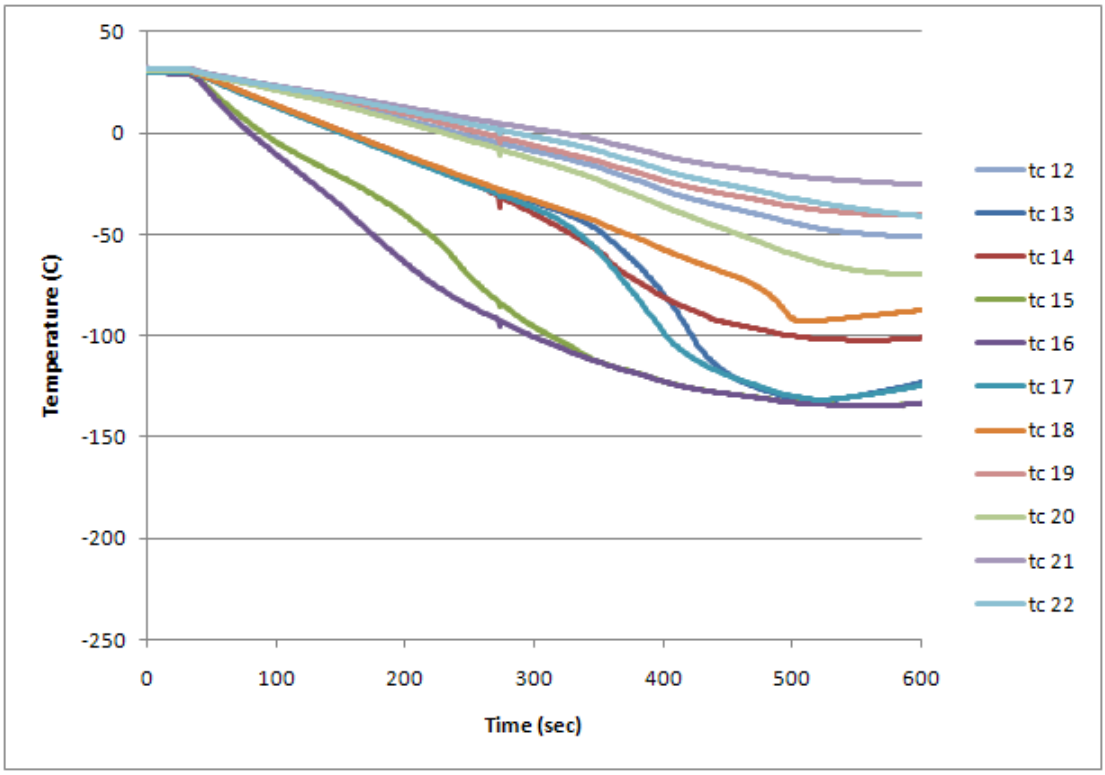

Figure 103. Test 10 – TCs 12-22

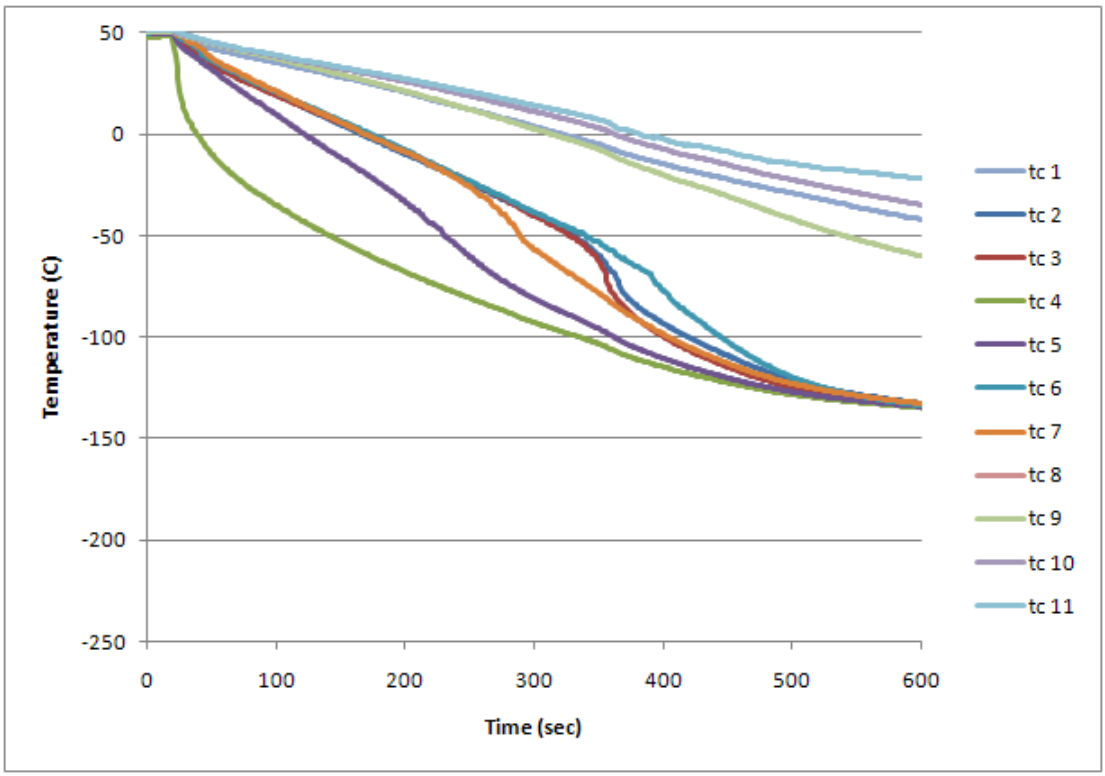

Figure 104. Test 11 – TCs 1-11

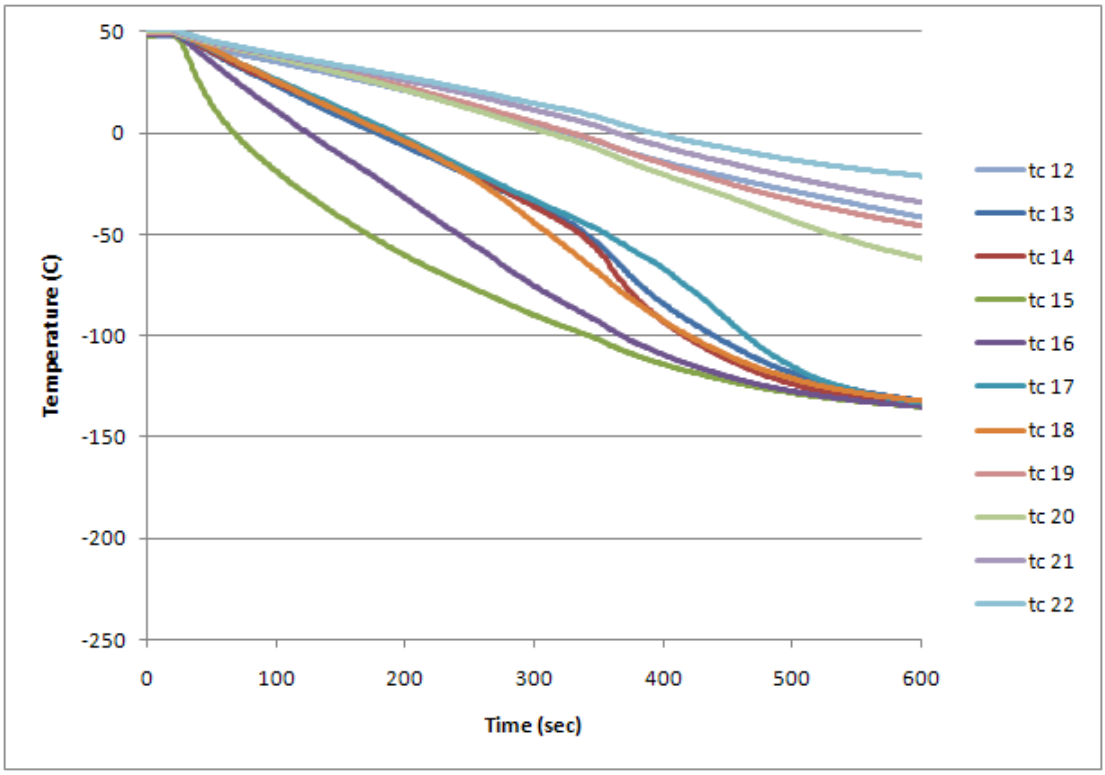

Figure 105. Test 11 – TCs 12-22

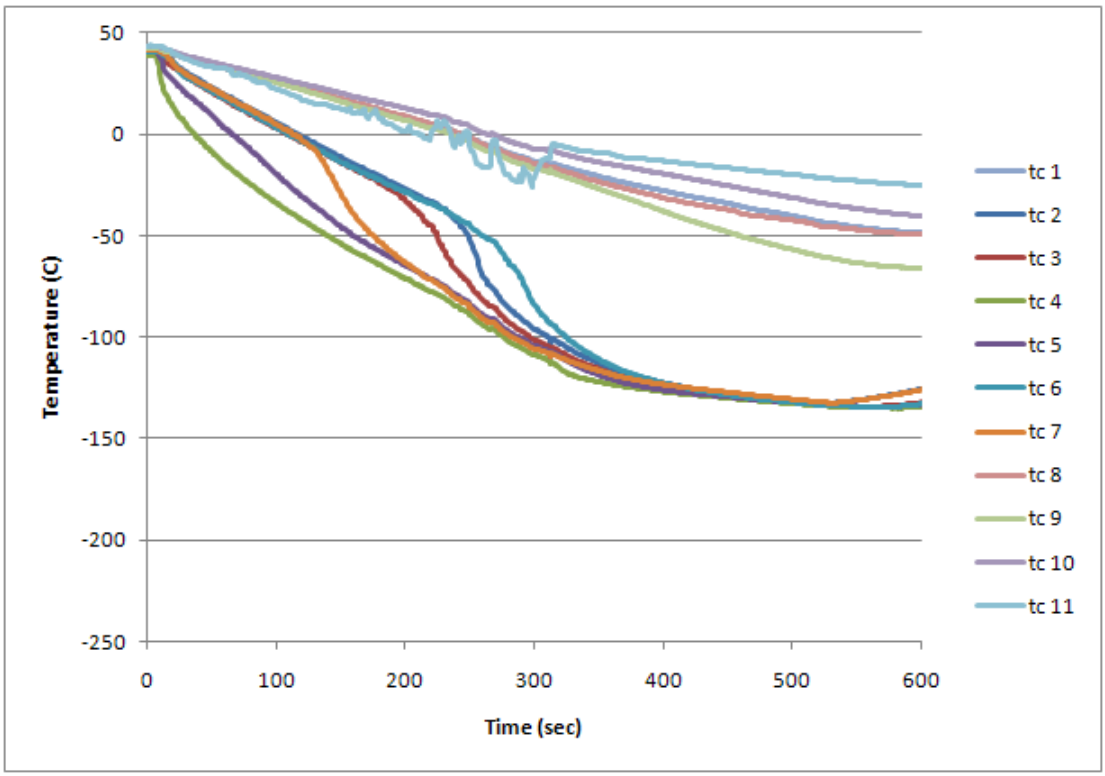

Figure 106. Test 12 – TCs 1-11

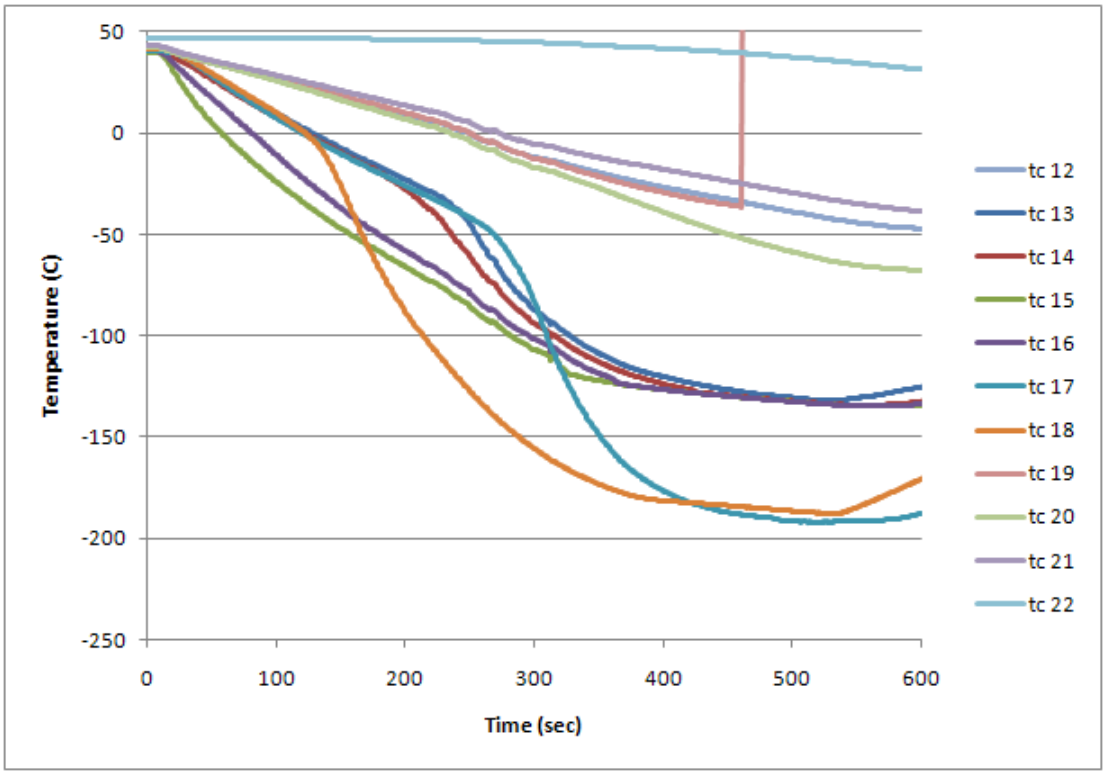

Figure 107. Test 12 – TCs 12-22

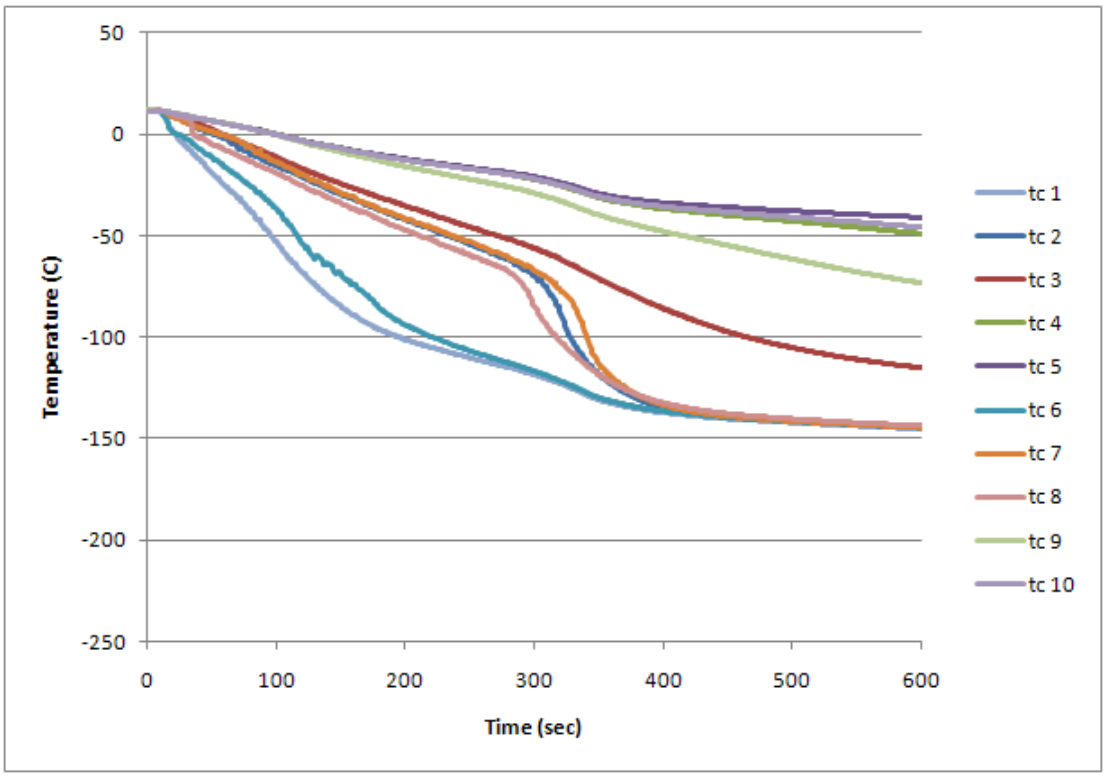

Figure 108. Test 17 – TCs 1-10

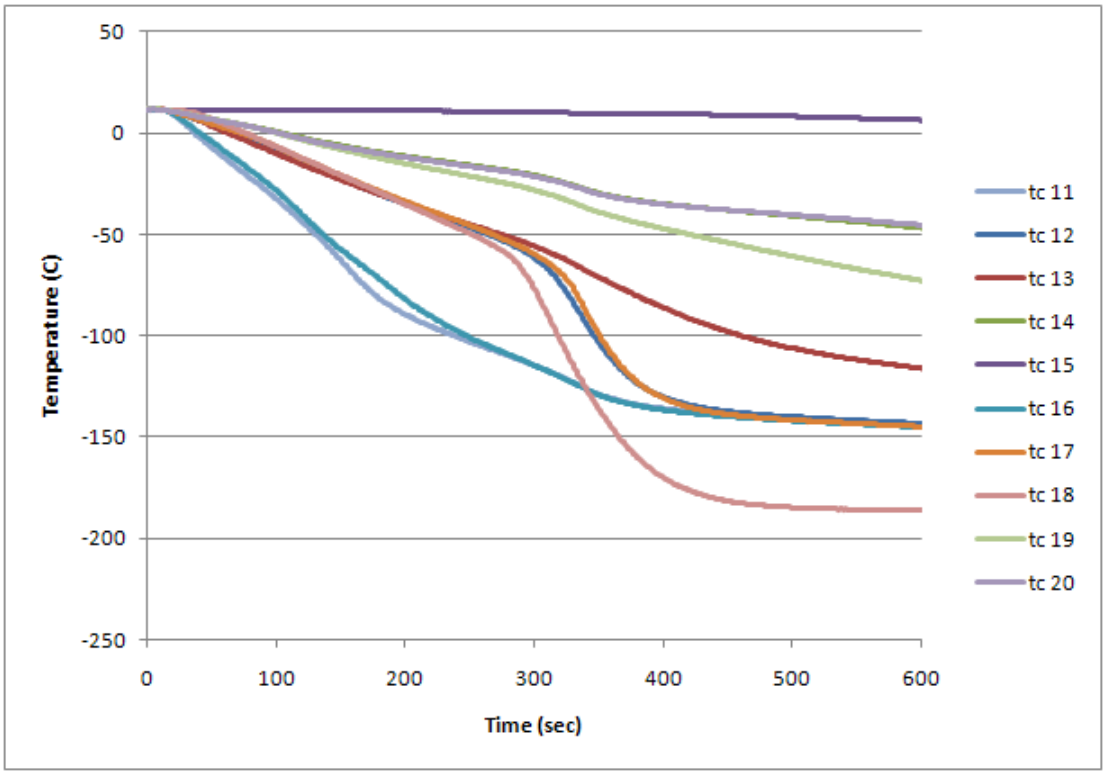

Figure 109. Test 17 – TCs 11-20

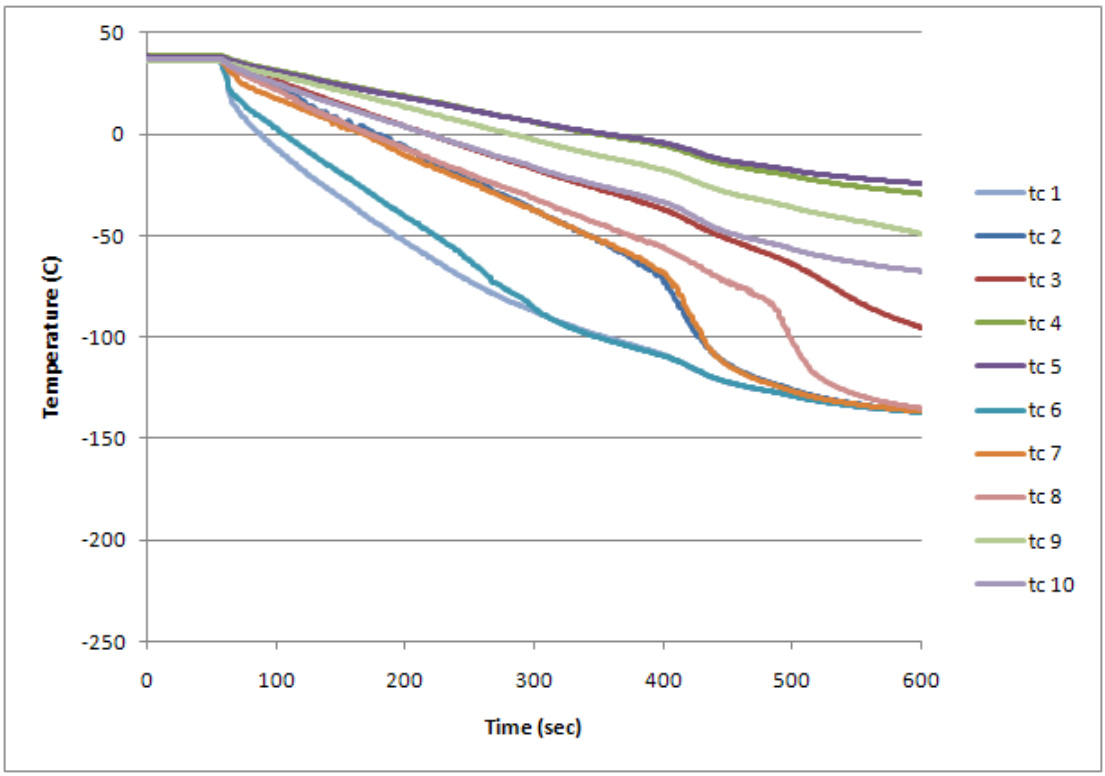

Figure 110. Test 18 – TCs 1-10

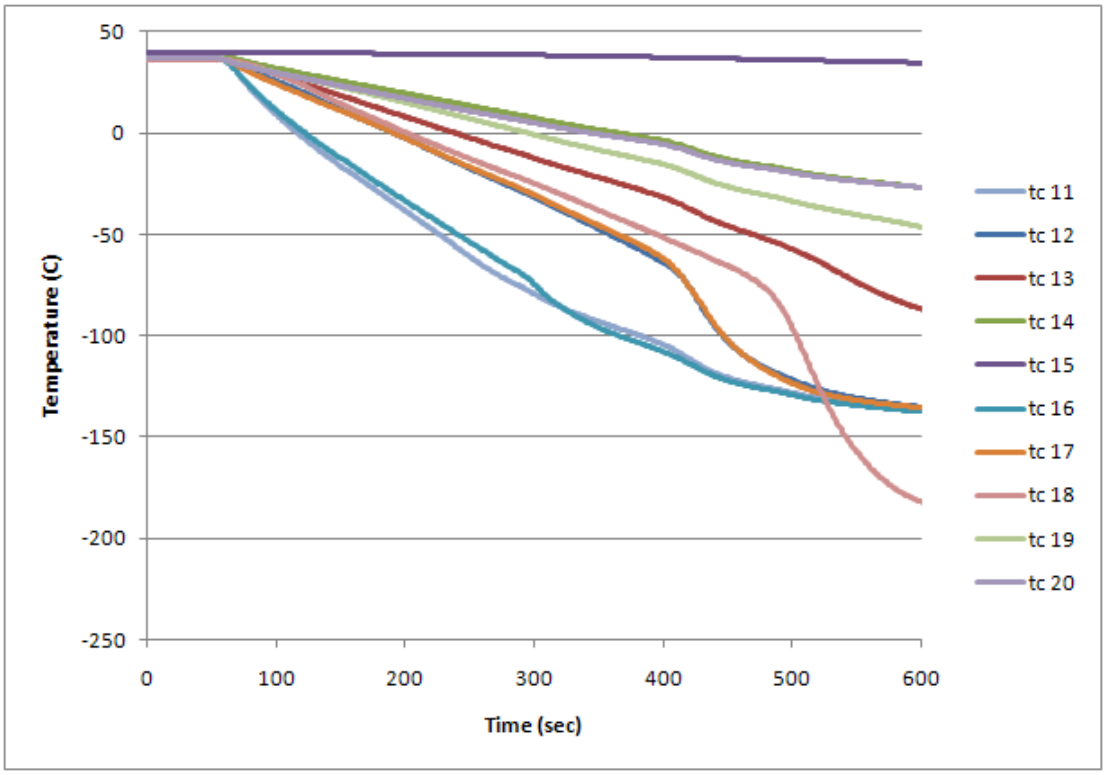

Figure 111. Test 18 – TCs 11-20

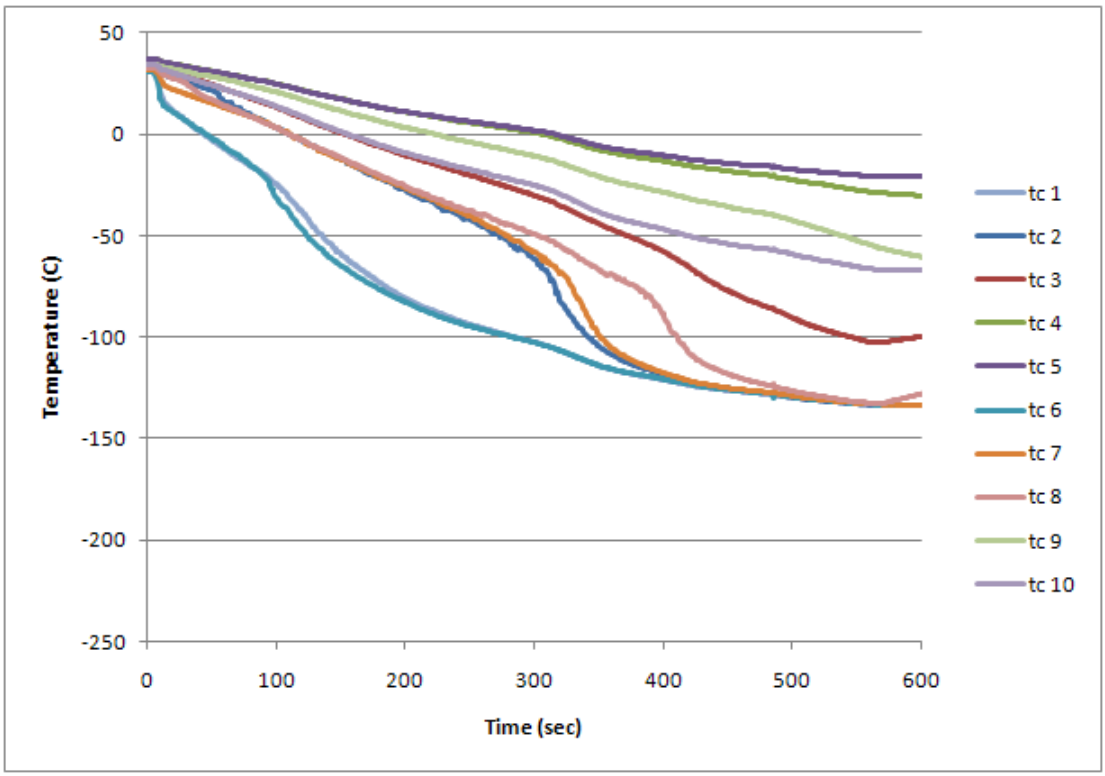

Figure 112. Test 19 – TCs 1-10

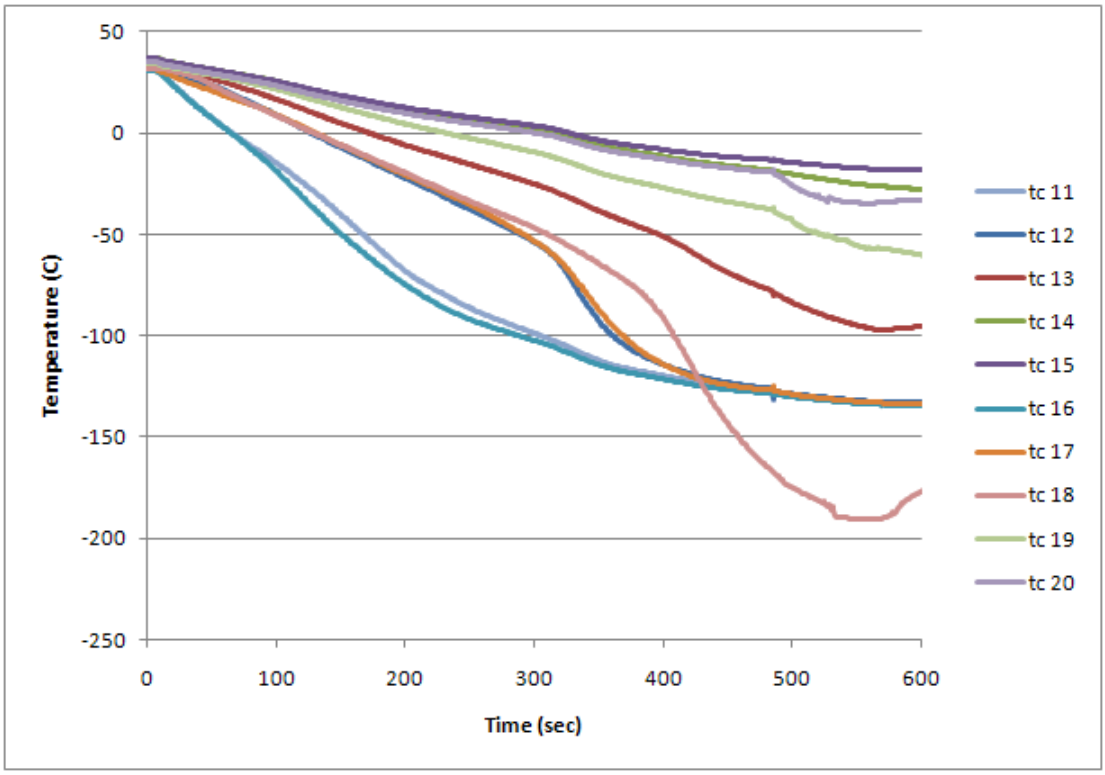

Figure 113. Test 19 – TCs 11-20

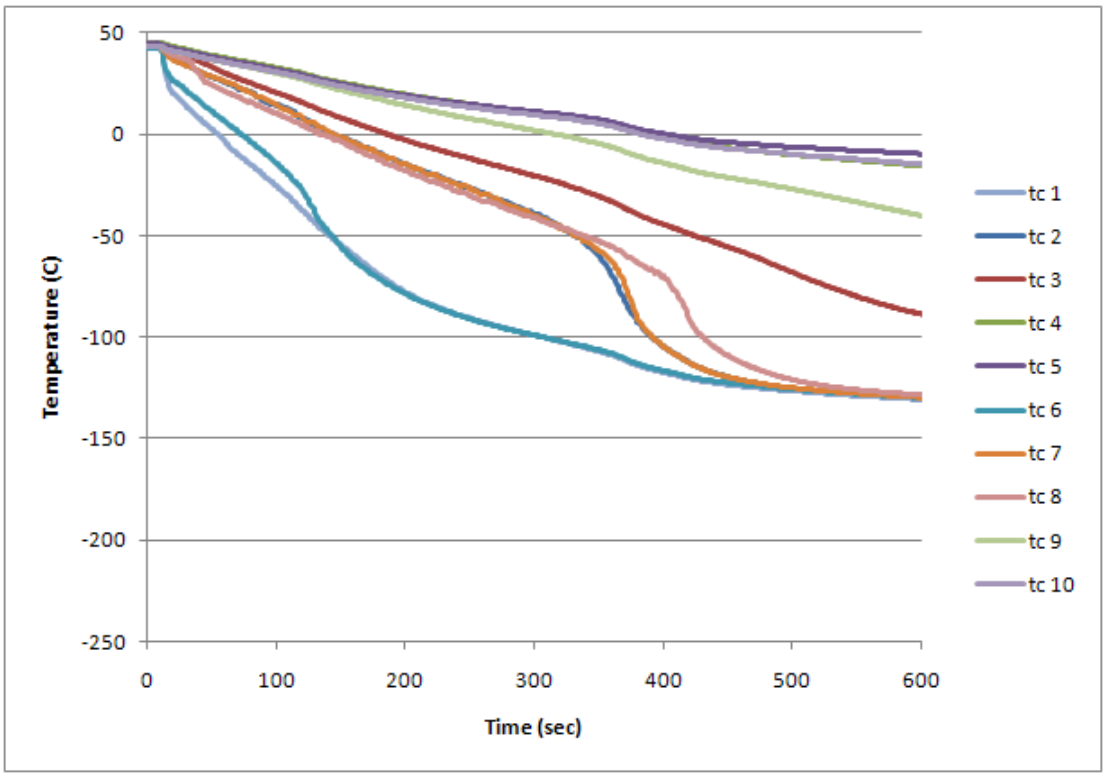

Figure 114. Test 20 – TCs 1-10

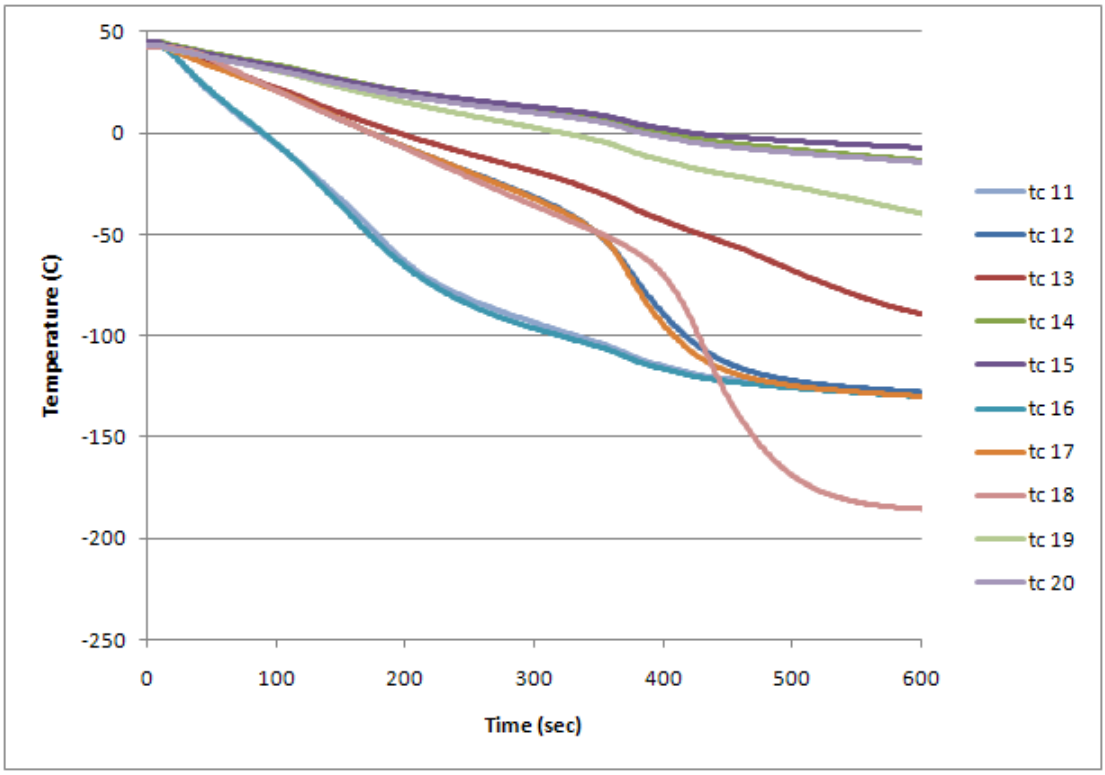

Figure 115. Test 20 – TCs 11-20

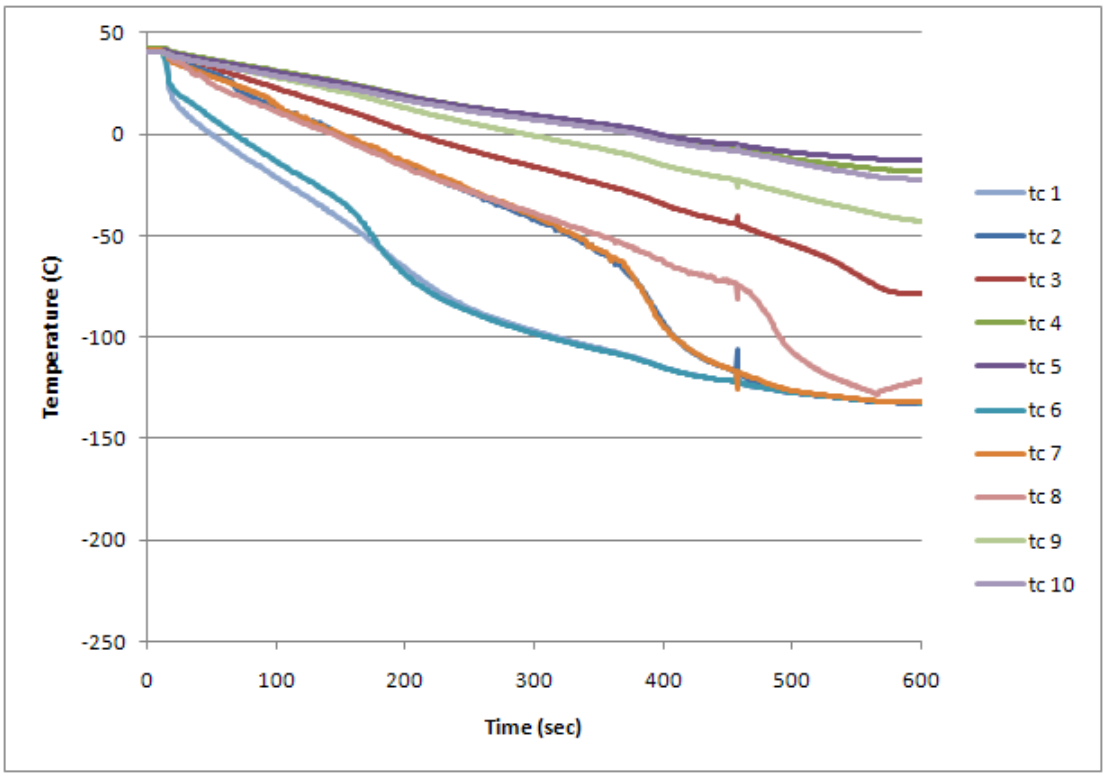

Figure 116. Test 21 – TCs 1-10

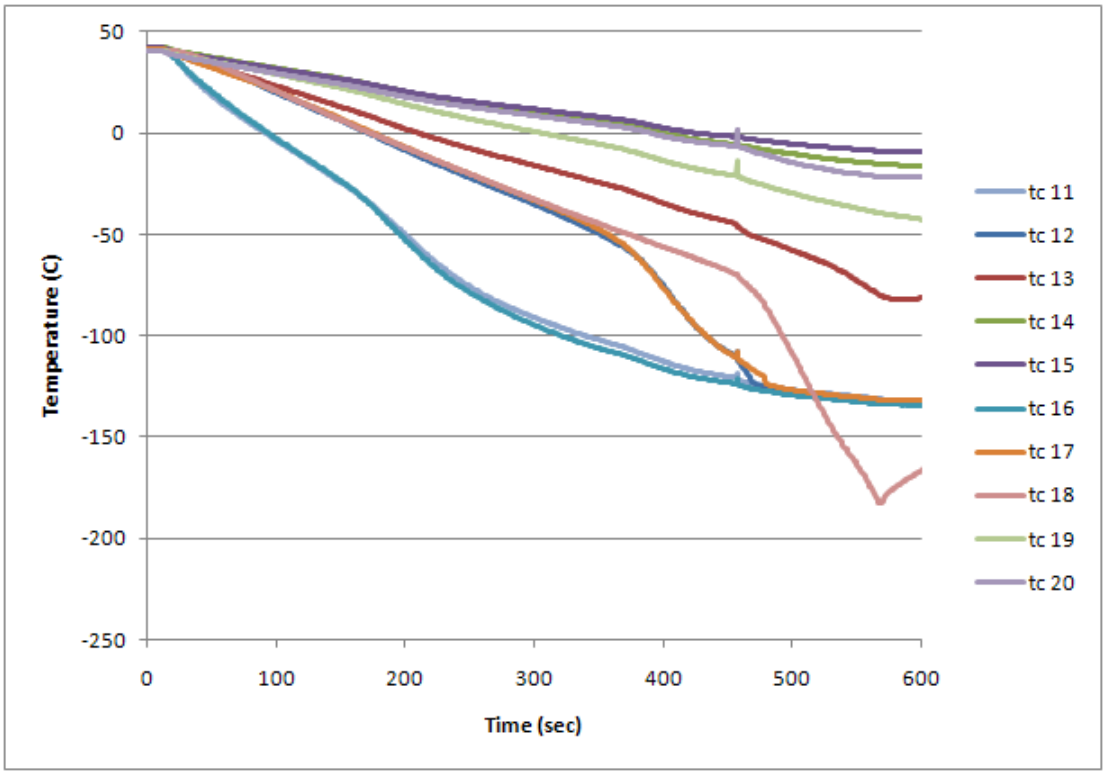

Figure 117. Test 21 – TCs 11-20

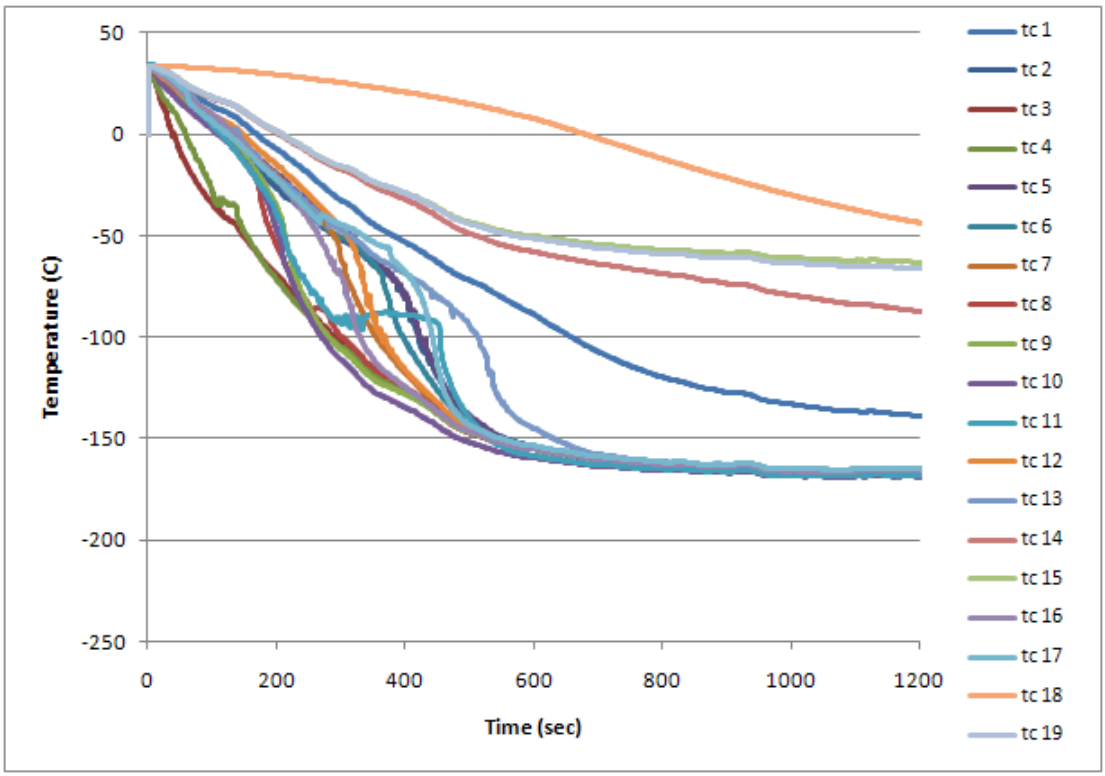

Figure 118. Test 13 – TCs 1-19

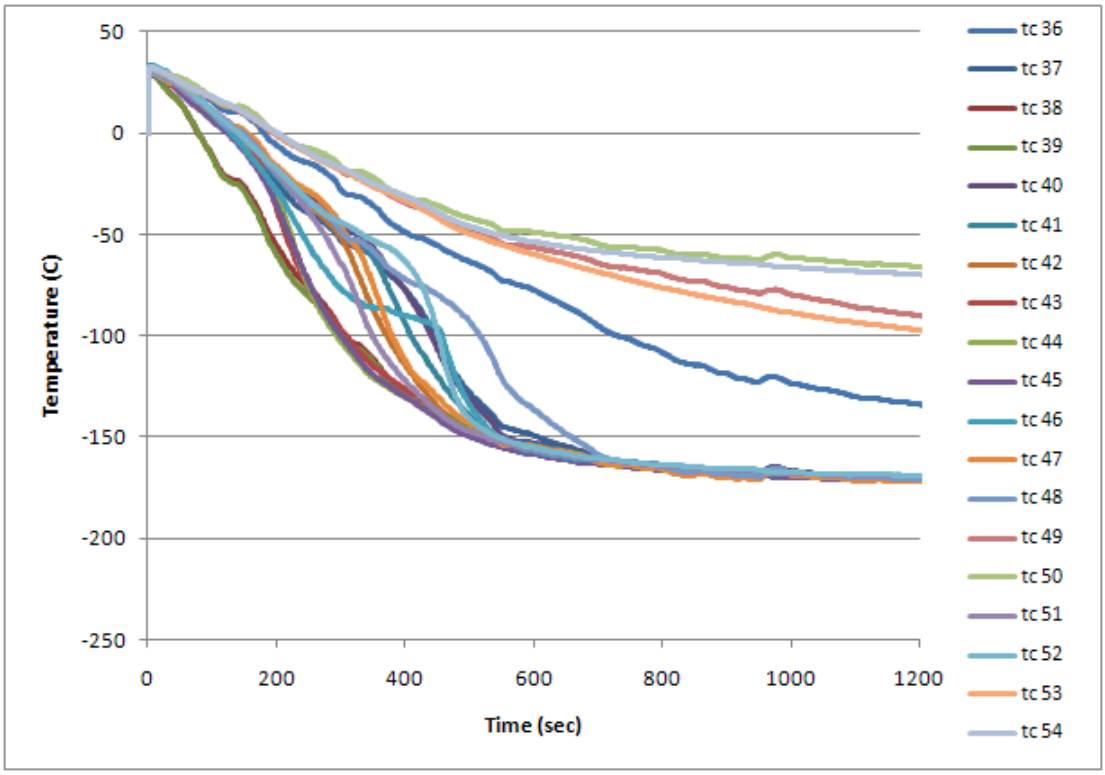

Figure 119. Test 13 – TCs 36-54

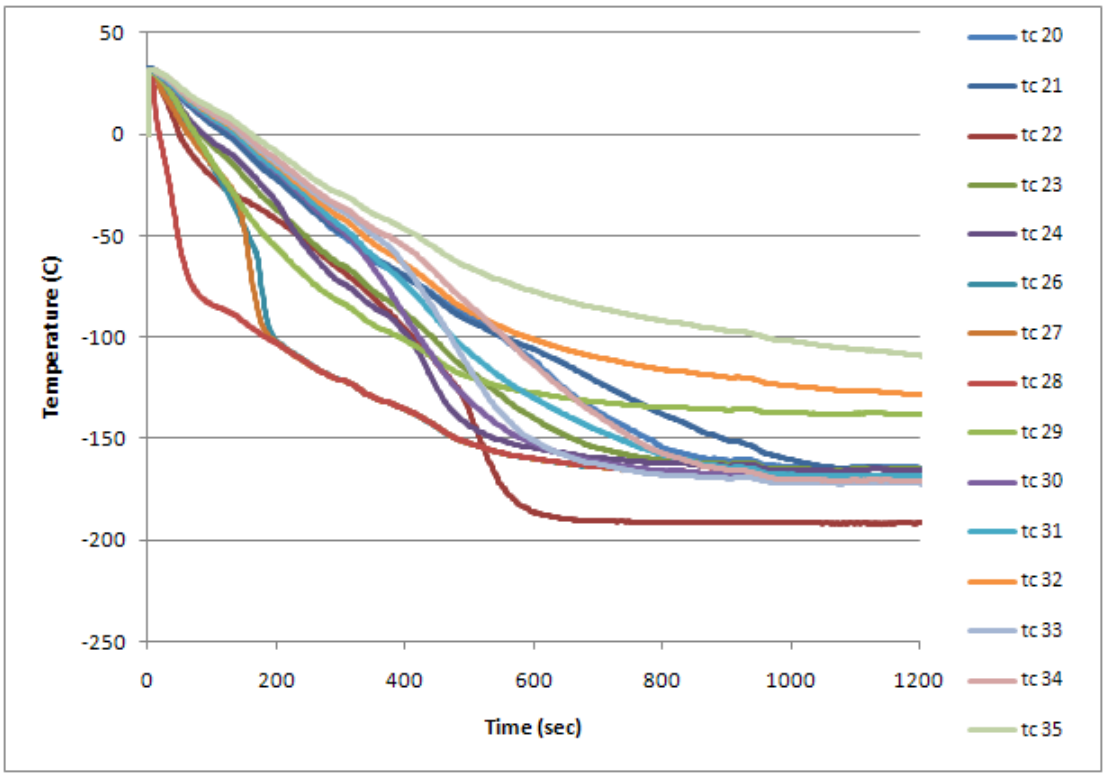

Figure 120. Test 13 – TCs 20-35 (TC 25 not used)

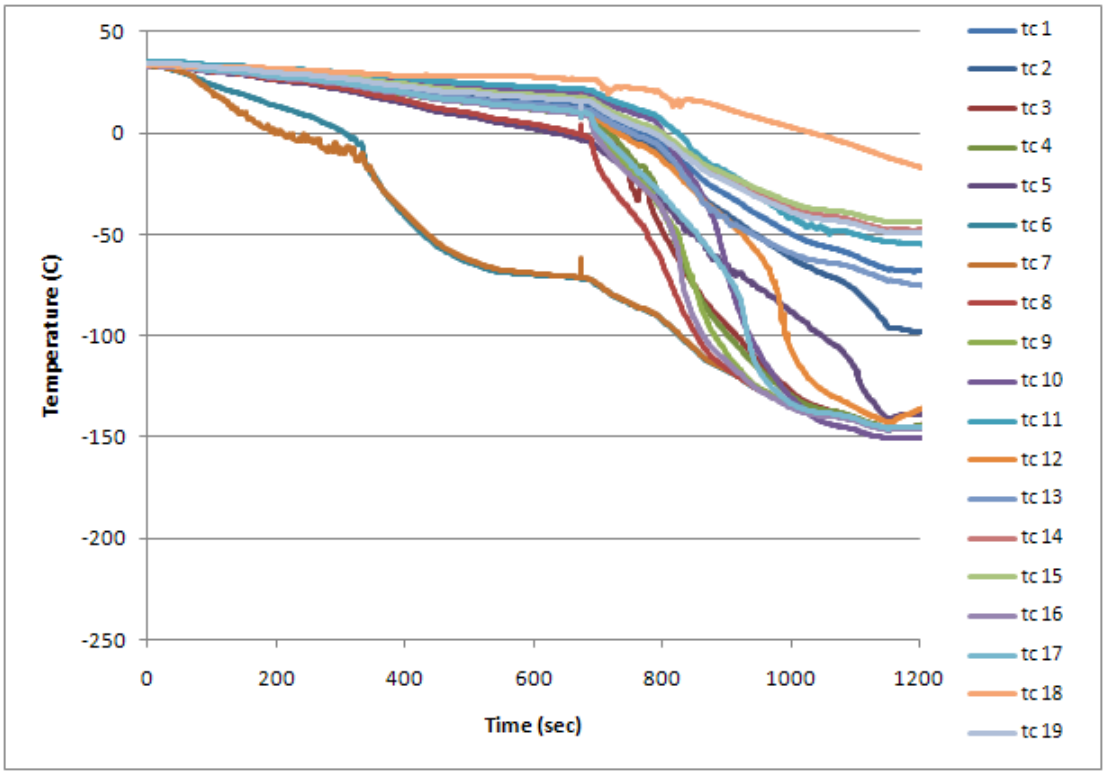

Figure 121. Test 14 – TCs 1-19

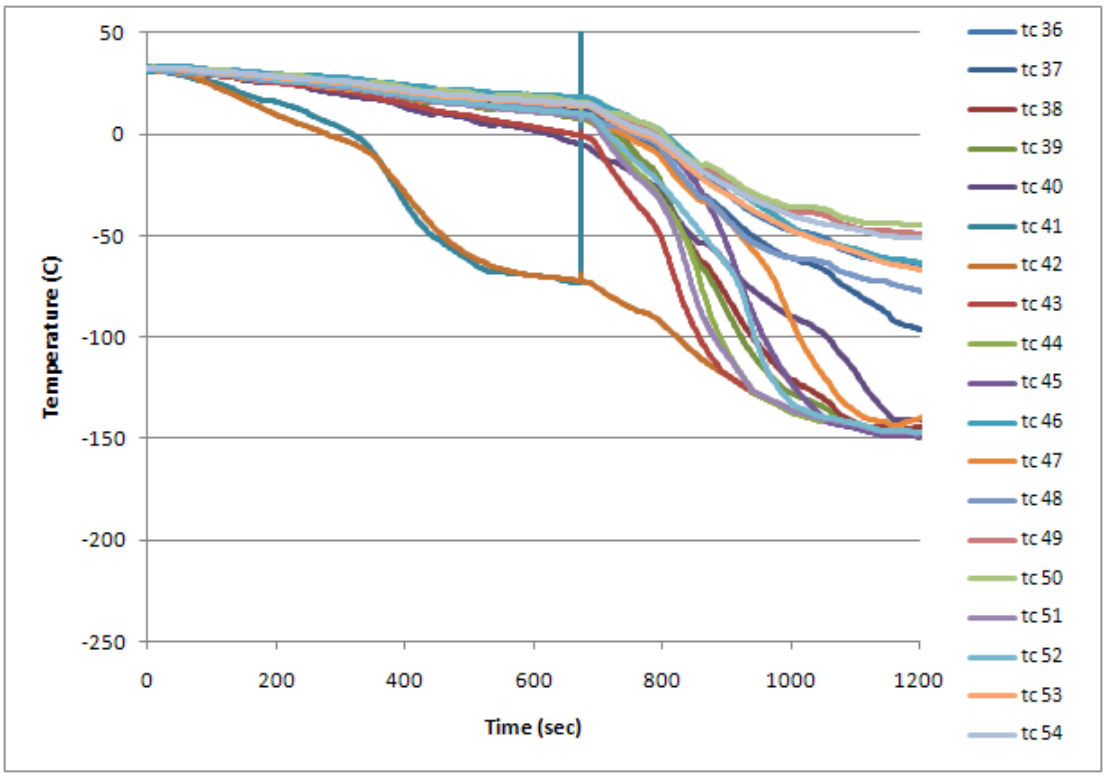

Figure 122. Test 14 – TCs 36-54

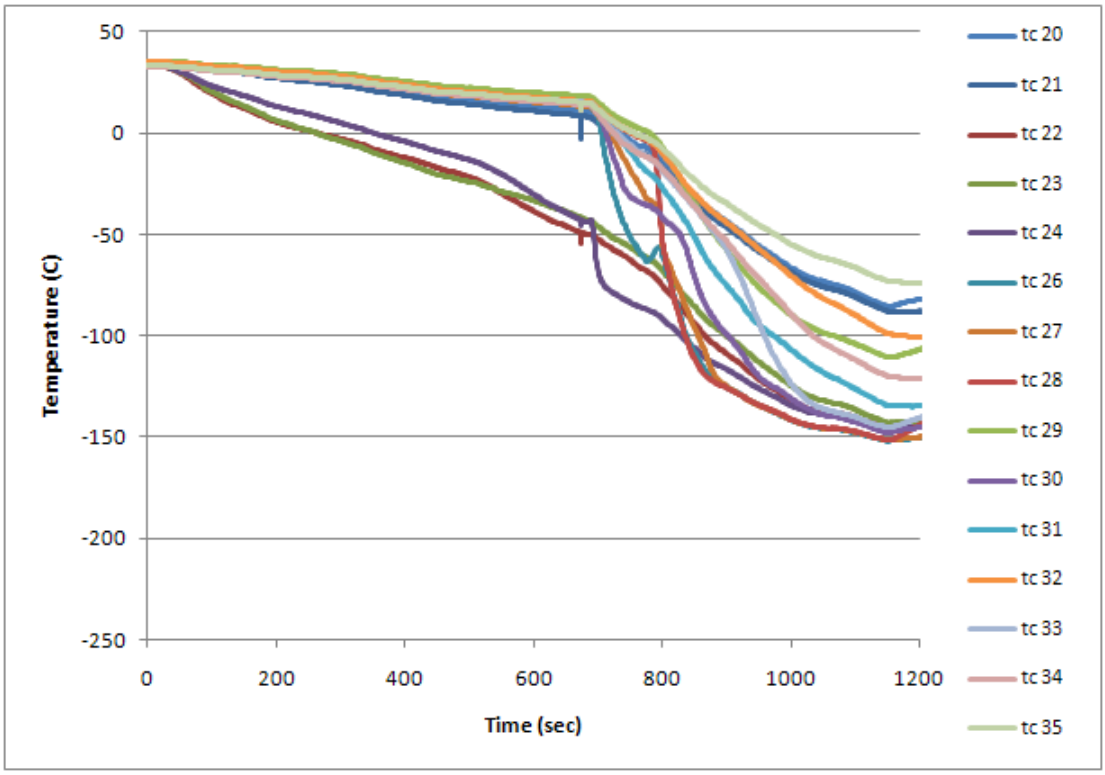

Figure 123. Test 14 – TCs 20-35 (TC 25 not used)

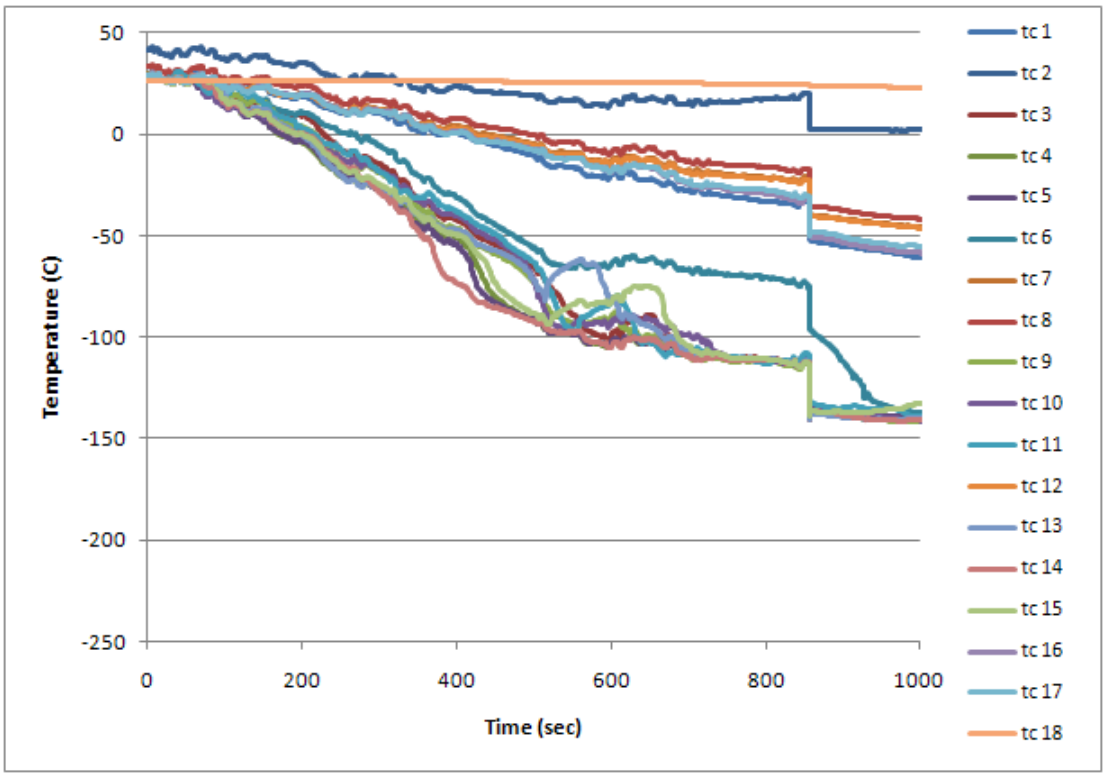

Figure 124. Test 16 – TCs 1-18

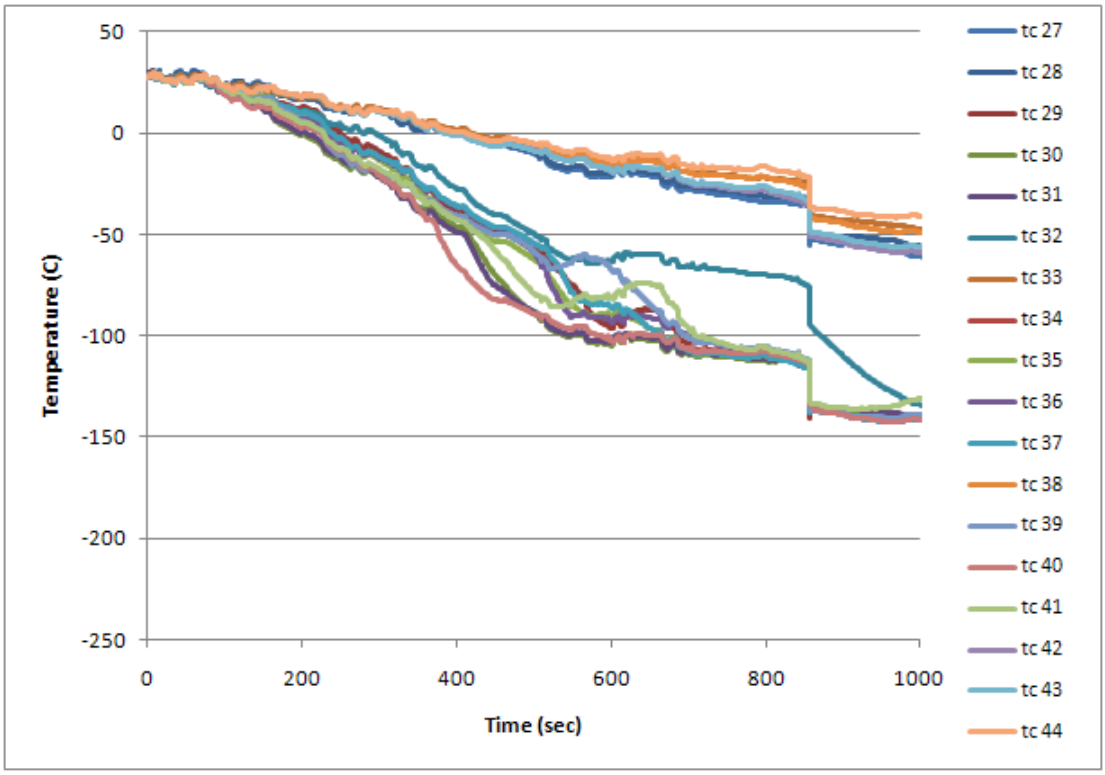

Figure 125. Test 16 – TCs 27-44

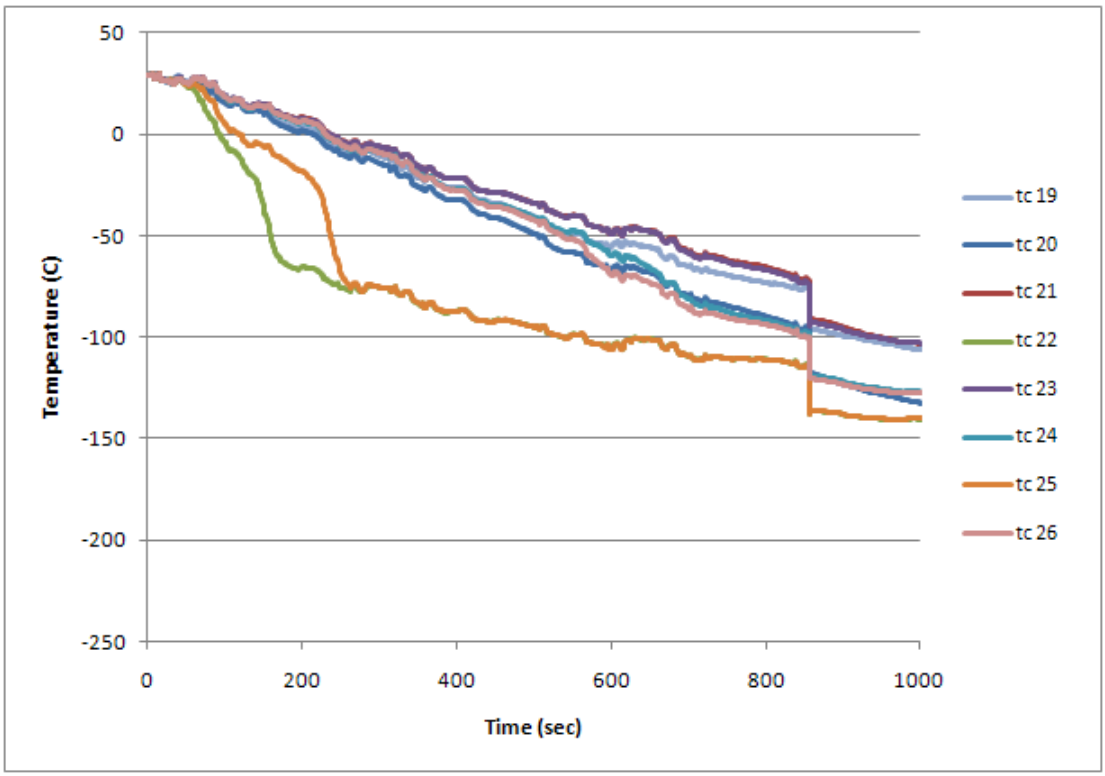

Figure 126. Test 16 – TCs 19-26

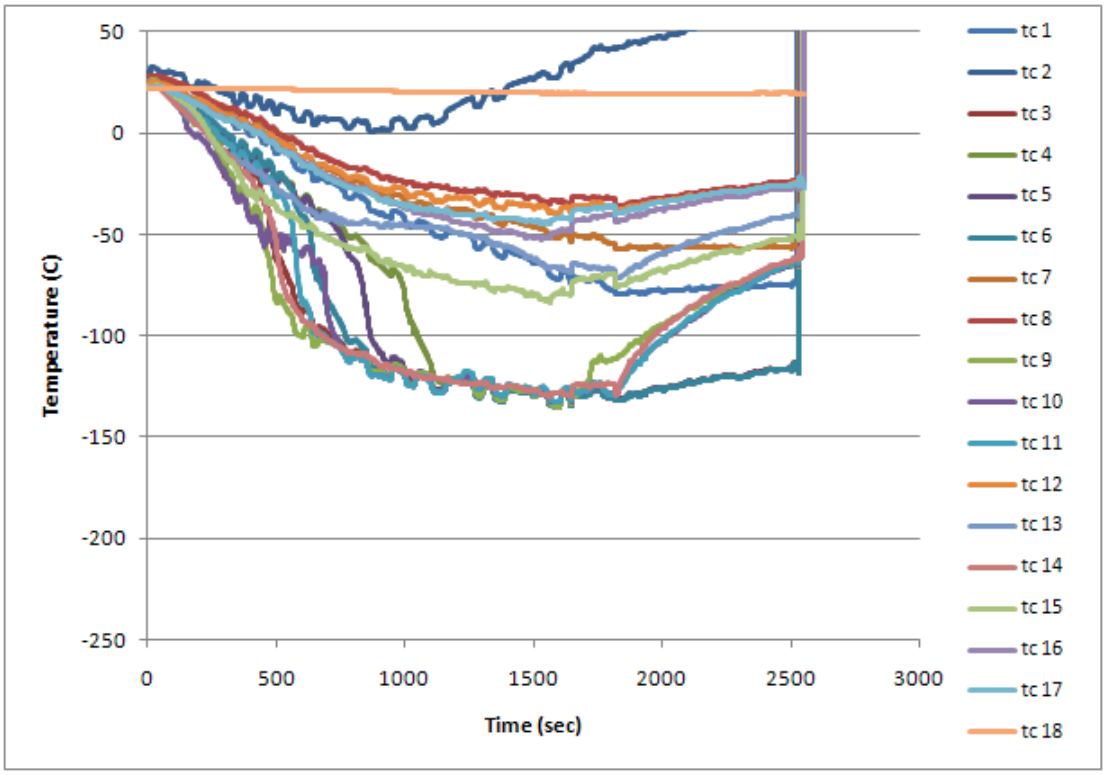

Figure 127. Test 22 – TCs 1-18

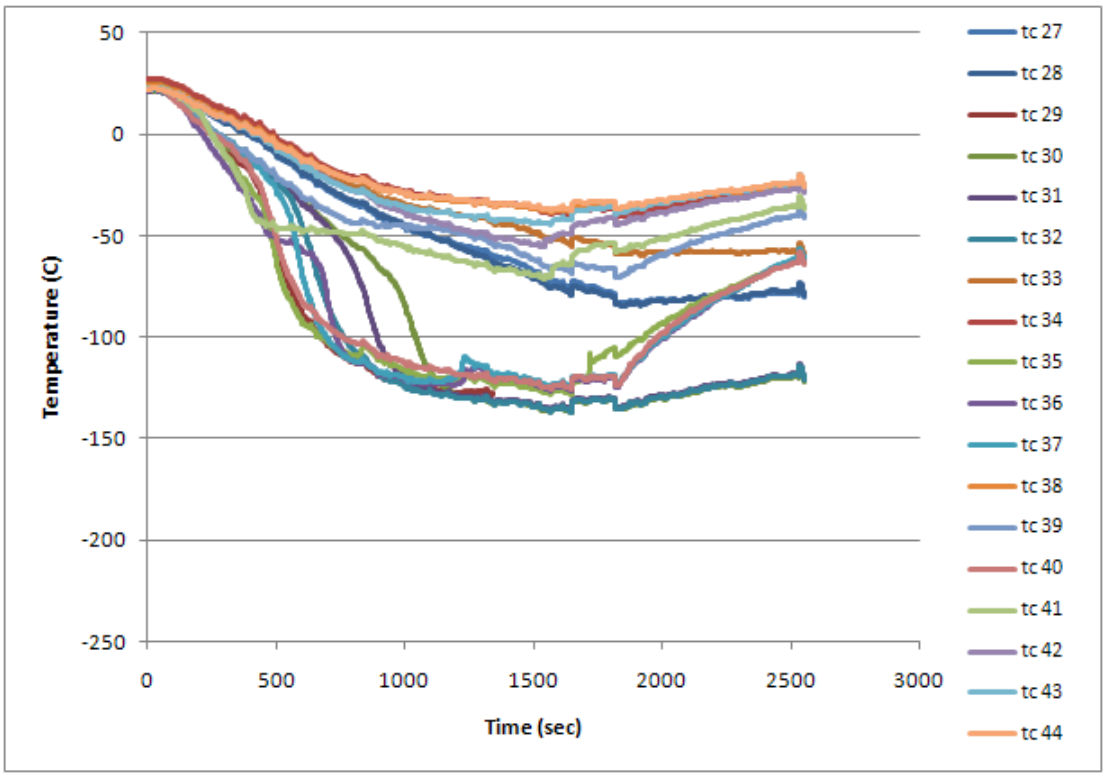

Figure 128. Test 22 – TCs 27-44

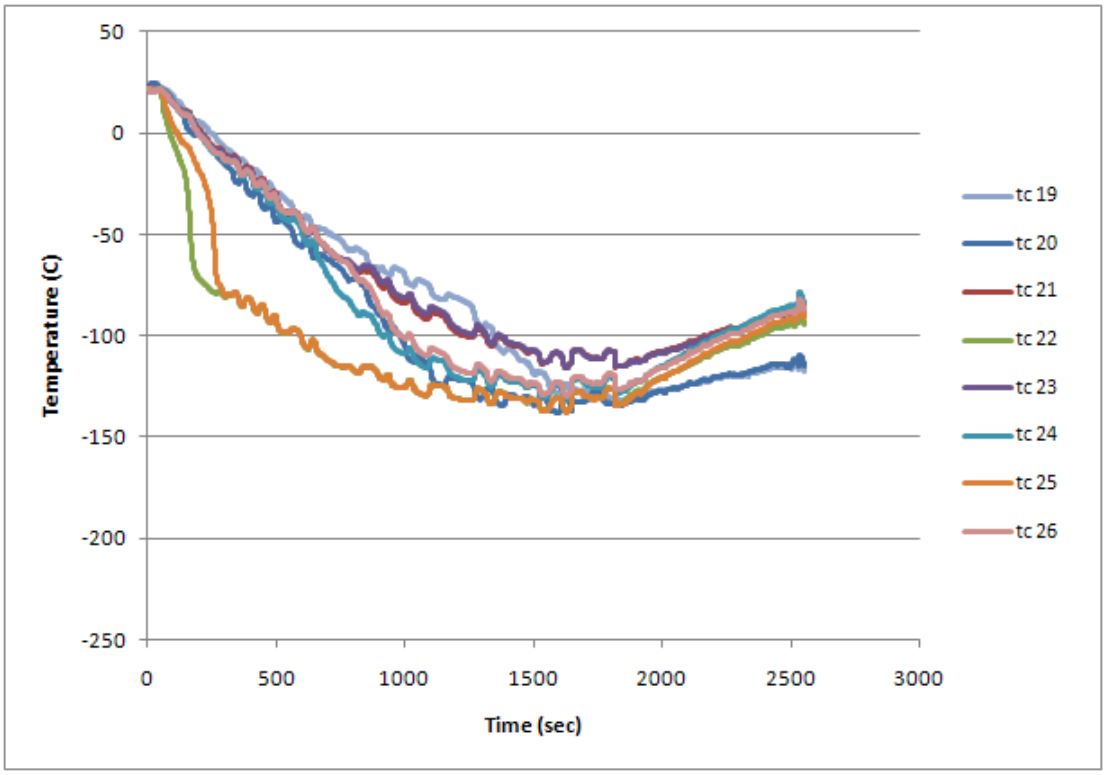

Figure 129. Test 22 – TCs 19-26

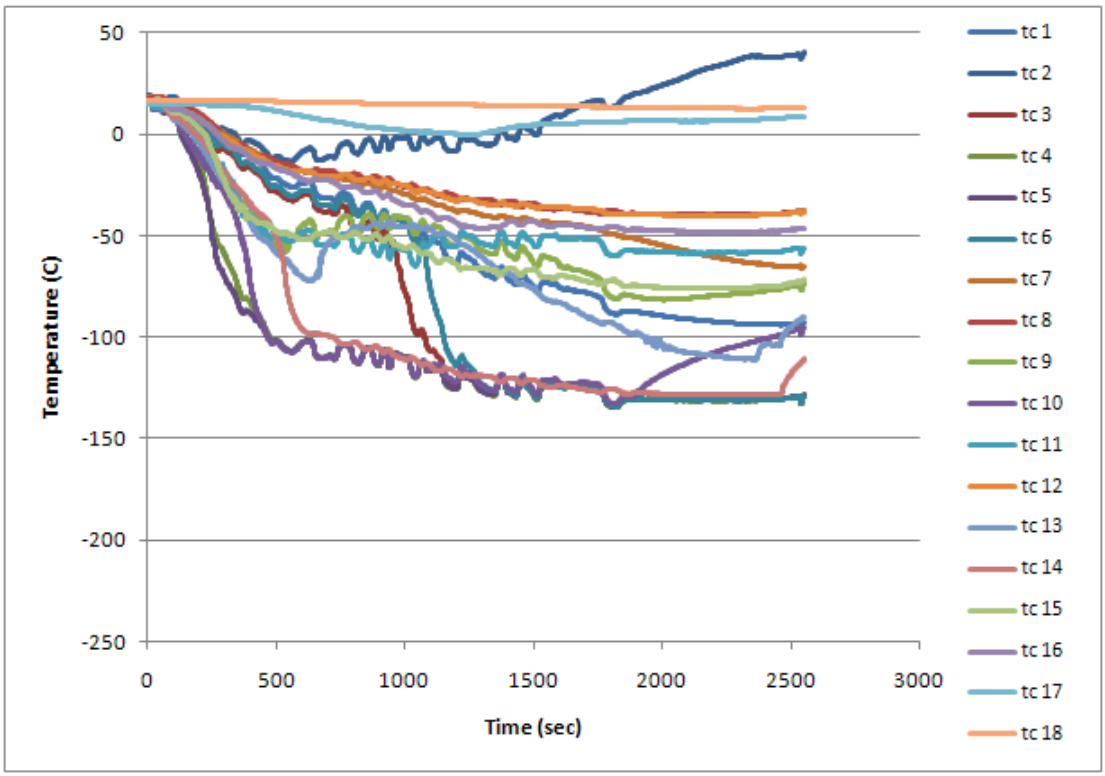

Figure 130. Test 23 – TCs 1-18

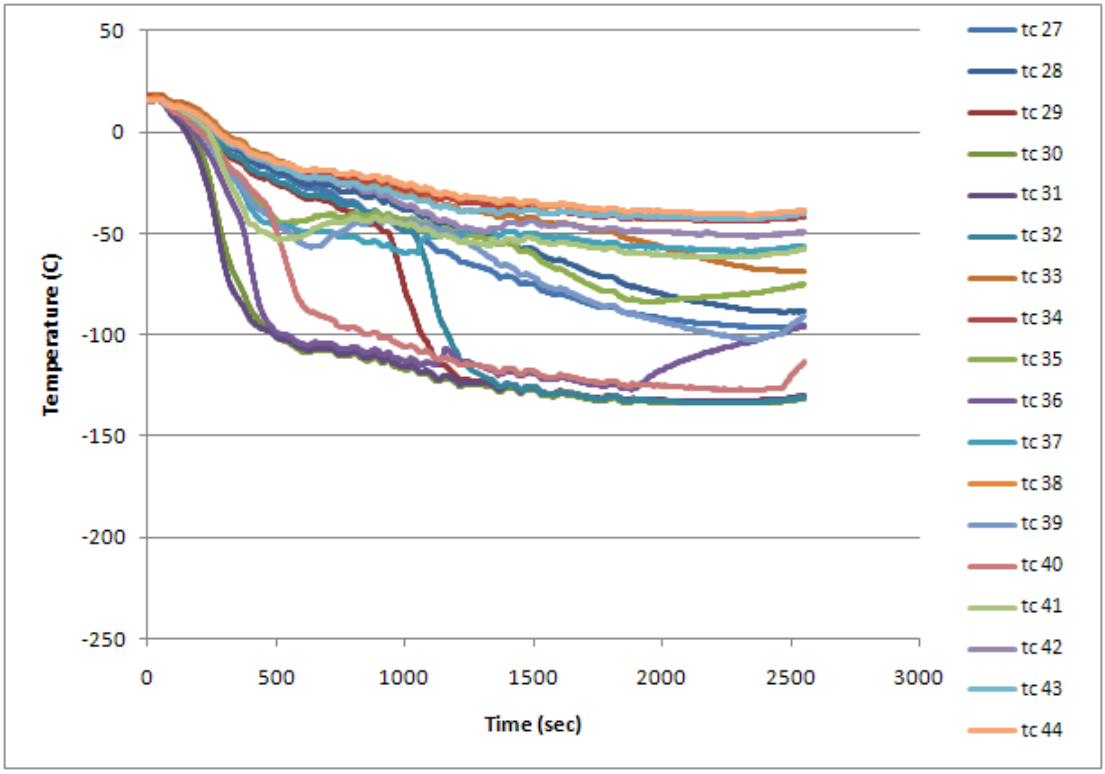

Figure 131. Test 23 – TCs 27-44

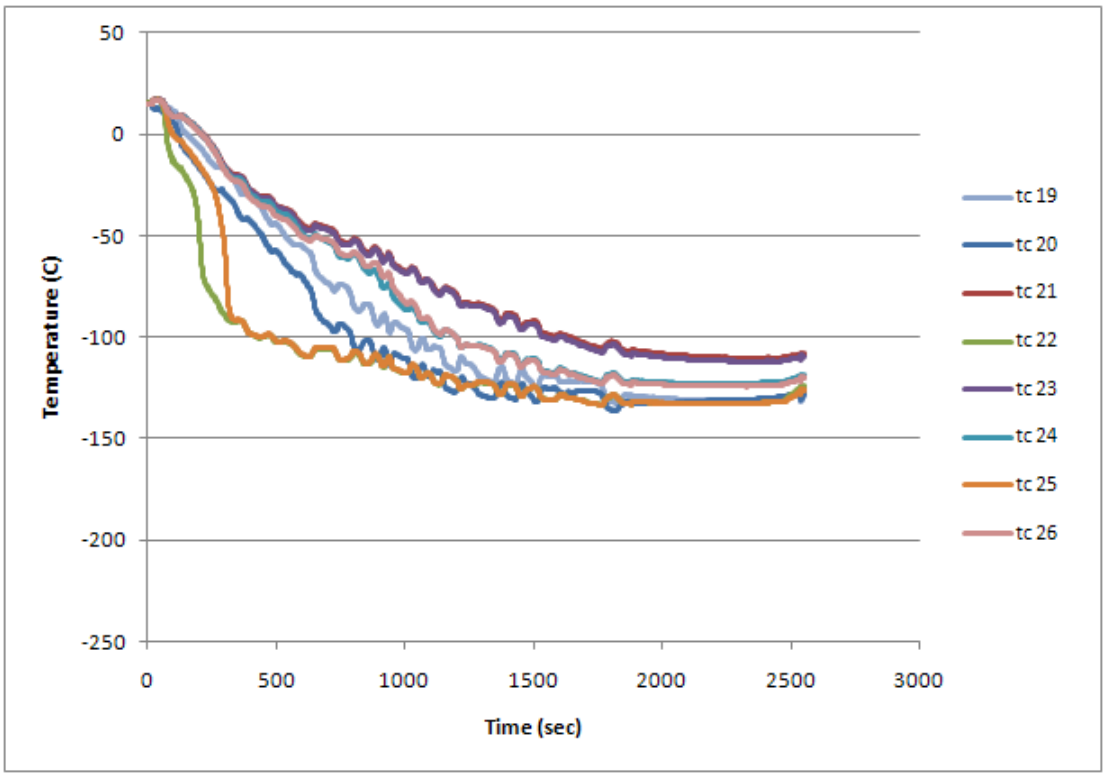

Figure 132. Test 23 – TCs 19-26

DISTRIBUTION

EXTERNAL DISTRIBUTION

Bob Corbin
Director, Oil and Gas Global Security and Supply
United States Department of Energy
Office of Oil and Natural Gas FE32
Forrestal Building
1000 Independence Ave SW
Washington DC 20585

SANDIA INTERNAL DISTRIBUTION

MS1135	R. Kalan, 1534
MS1108	M. Hightower, 6111
MS0744	J. Petti, 6233
MS0899	RIM - Reports Mgmt, 9532


Sandia National Laboratories